CHAPTER - IV

RESULTS AND DISCUSSION

Cynanchum tunicatum Retz. (Alston) is a climber, comes under Apocynaceae family. It is usually called as dog-strangling wine or mild weed. In Tamil, it is called as Aattu Moola Kodi. There are roughly 2980 species in 315 genera in this family. The genus *Cynanchum* has approximately 200 species, which have been used in folk medicine such as an antifebrile, antitumor, diuretic, anodyne, tonic, and effective against chronic hepatitis (Tawfiq et al., 1991). According to review of literature there were no scientific research evidence was recorded in *C. tunicatum*. Consequently, understanding the basic characteristics of this species was depicted providing a basic for further research.

Macroscopic and microscopic analysis were done for accurate identification of this species. The use of the erroneous species for medicinal purposes can be detrimental to end-users. Proper identification and authentication of herbal plants are essential to ensure traditional values such as efficacy, purity and quality. One of the rare species *C. tunicatum* is selected for our study, critical conservation is needed to secure the sustainability of the species. The standardized methods for *in vitro* micropropagation through PTC technique has been optimized.

The *in vitro* direct and indirect organogenesis were successfully regenerated and it was acclimatized in a field condition. The callus and plant extracts were obtained by sequential method using organic solvents. The preliminary qualitative and quantitative analysis were performed using both plant and callus extract. The FTIR, GC-MS, HPTLC and column chromatographic technique were scrutinized to characterize the bioactive compounds. The *in vitro* biological assays such as antimicrobial, antioxidant, anti-inflammatory, and anti-cancer activities. Though there were no previous scientific reports on *C. tunicatum,* this study was a novel finding. The molecular docking studies confirmed the highest binding score with the target cancer protein and bioactive compounds.

4.1. Ethnobotanical survey

An ethnobotanical survey was investigated in the Sirumalai forest, Dindigul district, Tamil Nadu. It revealed that *Cynanchum tunicatum* was used as folk medicine such as antifebrile, antitumor, diuretic, anodyne, tonic, and effective against chronic hepatitis by indigenous people. It sheds light on the traditional medicinal uses of *C. tunicatum* in the Sirumalai forest region.

4.2. Macroscopic observation

Cynanchum tunicatum is commonly known as Dog Strangling Vine or Milkweed. It is a perennial twinning herb predominantly found in tropical and temperate zone. Its leaves are simple, ovate, oblong, opposite, petiolate, and heart-shaped, base and tapering tip length of 3-15 cm long and 2-7 cm wide, fine hairs could be seen on adaxial surface.

It is slender climber produce white latex, with stems are pendulous and twinning, reaching up to 5 m in length. The flowers are borne on an umbel inflorescence, consists of 3-6 flowers, 5-15 mm long and 0.5-1 mm wide, pedunculate and white, forming umbels of 3-6 flowered, bisexual, yellow outside with 5 greenish-red lobes. The fruit is a simple, dehiscent dry follicle, green when immature and brown when mature, releasing seeds through a suture and it has taproot system (Figure 1).

Wang et al. studied the morphological characteristics of *Cynanchum* species including *C. auriculatum, Cynanchum bungei* and *Cynanchum wilfordii.* The roots of *C. auriculatum* are cylindrical, plump and tuberous. Tiny hairs were covered in its stem and leaves. Leaves are lanceolate, 4-12 cm long, oval and 4 -10 cm wide. Flowers are white, oval-shaped, individual with soft hairs present in the inner surface and follicles are 8 cm long and 1 cm diameter (Wang et al., 2021).

In *Cynanchum bungei,* the roots are cylindrical, mostly 3-6 in number with brown-white surface. It has slender stem with minute hairs and halberd-shaped leaf with 3-8 cm long, 1-5 cm wide. The lobes of the calyx are needle shaped and corolla are white or moderately yellowish green in colour with hairy, soft in the inner surface. The seeds are 4 cm long with several white filaments. The roots are grey- brown, spindle shaped in *Cynanchum wilfordii* and it has 10 cm long and 2 cm in diameter. It has a slender stem like other species, tiny soft hairs were present around the stem. Habitually, ovate leaves were present like as *C. tunicatum,* 5-6 cm long and 2-4 cm wide. The flowers have soft hairs present outside the calyx and corolla is oblong and yellowish in colour. The follicle is needle-shaped, 12 cm long and 1 cm diameter. The seed is dark brown in colour and ovate (Wang et al., 2021).

Ellmouni et al. observed the morphological characteristics of *Cynanchum leave,* the stem is herbaceous, climber, villous hairy covered at stem margins. Leaves are opposite, petiolate and it is 7 cm long with reddish-green in colour, Glabrous blade, cordate, ovate, acute, with 10 cm long and 8 cm broad. Unlike *C. tunicatum*, its inflorescence is axillary umbellate cyme. It has hairy peduncles with 8 cm broad and pedicel is pubescent with 1 cm long. Corolla were

white, glabrous, 5 lobes with 7 mm long and 3 cm broad. Calyx has 5 green lobes, pubescent and ovate.

Figure 1. Macroscopic observation of *C. tunicatum*

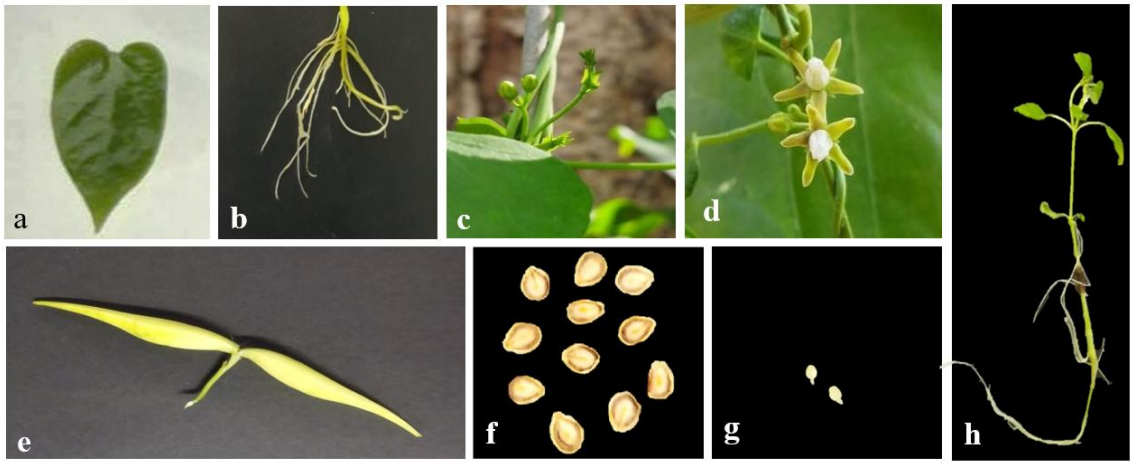

a) leaf, b) root, c) bud, d) flower, e) pod, f) seed, g) embryo, h) whole plant

4.3. Microscopic observation of *C. tunicatum*

Plant anatomy is one of the oldest disciplines in plant science, with a vast body of accumulated knowledge that has given rise to various modern branches of the field (Sokoloff et al., 2021). 10x, 40x and 100x magnification lens were used for microscopic analysis. The detailed anatomical observation of *C. tunicatum* from leaf, stem, and root were examined microscopically including the cell size, shape, arrangement, distribution, types of crystal, and starch distribution.

4.3.1. Anatomy of leaf

The transverse section of *C. tunicatum* was investigated under the light microscope. The multicellular epidermal cell consists of thin and uniseriate, irregular, oblong-shaped cells, which are distinct from inner tissue and covered by a thin layer of cuticle. The multicellular epidermal hairs were observed on upper epidermal layer. The abaxial epidermal cells appeared larger than the adaxial epidermal cell. Both epidermis layers showed straight anticlinal walls. The prominent underlying single-layered epidermis on the abaxial surface of the central midrib. The presence of arc-shaped vascular bundle was observed under the starch-filled chlorenchyma cells. The calcium oxalate crystal was embedded on the vascular bundle compressed of a phloem followed by a protoxylem and metaxylem without bundle sheath. The periclinal

parenchymatous cells were filled in the vascular bundle. The long-armed irregular and rounded-shaped parenchymatous, spongy and mesophyll cells were present around the vascular bundle (Figure 2).

The anatomy of the leaf was determined in two species such as *Thuarea involute* and *Ischaemum muticum.* Leaves are succulent in nature which contained leaf midrib, bulliform cells, vascular bundles, sclerenchymatous cells, and bundle sheath. There are three types of sclerenchyma cells which are present in the upper leaf, midrib, and epidermal cells. *Imperata cylindrica* showed greater number of vascular bundle arches and area. In contrast, *T. involuta* resembles anatomical traits of *I. muticum*, especially with a larger chlorophyll content and greater bundle sheath area. Moreover, *I. cylindrica* revealed dense sclerenchymatous cell than its counterparts. Notably, significant differences in various quantitative grass traits, such as bundle sheath, leaf thickness, vascular bundle, chlorophyll content, sclerenchymatous tissue were observed (Rindyastuti et al., 2021). Sayed et al. studied anatomical features of various species of leaf blades. Calcium oxalate crystals were existed in *C. acutum* (Sayed et al., 2017).

The leaf of *Plumeria alba* is characterized as thin lamina and thick midrib extended from upper portion of midrib. The adaxial side of the midrib was flat, less prominent central ridge, while lower portion was wide, semicircular and even, measuring 1.8 mm length and 2.5 mm breath. The midrib comprised a thin epidermal layer blending into inner tissues. Its cortex tissue consists of small collenchyma cells at the outer region, transitioning into parenchyma. The collenchyma is 50 μm wide at lower surface and 150 μm wide at upper surface. Thin laticifers, thick-walled and dispersed within the ground tissue, occasionally it wide and thin-walled with no visible contents. The vascular bundle includes angular xylem elements, a thin layer of phloem, bowl-shaped strand along with outer metaxylem and inner phloem are present within the vascular arcs (Imrana & Asif, 2020).

Figure 2. Anatomical structure of leaf from *C. tunicatum*

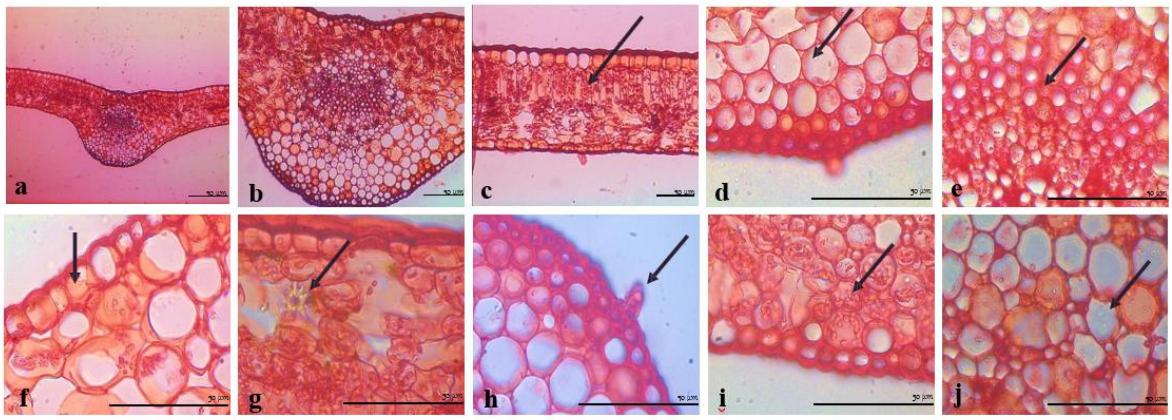

a) Leaf midrib in Transverse section b) Enlarged midrib portion c) Palisade cells d) Sclerenchymatous cells e) Vascular bundle f) Upper epidermis g) Calcium Oxalate crystals h) Epidermal hair j) Starch grains j) Cortex

4.3.2. Anatomy of stem

The stem anatomy comprised of epidermis, vascular bundle, and pith. The uniseriate epidermal layer was compactly arranged without intercellular space and it was covered by a thin layer of cuticle. The paracytic stomata were observed in the epidermal layer. It is a minute pore, which allows gases such as oxygen, carbon dioxide, and water vapor. Below the single-layered epidermis, 3-5 layers of hypodermis were present, it was isodiametric, thin cells and closely arranged. The periclinal chlorenchyma cells occupied up to 3-4 layers beneath the hypodermis. The fibrous pericycle cells were scattered in the hypodermal cells, which were compactly arranged. Phloem cells were present in between the fibrous pericycle and xylem cells. Latex cells are present amidst the parenchyma cells around the central vascular bundle. The metaxylem and protoxylem are surrounded by the midrib region called the pith (Figure 3).

In *Gymnosporia senegalensis*, the stem cross-sectioning showed a circular shape with an outer layer of epidermis. Below the epidermis, layers of cells such as parenchymatous and collenchymatous and sclerenchymatous cells were observed. The endodermis is the innermost layer of cortex formed a single layer. Vascular bundles were arranged in a V-shape consist of five bundles within the parenchymatous region and xylem is lignified. The arrangement of vascular bundles served as a significant marker for species identification and differentiation in plants. The pith encomposed large, thin-walled parenchymatous cells with a cavity-like structure in the middle (Jain & Janmeda, 2023).

The stem of *Mollinedia clavigera,* determined a circular shape, uniseriate epidermis protected by a layer of thin cuticle. The cortex contained few layers of parenchymatous tissues, interspersed with single or grouped brachy sclereids. The endodermis which contained prismatic crystals and starch grains marks the boundary of the cortex. In vascular bundle, the phloem lies outward and the xylem in inward position, accompanied by brachy sclereids and perivascular fiber caps next to phloem. The pith comprised of thin-walled parenchyma cells along with scattered starch grains, styloids with sharp ends and calcium oxalate crystals and it is similar to mesophyll, midrib, and petiole (Homem et al., 2020).

Figure 3. Anatomical structure of stem from *C. tunicatum*

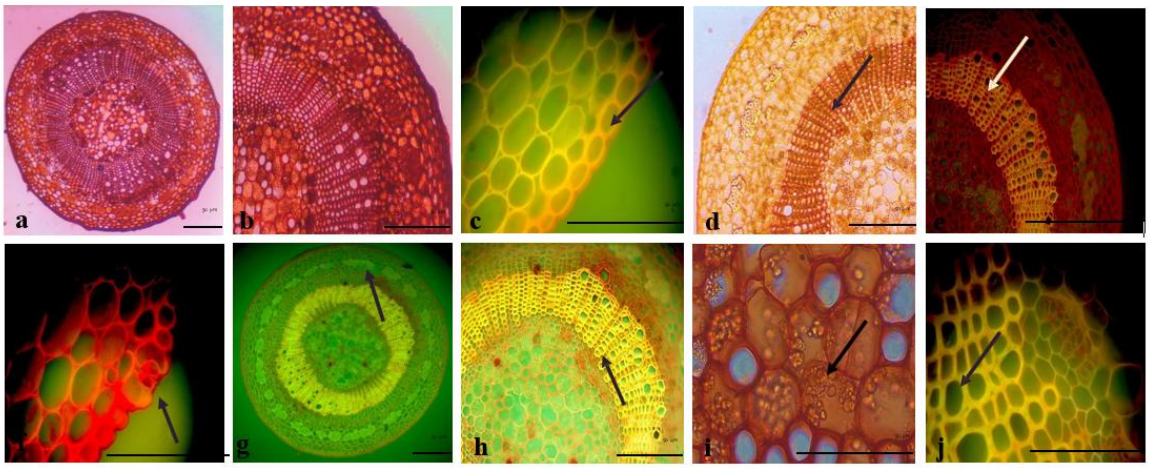

a) Transverse section of stem b) T.S of stem portion enlarged c) Upper epidermis with layer of cuticle d), e) Xylem cells f) Stomata g) Pericycle h) Vascular bundle i) Storage grains j) Enlarged xylem cells

4.3.3. Anatomy of root

The epidermal layer was thick, oblong shaped, uniseriate, arranged without intercellular space and covered with uniseriate cuticle layer. Beneath the epidermal layer, hypodermis consists of 5-6 layers of periclinal and anticlinal cell division. The prominent vascular bundle encompassed of xylem, phloem and crystals were scattered in druses form in hypodermis. It provides mechanical strength to the plant (Figure 4).

Crystals were observed in both leaf and stem from *C. acutum*. They were abundant in the stem cortex but sparse in the leaves, where druse crystals were located around the midrib the minor veins near xylem vessels (Tütüncü Konyar et al., 2014). The roots of *Rhus succedanea* exhibited similar histological features to *Pavonia odorata*, such as cork, cortex with

parenchymatous cells, pericycle, collateral vascular bundles, and a central pith (Khan et al., 2020).

The anatomy of roots of *Calotropis gigantea* both purple and white flower variants were similar. The well-developed periderm consisted of about 10-12 layers of different irregular shaped cells. The rectangular, barrel, or elongated-shaped endodermis cells were detected at the peripheral region of the cortex. The vascular bundles were well-developed and scattered. Vessels were solitary, round, or irregular or multiples of 2-3 rounds or irregular and semi-ring-porous, mainly in radial and/or diagonal, radial-oblique. Thickenings were alternate, oval-shaped, and with slit-like apertures. The epidermis of the stem was multicellular consisting of highly packed barrel to rectangular-shaped cells with a thick cuticle and covered with a thick coat of trichomes. Large, elongated trichomes were present in the purple form while the white form had uniseriate, elongated, and uniseriate multicellular trichomes. The cortex compressed of 2-3 layers of collenchyma cells adjacent to the epidermis followed by several layers of parenchyma cells. The small patches of sclerenchyma fibers were observed in pericycle (Abeysinghe & Scharaschkin, 2022).

Figure 4. Anatomical structure of root from *C. tunicatum*

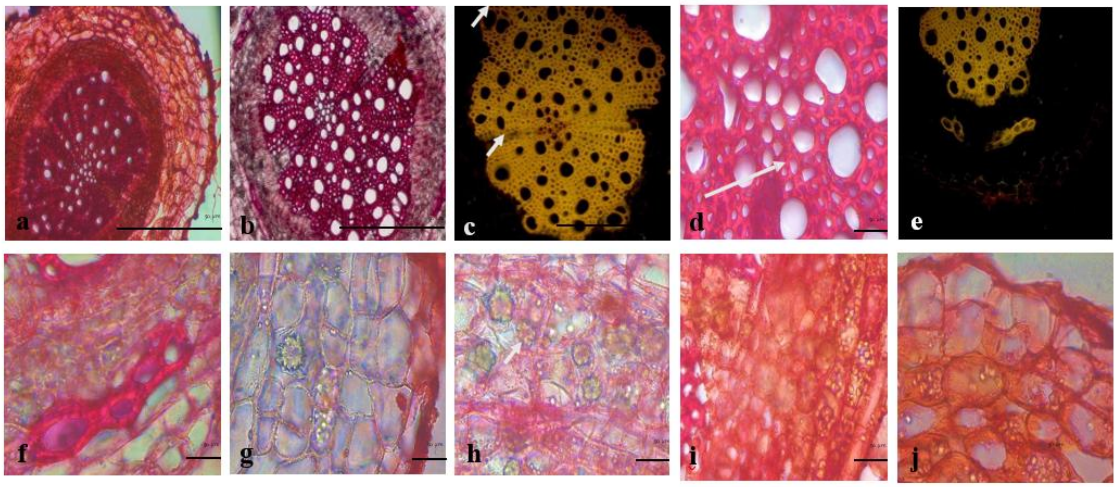

a) Transverse section of root b) Enlarged portion of a root c) Vascular bundle d) Xylem cells e), f) Phloem cells g) Calcium Oxalate crystals h) Latex cells i), j) Starch grains

4.4. Plant Tissue Culture

The optimization of seed culture from *C. tunicatum* using abiotic factors such as pH, photoperiod, and sucrose concentration. The callogenesis, somatic embryogenesis, and

organogenesis were optimized. The flow diagram showed the graphical representation for the experimental manipulation (Figure 5).

Figure 5. Workflow in Plant tissue culture

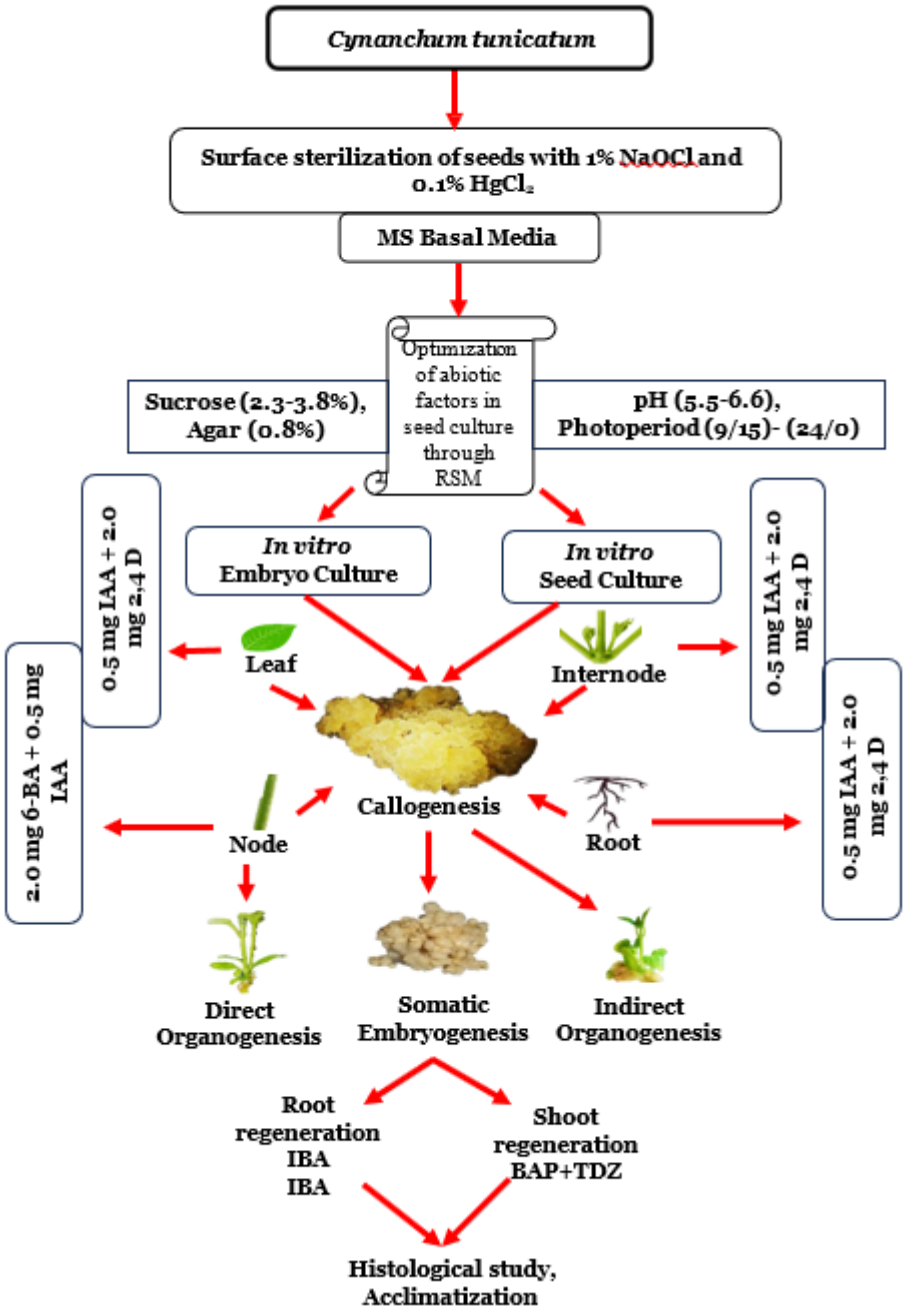

4.4.1. Sterilization

Surface sterilization is a process of preparing explants to remove the dust in debris with using sterilizing agents. Different durations of $NaHCl_3$ and $HgCl_2$ were used to optimize the sterilization technique of *in vitro* seed germination of *C. tunicatum* (Table 1). The surface sterilization was carried out with the running tap water for 20 minutes followed by 1% $NaHCl_3$

for 10-20 minutes and washed with double distilled water. Then 0.1% $HgCl_2$ were washed for three minutes followed by double distilled water.

Table 1. Effect of surface sterilization of *C. tunicatum* seeds with 1% sodium hypochlorite and 0.1% mercuric chloride

S.No	$NaHCl_3$/min	$HgCl_2$/min	Germination percentage (%)
1.	10	2	84.3 ± 2.5^{c}
2.	20	3	**96.6 ± 2.5^{a}**
3.	30	4	92 ± 1.0^{b}

Values represent mean ± standard deviation of tree replicates per treatment. Means in a column with same letter are significantly ($p \leq 0.05$) difference according to DMRT.

The first experiment was analysed with 10 minutes $NaHCl_3$ and 2 minutes $HgCl_2$ and the results showed 84.3% of germination rate. The maximum germination rate (96.6%) was achieved when $NaHCl_3$ rinsed for 20 minutes and $HgCl_2$ for 3 minutes. Increasing the time duration of 30 minutes $NaHCl_3$ and 4 minutes $HgCl_2$ showed a 92% germination rate in which the pods turned into light brown colour. The exposure of sterilizing agents should be in appropriate duration because the lesser duration increases the rate of contamination and higher duration affects the explants.

Similarly, the sterilization protocol was studied by Singh et al. the maximum sterilization percentage of *in vitro* aseptic culture was obtained from 1.0% Bavistin + 5% Sodium hypochlorite + 0.1% Mercuric chloride + 70 % Ethanol in Banana (Singh et al., 2022). In Tulip buds, 0.1 % mercuric chloride and Tween 20 were observed a maximum survival rate reached 96%. The sterilizing agent helps to eliminate microorganisms like fungi, bacteria, and viruses (Ibrahim & Draaj, 2020). Liquid disinfectants used for decontamination such as sodium hypochlorite, hydrogen peroxide (H_2O_2), and glutaraldehyde were examined to inactivate the lipid and non-lipid enveloped for the model microorganism (Kindermann et al., 2020). Sorokin (2021) achieved the maximum percentage of seed germination rate in 1% H_2O_2 solution used (Sorokin et al., 2021). Sodium hypochlorite is a commonly used well-known bactericide, which is highly potential to reduce microorganism level present in plant species (Ahmadpoor et al., 2022). The supplementation of 0.2 % $HgCl_2$, ethanol (70%–90%), mercuric chloride (0.1%), and formaldehyde (40%) revealed 100% disinfection in endophytes (Sahu et al., 2022).

4.4.2. Response Surface Methodology in Seed Culture

The healthy seeds were selected for seed culture to obtain disease-free plantlets. The seeds were cultured on MS medium without PGRs (Murashige & Skoog, 1962). The maximum germination rate of *in vitro* seed culture of *C. tunicatum* showed 96% (Figure 6). There are three abiotic factors were chosen for RSM analysis such as pH, photoperiod and sucrose concentration. These factors play a crucial role in *in vitro* germination percentage of seed. *In vitro* germination of seed is essential for obtaining young plantlets, moreover it serves a valuable source of explant for various *in vitro* cultures (Sorokin et al., 2021). The basal medium act as a primary source of macronutrients, micronutrients, vitamins, minerals and ions for the development of seed (Kim et al., 2019; Hesami et al., 2021). Therefore, seed culture of *C. tunicatum* established an appropriate method for the conservation of endemic plant species.

Figure 6. Optimization of abiotic factors through Response surface methodology in Plant tissue culture

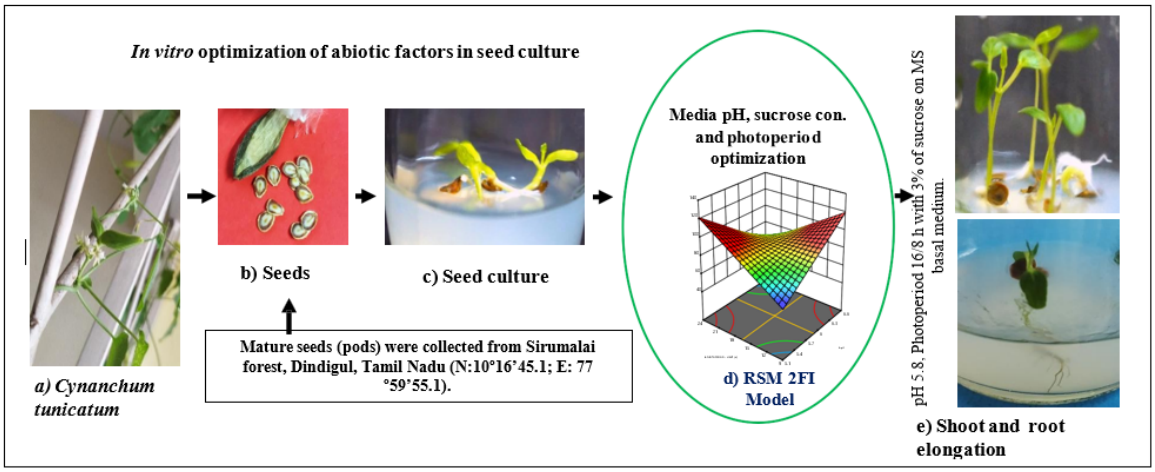

a) *Cynanchum tunicatum* b) Seeds of *C. tunicatum* c) *In vitro* seed culture d) RSM for abiotic factors e) Shoot and root elongation of *C. tunicatum*

4.4.3. Optimization of *in vitro* seed culture using RSM

Optimizing abiotic factors significantly contributed to achieving the highest seed germination percentage of *C. tunicatum*. Response surface methodology was applied to optimize various abiotic factors. Three replicates were used for each variation of all the parameters. Three independent parameters were investigated such as pH (5.1-6.6), photoperiod (9/15-24/0), and sucrose concentration (2.3-3.8%) on MS medium was used without PGRs. The data set was aliased with Two-Factor interaction model (2FI model) (Dron et al., 2002).

4.4.4. Effect of pH on seed germination percentage

The variation of pH affects the germination percentage in seed culture of *C. tunicatum.* The pH 5.8 on the medium achieved the maximum germination of 96.6% in *C. tunicatum*. Leifert et al. analyzed the determination of optimal pH buffering values ranging from 2.6 to 5.8 across various species for growth (Leifert et al., 1992). The pH changes could impact the viability of organogenesis and rhizogenesis. MS basal medium was typically maintained a pH ranging from 5.6 to 5.8. In *Mucuna monosperma*, the factors were optimized including tyrosine 0.978 g L^{-1}, pH 5.85, SDS 34.55 mg $L^{-1}$and copper sulphate 21.14 mg L^{-1} for the maximum melanin yield of 0.887 g L^{-1} using Response surface methodology (Inamdar et al., 2014) (Figure 7a, 8).

4.4.5. Effect of photoperiod – seed germination percentage

Photoperiod is a crucial abiotic factor which influence the growth and germination rate. Absolute darkness might impact germination percentages in both *in vivo* and *in vitro* plants. The absence of light can modify the germination percentage in *in vitro* cultures. This study proves a photoperiod of 16/8 hours of light /dark reached the highest germination percentage of 96% in *C. tunicatum* (Figure 7b, 8). A continuous dark period affected the germination percentage and showed a maximum seed germination at 8-hour dark condition (Figure 7c, 8).

Photoperiod demonstrated the highest growth percentage and enhanced yield (Flores et al., 2021). The optimal photoperiod has been found to promote flowering and augment plant growth in *Cannabis sativa* (Moher et al., 2021). Although light quality and intensity may seem straightforward, they represent complex factors that interact with variables like sucrose levels, influencing shoot development and growth in a non-linear, multifactorial manner (Hesami & Jones, 2021). The alternating light and dark photoperiod can induce changes in cellular composition. *Isochrysis galbana* exhibited high biomass production under an 18/6 photoperiod, making it a promising candidate for biodiesel production (Che et al., 2019).

Reducing the duration of the dark period impacts the plant regeneration capacity. There was no observable increase in the germination rate in *Triticum timopheevii* with the reduction of the dark period (Miroshnichenko et al., 2021). Low light intensity impedes photosynthetic efficiency, while high levels can damage certain components of the photosynthetic apparatus and restrict pigment synthesis (Cioć et al., 2018). Each stage of *in vitro* development necessitates specific light and dark conditions for optimal growth (Batista et al., 2018). The effect of a dark period can change the germination percentage in *in-vitro* culture.

Figure 7. Graphical representation of optimization of abiotic factor (RSM)

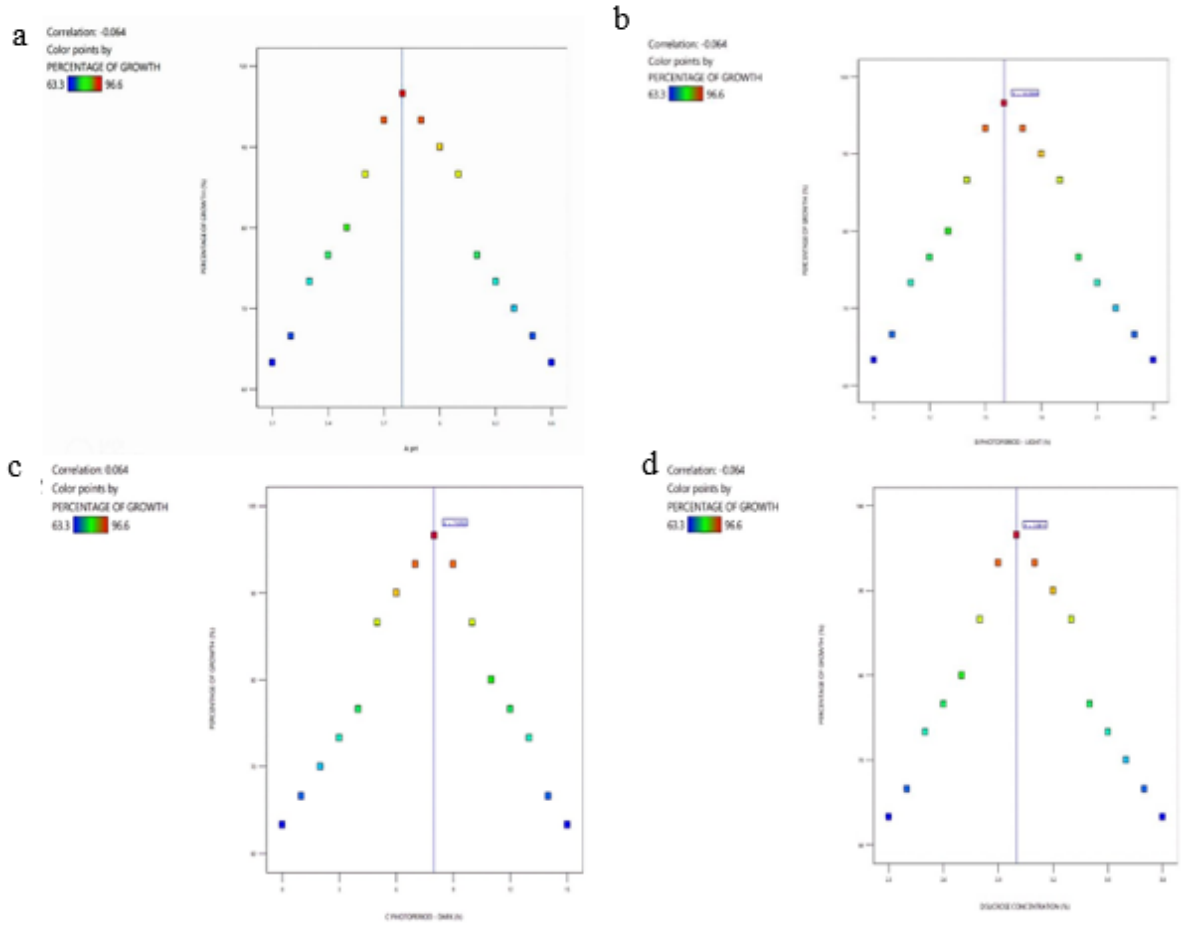

(a) Percentage growth of pH (a) Percentage growth of photoperiod (Light) (c) Percentage growth of photoperiod (Dark) (d) Percentage growth of sucrose concentration.

4.4.6. Effect of sucrose concentration on seed germination percentage

In this present experimental analysis, sucrose concentration was investigated as a third abiotic factor and aimed to evaluate sucrose concentrations ranging from 2.3 to 3.8 % in seed culture of *C. tunicatum*. The highest germination percentage (96%) was achieved with MS medium with 3% sucrose, resulting in healthy and rapid seedling germination (Figure 7d, 8). Sucrose served as the primary carbon source in *in-vitro* culture and was associated with foliar expansion, increased growth, biomass accumulation, and enhanced growth in *Vernonia condensata* (Fortini et al., 2021).

Nonetheless, 3% sucrose was identified as optimal for maximizing shoot length in *in vitro* culture. Similarly, in the micropropagation of *Cannabis*, a 3% sucrose concentration was commonly utilized for caulogenesis and its development (Hesami, Baiton, et al., 2021). For example, a half-strength MS basal medium amended with 3% sucrose demonstrated higher seed germination percentages in *Eustoma grandiflorum* (Roni et al., 2018). Results indicated that *in vitro* seed cultures were optimized with various abiotic factors such as pH, photoperiod, and sucrose concentration.

Figure 8. Effect of basal medium on *in vitro* seed culture with various abiotic factors (pH, photoperiod and sucrose concentration) of *C. tunicatum*

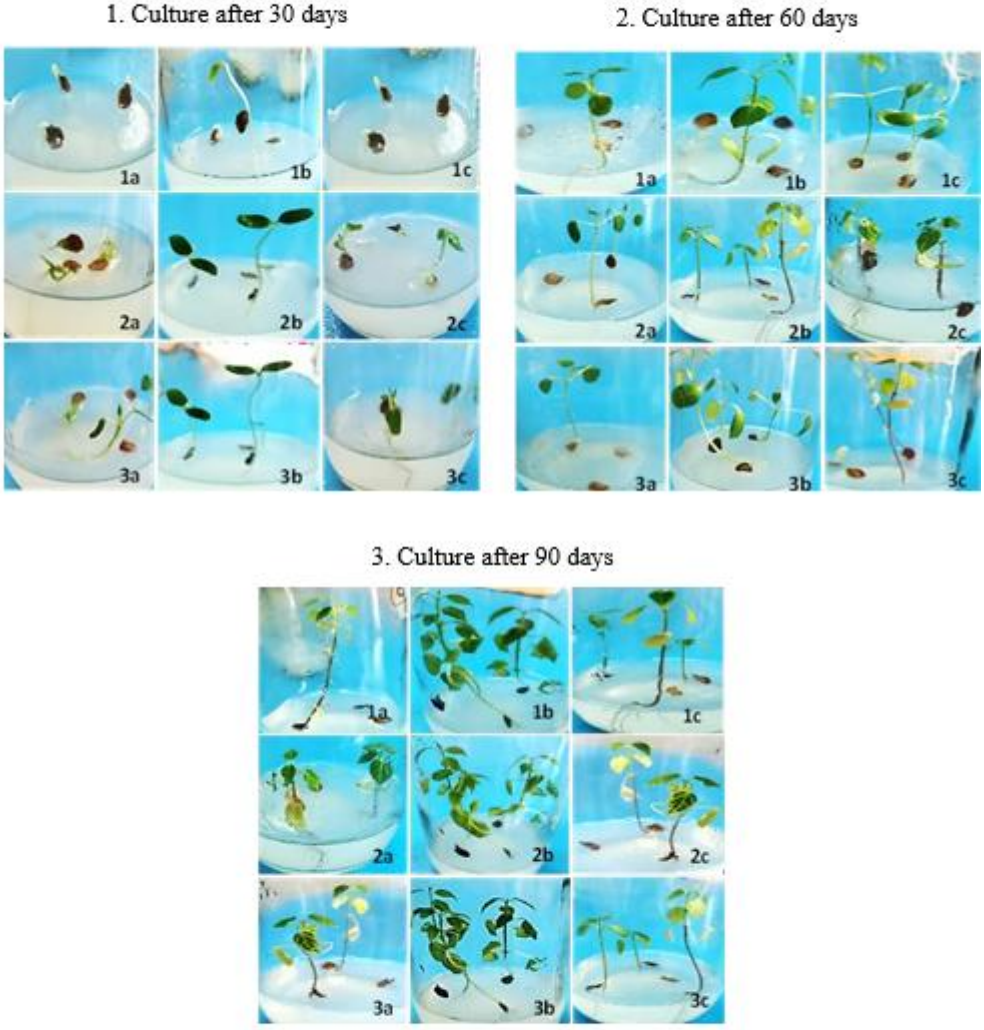

(1a) MS media with pH 5.1; (1b) MS media with pH 5.8; (1c) MS media with pH 6.6; (2a) MS media with photoperiod 9/15hrs (L/D); (2b) MS media with photoperiod 16/8hrs (L/D); (2c) MS media with photoperiod 24/0hrs (L/D); (3a) MS media with sucrose concentration is 2.3%; (3b) MS media with sucrose concentration is 3%; (3c) MS media with sucrose concentration is 3.8%.

4.4.7. A statistical representation of ANOVA

An analysis of variance, lack-of-fit test, and three R^2 statistics was analysed for pH, photoperiod (light and dark), and sucrose concentration. The seed culture of *C. tunicatum* exhibited optimal results under appropriate abiotic conditions. The adjusted R^2 value and predicted R^2 value ranging 0.8737 to 0.8905. The total model effect was highly significant ($p <$ 0.0001), suggesting that inappropriate abiotic factors adversely affected growth. ANOVA revealed significant terms, with p <0.0001, indicating good agreement among these values. The overall model effect was highly significant ($p < 0.0001$), suggesting significant factor effects on pH, photoperiod, and sucrose concentration (Table 2).

Table 2. Percentage of growth in *in-vitro* seed culture of *C. tunicatum*

Source	Sum of Squares	Df	Mean Square	F-value	p-value	
Model	1701.10	2	850.55	52.86	< 0.0001	Significant
A-pH	7.80	1	7.80	0.4848	0.4985	
B-Photoperiod Light	0.0000	0				
C-Photoperiod Dark	0.0000	0				
D-Sucrose Concentration	0.0000	0				
AB	1693.29	1	1693.29	105.24	< 0.0001	Significant
AC	0.0000	0				
AD	0.0000	0				
BC	0.0000	0				
BD	0.0000	0				
CD	0.0000	0				
Residual	209.16	13	16.09			
Cor Total	1910.26	15				

4.4.8. Growth percentage in plots

The percentage of growth was graphed in a Predicted vs. Actual plot (Figure 9a). The perturbation plot indicated that other factors were confounded, with the growth percentage plotted by varying only pH (coded as A) across its range. Design-Expert defaulted to using all

factor midpoints (coded as 0) as the reference point. A factor exhibiting a steep slope or curvature indicated sensitivity of the response to that factor, while a relatively flat line suggested insensitivity to change. The perturbation plot depicts the percentage of growth (Figure 9b).

Figure 9. Optimization of *in vitro* seed culture of *C. tunicatum*

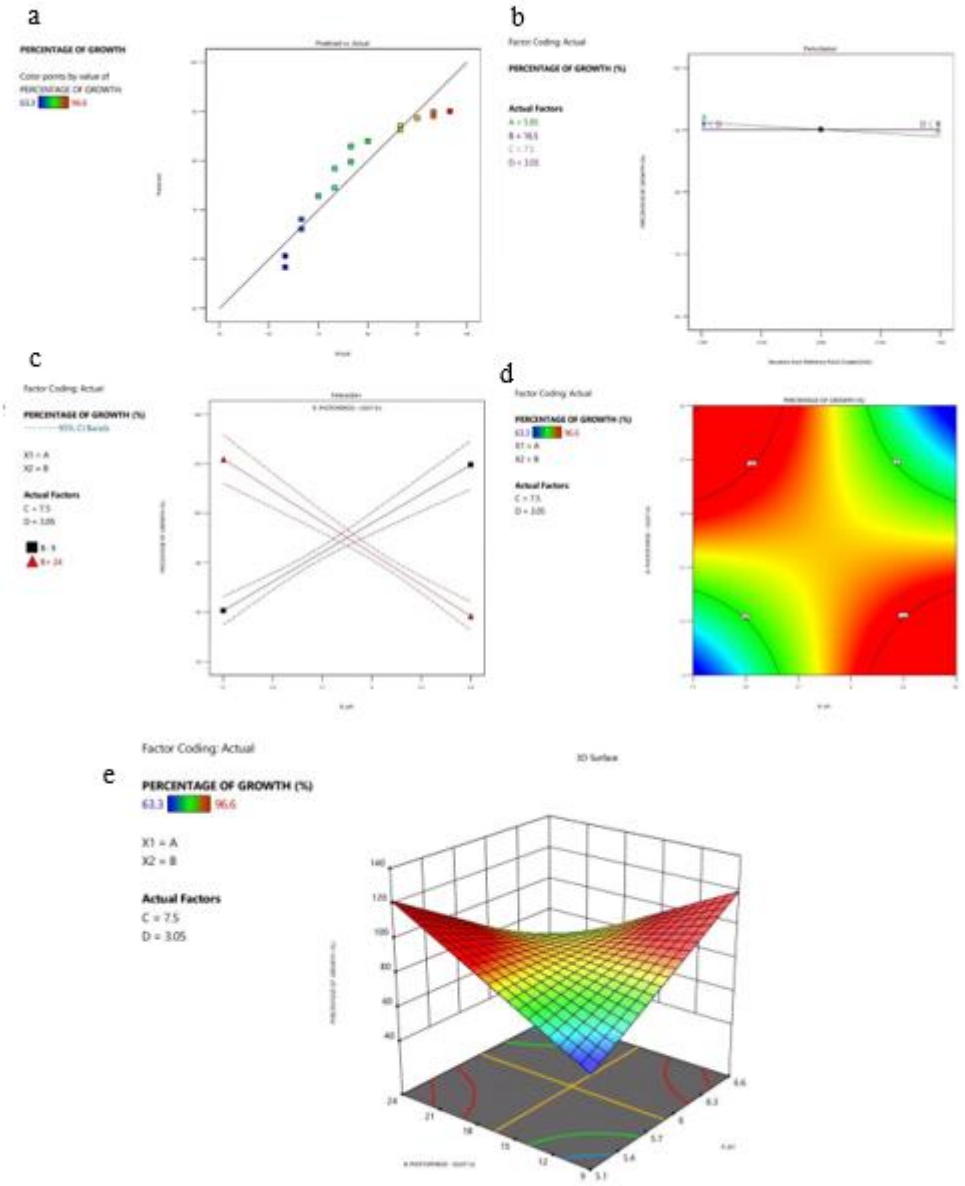

a) Predicted vs Actual plot b) Perturbation c) Interaction d) Percentage of Growth e) Three-Dimensional surface

An interaction was observed when the percentage growth (response) varied with the combined effect of pH, photoperiod, and sucrose concentration (factors). Analysis of other interactions was not possible as the model was aliased (Figure 9c). The contour plot served as a two-dimensional representation of the response (% growth) plotted against a pair of numerical

factors (pH, photoperiod–light, dark, and sucrose concentration). Aliased terms were excluded from this plot (Figure 9d). The three-dimensional response surface plot depicted the relationship between photoperiod and percentage growth for seed germination of *C. tunicatum*. These plots provide a comprehensive view of growth percentage in a three-dimensional context (Figure 9e).

4.4.9. Embryo culture

Mature embryos were carefully removed from seeds of *C. tunicatum* and the explants were treated on MS basal medium without plant growth regulators. *In vitro* embryo culture germinating after a week of inoculation. The *in vitro* zygotic embryos were germinated at 15 days post-inoculation and plantlets were achieved by 50th day which results in 98% of germination rate (Figure 10). There is no callus formation was observed. Embryo culture showed the fastest germination rate and reduced the high risk of contamination compared to seed culture. *In vitro* seed culture and embryo culture was used as an explant for callus induction.

Figure 10. *In vitro* Embryo Culture of *C. tunicatum*

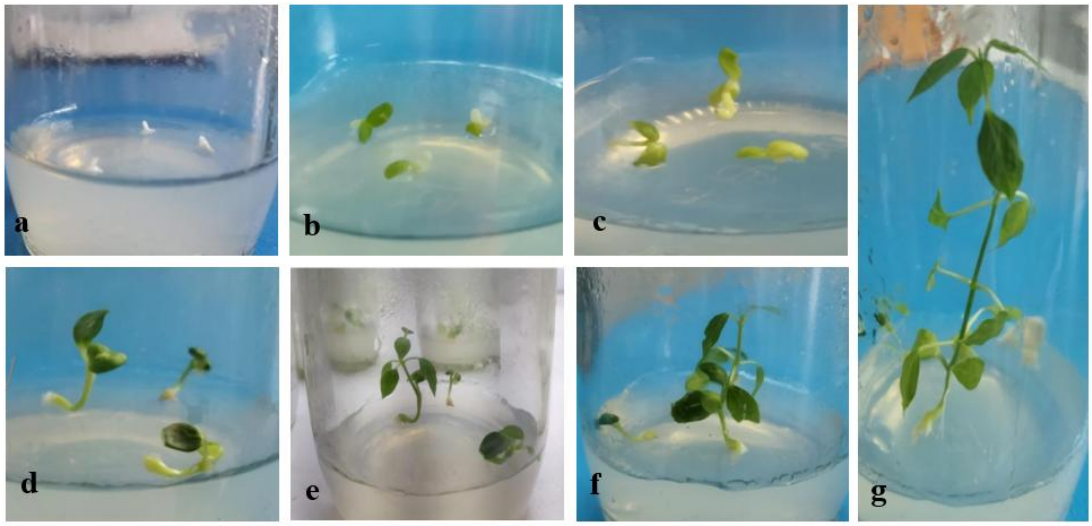

a) On the day of inoculation b, c) 7th day of inoculation d) 14th day of inoculation e) 21st day of inoculation f) 30th day of inoculation g) 45th day of inoculation

4.4.10. Callus Culture in Leaf Explant

A detailed experimental trial was conducted to optimize the callus induction for leaf explant of *C. tunicatum* using different hormonal concentrations and combinations such as 2, 4D, BAP, IAA, IBA and NAA. Healthy leaf explants were obtained from *in vitro* seedlings and explants started producing a mass of cells at the cut edge, after a week of inoculation. The shape of the leaf completely disappeared and formed a white mass of friable calli at 6th week of

culture. The highest percentage was obtained in leaf explant of *C. tunicatum* showed 89% at 2 mg L^{-1} of 2,4 D + 2 mg L^{-1} IAA. The growth rate and percentage response were excellent in the combination of IAA and 2,4 D (Table 3 and Figure 11a).

Table 3. Optimization of callus induction using different PGRs with different explants

MS Medium with PGRs combinations (mg L^{-1})	Explants and callus induction (%)			
	Leaf	Node	Internode	Root
1 2,4 D + 1 IAA	86±2.65^{c}	82.6±1.06^{c}	83±1.83^{c}	82.92±1.45^{cd}
1 2,4 D + 2 IAA	83±1.00^{f}	83.2±2.20^{b}	82±0.34^{d}	83.48±0.91^{c}
2 2,4 D + 1 IAA	87±2.50^{b}	83.2±1.21^{b}	85±0.83^{b}	89.49±1.07^{b}
2 2,4 D + 2 IAA	**89±0.95^{a}**	**85.6±0.68^{a}**	**90±1.00^{a}**	**94.57±1.00^{a}**
1 2,4D + 1 IBA	85±2.20^{d}	74.8±0.72^{gh}	77±4.68^{f}	78.55±3.36^{g}
1 2,4D + 2 IBA	83±1.71^{f}	76.0±1.69^{f}	79±3.86^{e}	80.59±3.95^{e}
2 2,4D + 1 IBA	85±0.98^{d}	74.3±1.29^{gh}	77±6.44^{f}	80.49±4.68^{e}
2 2,4D + 2 IBA	81±1.13^{h}	77.4±1.77^{e}	78±3.65^{ef}	80.12±2.54^{e}
1 IAA + 1 IBA	73±1.45^{m}	76.4±0.50^{f}	74±2.17^{h}	75.00±1.46^{h}
1 IAA + 2 IBA	75±2.50^{l}	77.7±1.17^{e}	78±0.37^{ef}	78.47±0.94^{g}
2 IAA + 1 IBA	73±1.01^{m}	70.4±1.07^{l}	71±2.07^{j}	72.45±2.53^{j}
2 IAA + 2 IBA	76±1.53^{k}	71.7±2.64^{jk}	72±2.22^{i}	73.67±2.43^{i}
1 2,4 D + 1 NAA	77±1.15^{jk}	72.0±3.02^{j}	72±3.32^{i}	73.70±2.55^{i}
1 2,4 D + 2 NAA	78±0.55^{j}	76.8±2.86^{f}	77±0.95^{f}	78.11±1.35^{g}
2 2,4 D + 1 NAA	84±1.10^{e}	73.8±1.63^{i}	77±5.21^{f}	79.92±5.26^{f}
2 2,4 D + 2 NAA	82±0.61^{g}	72.7±2.12^{j}	72±1.73^{i}	79.62±6.17^{f}
1 BAP + 1 2,4 D	69±0.61^{o}	77.8±0.58^{e}	77±0.81^{f}	82.93±4.83^{cd}
1 BAP + 2 2,4 D	67±2.00^{o}	67.4±1.78^{m}	66±1.19^{l}	67.17±0.40^{k}
2 BAP + 1 2,4 D	71±2.58^{n}	64.9±1.27^{n}	66±2.28^{l}	67.25±2.24^{k}
2 BAP + 2 2,4 D	77±1.21^{jk}	67.7±2.08^{m}	68±0.42^{k}	71.81±6.60^{jk}
1 BAP + 1 IAA	80±2.26^{i}	71.9±1.59^{jk}	73±1.14^{hi}	77.90±5.22^{gh}
1 BAP + 2 IAA	81±0.66^{h}	75.9±2.4^{g}	76±0.41^{g}	78.18±3.77^{g}
2 BAP + 1 IAA	83±1.12^{f}	81.9±2.52^{d}	76±2.02^{g}	81.67±3.12^{d}
2 BAP + 2 IAA	81±0.94^{h}	82.8±0.55^{c}	74±1.52^{h}	80.04±4.49^{e}

Values represent mean ± standard deviation of tree replicates per treatment. Means in a column with same letter are significantly ($p \leq 0.05$) difference according to DMRT.

According to Kumar et al. the maximum callus development of leaf explant from *Gerbera jamesonii* achieved in the combination of 2mg L^{-1} 2,4-D and 2 mg L^{-1} Kinetin while BAP induced lowest callus induction (Kumar et al., 2022). The MS basal medium containing 2, 4-D

Figure 11a. Effects of different concentrations of PGRs on callus induction from leaf explant of *C. tunicatum*

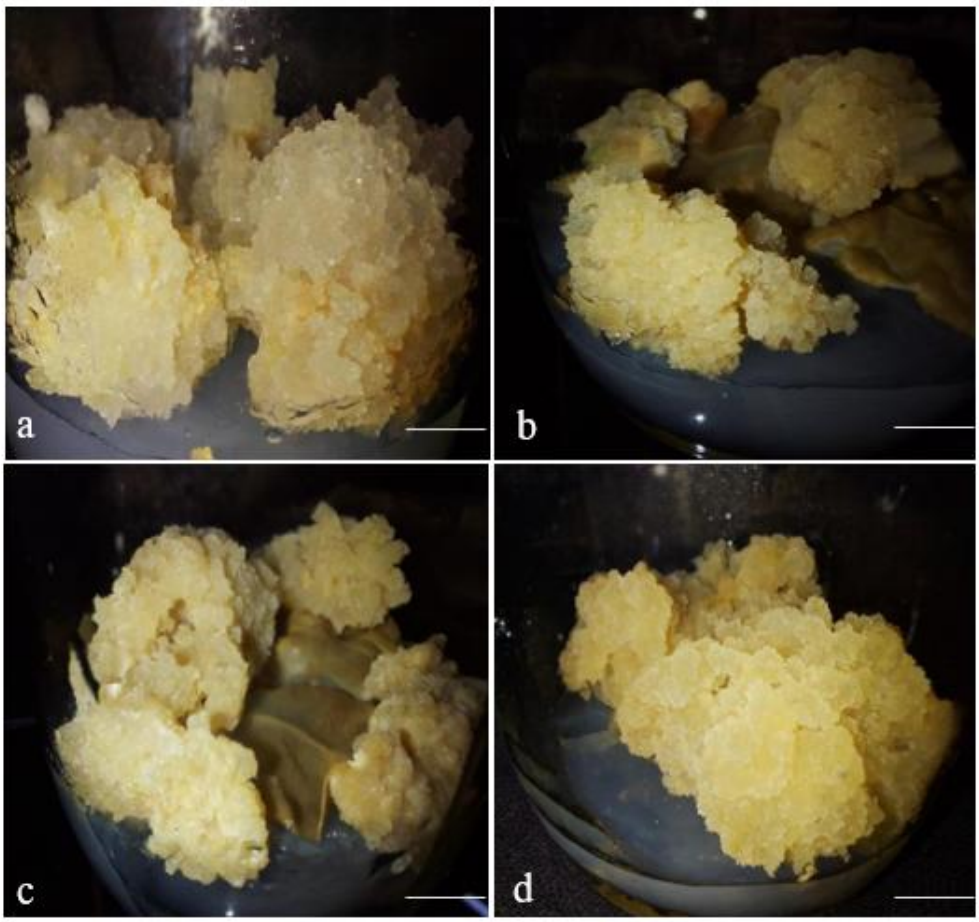

a) Whitish friable callus was observed on 2 mg L^{-1} 2,4 D + 2 mg L^{-1} IAA
b) Yellowish friable callus was observed on 1 mg L^{-1} 2,4D + 1 mg L^{-1} IBA
c) Whitish friable callus was observed on 2 mg L^{-1} 2,4 D + 1 mg L^{-1} NAA
d) Yellowish white friable callus was observed on 2 mg L^{-1} IAA + 2 mg L^{-1} IBA

Photographs were took at 45th day old calli. *Scale bar indicates 0.5 cm

(4.5 mg L^{-1}) was appropriate for callus development from leaf explants of *Dianthus caryophyllus* (Mahood, 2021). Zaman et al., studied various PGRs such as picloram and 2,4-D which leads to form a callus development of leaf explant from *Polyalthiabullata* (Kamarul Zaman et al., 2020).

The highest callogenesis of *Crinum americanum* leaf explant was evaluated from MS medium contained 2,4-D (2.5 mg L^{-1}) and 6-BA (10 mg L^{-1}). The compact and embryogenic calli were obtained (Copeland et al., 2020). The hormonal combination of BAP (2.0 mg L^{-1}) and IBA (0.5 mg L^{-1}) was induced for the highest callus percentage of leaf explant from strawberry (Yeasmin et al., 2022). The maximum callus (94.68%) was noted from leaf explants of *Bacopa monnieri* on MS + 1.5 mg L^{-1} 2,4-D + 0.4 mg L^{-1} Kin (Kumari, 2019). Mwaniki et al. studied *Coffea arabica* leaf explant, in which the maximum callus induction (0.53 + 0.11 µM) was observed on 1/2 MS media with 2,4-D + BAP and its fresh weight 0.97±0.01 g were obtained (Mwaniki et al., 2019).

4.4.11. Callus induction from nodal explant

The nodal explants of *C. tunicatum* which produced both callogenesis and direct organogenesis according to the plant growth regulators. The nodal explant when cultured on MS basal medium enriched various concentrations of cytokinin (BAP) produced multiple shootlets. The explants were inoculated on MS media with PGRs such as IAA, IBA, NAA and 2,4 D, it developed mass of friable callus. The maximum percentage of nodal explant of *C. tunicatum* reached 85 % in the combination of 2,4 D (2.0 mg L^{-1}) + IAA (2.0 mg L^{-1}). The growth rate was successful whereas the percentage response was higher. Overall maximum growth was achieved at IAA + 2,4 D for callus induction (Table 3 and Figure 11b).

Ansari and Vimala studied the different hormones such as 2,4-D, Kn, IAA, IBA, NAA, BAP and concentration ranged from 0 to 4 mg L^{-1} to optimize the induction of callus of *Urena lobata*. The maximum callus was successfully produced at 1 mg L^{-1} 2,4 D + 2 mg L^{-1} Kin + 2.0 mg L^{-1} BAP (Ansari & Vimala, 2022). In *Bougainvillea glabra*, the maximum callus induction (73 %) of nodal explant in MS media supplemented with a combination of 7.5 µM 2,4-D (7.5 µM) + BAP (0.5 µM) (Nasrat et al., 2022). The callus production was observed by Ghazali et al. showed the maximum callus induction (100%) from *Clinacanthus nutans* nodal explant was obtained on MS medium enriched with NAA (1.5 mg L^{-1}) compared to other concentrations and its fresh weight reached 1.470 ± 0.225 gm (Ghazali et al., 2021).

Figure 11b. Effects of different concentrations of PGRs on callus induction from nodal explant of *C. tunicatum*

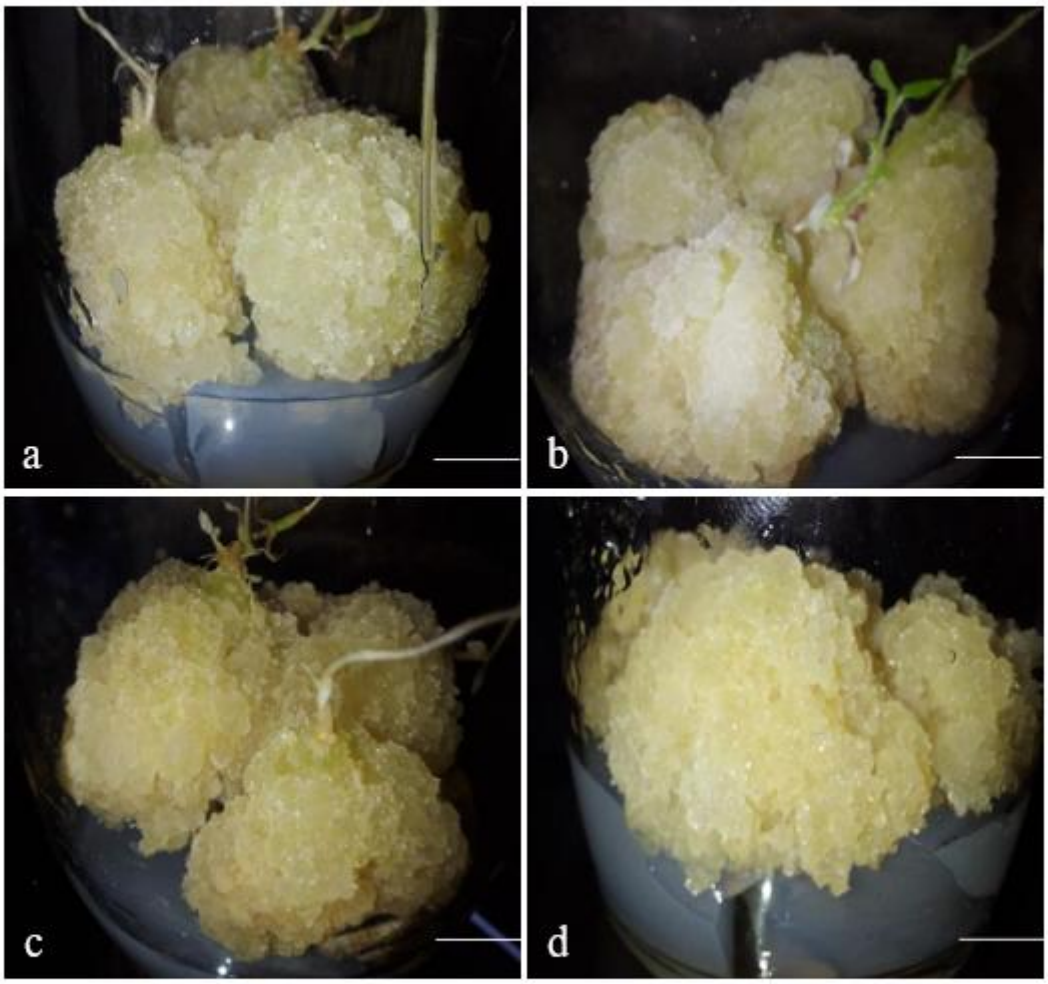

a) Whitish friable callus was observed on 2 mg L^{-1} 2,4 D + 2 mg L^{-1} IAA
b) Yellowish friable callus was observed on 2 mg L^{-1} 2,4D + 2 mg L^{-1} IBA
c) Whitish friable callus was observed on 1 mg L^{-1} 2,4 D + 1 mg L^{-1} IAA
d) Yellowish white friable callus was observed on 1 mg L^{-1} 2,4 D + 2 mg L^{-1} NAA

Photographs were took at 45th day old calli. *Scale bar indicates 0.5 cm

Azman et al. examined the different hormonal combinations of callus induction of nodal explant of *Tacca integrifolia*. The maximum callus was observed on MS basal medium fortified with BAP (1.0 mg L^{-1}) which appeared green and compact calli (Azman et al., 2023). According to Aghbolaghi et al. MS basal medium amended with 3 mg L^{-1} 2,4-D + 0.4 mg L^{-1} BAP evoked the callus proliferation percentage up to 60% from *Stipagrostis pennata* nodal explant (Asadi

Aghbolaghi et al., 2020). The highest callus induction percentage (98.3%) was obtained from nodal explant of *Centratherum punctatum* treated with BAP (4.0 mg L^{-1}) + Kin (3.5 mg L^{-1}) (Talan et al., 2023). In *Mansonia altissima*, the nodal explant showed the maximum intensity of callus (95%) on MS basal medium amended with 4.0 µM IAA + 50.0 mg L^{-1} L-ascorbic acid (Oseni et al., 2022). The hormone 2,4 D stimulated the callus proliferation of *Abies koreana* (Guo & Jeong, 2021). Mahood analysed Kin (0.4 mg L^{-1}) + 2,4 D (2.0 mg L^{-1}) showed maximum callus development from nodal explant of *Dianthus caryophyllus* (Mahood, 2021).

4.4.12. Callus induction from internodal explant

The *in vitro* internodal explants of *C. tunicatum* callus proliferation was obtained on MS medium with IAA (2.0 mg L^{-1}) + 2,4 D (2.0 mg L^{-1}) provoked highest callus induction percentage (90%). The explants were developed into light brown compact calli while MS media fortified with BAP. The color and intensity of the callus varied significantly (Table 3 and Figure 11c).

Kumari et al. induced calli from internodal explants of *Bacopa monnieri* on MS medium amended with 2,4-D (1.5 mg L^{-1}) + Kn (0.4 mg L^{-1}) showed 88.72% (Kumari, 2019). In *Ardisia silvestris,* enriched with 1 mg L^{-1} TDZ revealed the highest callus induction rate from internodal explant of 77.8% (Minh et al., 2021).

The highest callus proliferation was obtained from internodal explant of Desiree and Sarnav varieties of *Solanum tuberosum*. The results revealed that 92% of the Desiree variety and 100% of the Sarnav variety at NAA (1 mg L^{-1}) + BAP (1.5 mg L^{-1}) (Babadjanova et al., 2024). Kulus & Tymoszuk observed the highest dry weight (30.8%) in the calli derived from the internodal explant of *Lamprocapnos spectabilis* (Kulus & Tymoszuk, 2020). The friable calli was obtained from the internodal explants of *Ruta graveolens*, in the hormonal combinations of 2,4 D (1.5 mg L^{-1}) + NAA (1.5 mg L^{-1}) achieved 90 % when compared to other combinations (Hussain & Nathar, 2020). The successive induction of calli from internodal explants (85.4%) on MS basal medium enriched with 2,4 -D (2.5 mg L^{-1}) + BAP (0.5 mg L^{-1}) in *Withania coagulans* (Mirjalili & Esmaeili, 2022).

Hadi et al. reported the efficient protocol for callus proliferation of internodal explants of *Stachys schtschegleevii.* The maximum callus frequency (<70%) was obtained on MS basal medium with TDZ (0.3 mg L^{-1}) and 2,4-D (0.7 mg L^{-1}) (Hadi et al., 2023). The highest callus development was acquired on 0.1 mg L^{-1} BAP + 1.0 mg L^{-1} NAA from internodal explant of *Artemisia ludoviciana* (Sánchez-Ramos et al., 2022). Al-Saedi and Abdulhalem experimented

Figure 11c. Effects of different concentrations of PGRs on callus induction from internodal explant of *C. tunicatum*

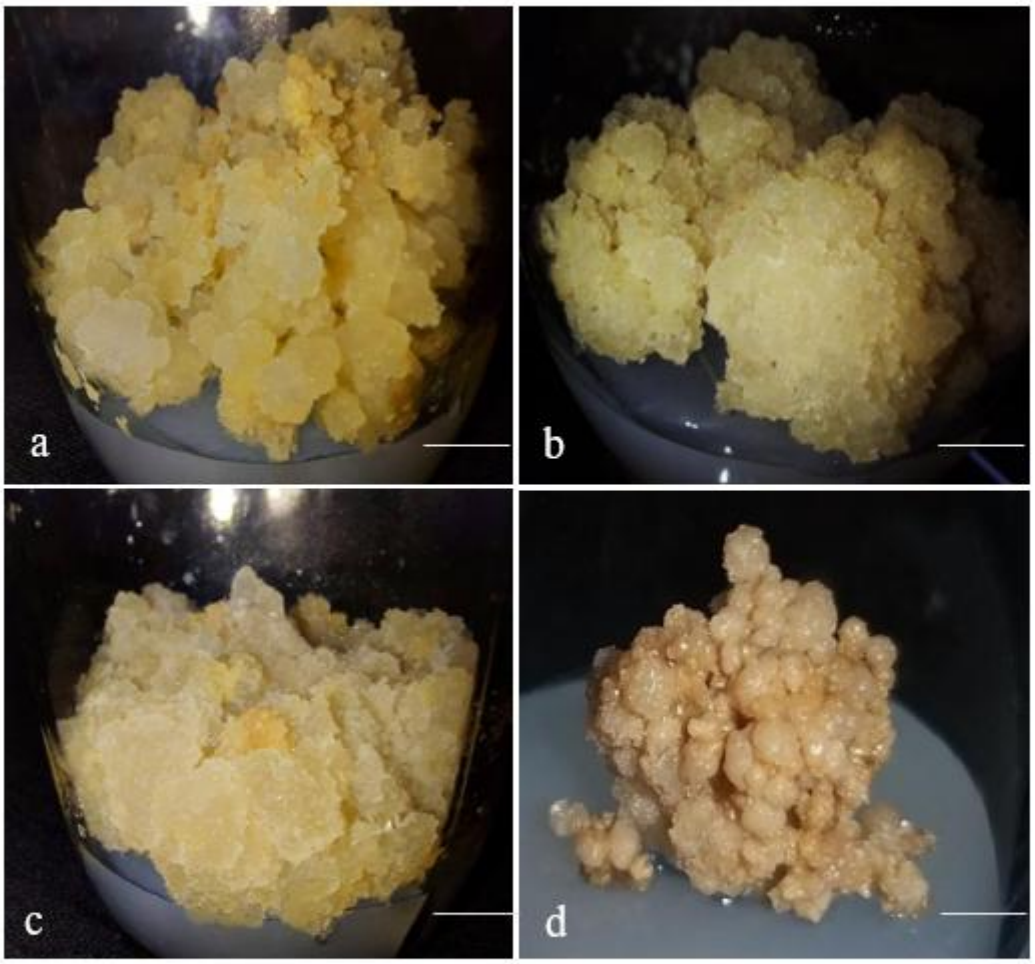

a) Whitish friable callus was observed on 2 mg L^{-1} 2,4 D + 2 mg L^{-1} IAA
b) Yellowish friable callus was observed on 2 mg L^{-1} 2,4D + 2 mg L^{-1} IBA
c) Whitish friable callus was observed on 1 mg L^{-1} IAA + 2 mg L^{-1} IBA
d) Brownish compact callus was observed on 2 mg L^{-1} BAP + 1 mg L^{-1} IAA
Photographs were took at 45th day old calli. *Scale bar indicates 0.5 cm

with maximum callus initiation (50%) on MS basal medium complemented with BAP (5 mg L^{-1}) in internodal explant of *Phaseolus vulgaris* (Al-Saedi & Abdulhalem, 2020). The optimal treatments of internodal explant of *Melastoma malabathricum* for callus formation were obtained in TDZ (0.1 mg L^{-1}), TDZ (1 mg L^{-1}), NAA (0.1 mg L^{-1}), and NAA (1 mg L^{-1}) and a combination of TDZ (0.1 mg L^{-1}) and NAA (0.1 mg L^{-1}) (Karimah et al., 2020). The internodal explants of *Rhodiola dumulosa,* the maximum callus proliferation has reached 90.03% at the concentration of BAP (0.85 mg L^{-1}), NAA (0.34 mg L^{-1}), and 2,4-D (0.33 mg L^{-1}) (Lu et al.,

2023). The maximum callus initiation (88.0 %) was achieved on MS medium fortified with IBA (1.5 mg L^{-1}) + BAP (4 mg L^{-1}) from internodal explant of *Ficus carica* (Shallal et al., 2021).

4.4.13. Callus induction from root explant

The optimized protocol for the *in vitro* callus development of root explants from *C. tunicatum*. Compared to all explants, root explants showed maximum percentage of callus formation. In the second week of inoculation, explants started to produce an undifferentiated mass of cells. Explants were sub cultured at regular intervals of every three weeks. Results revealed successful cell proliferation and callus initiation. The highest callus percentage (94%) was observed in combination of 2,4 D (2.0 mg L^{-1}) + IAA (2.0 mg L^{-1}) followed by 2,4 D (2.0 mg L^{-1}) + IAA (1.0 mg L^{-1}) achieved 89.43 %. Explants produced both friable and compact calli depending on plant growth regulators (Table 3 and Figure 11d).

Dar et al. studied the callus development from *Atropa acuminata* (root explant). The maximum callus percentage (100%) was observed on MS media amended with BAP (0.5 mg L^{-1}) + NAA (1.0 mg L^{-1}) (Dar et al., 2021). In root explant of *Euphorbia peplus,* the maximum callus induction (100%) was observed at BAP (2 mg L^{-1}) and 2,4 D (0.5 mg L^{-1}) (Mousa, 2023). In addition to that, Zuhra et al. observed the maximum callus induction (80%) on MS media supplemented with IAA (1.0 µM) + BAP (5.0 µM) from root explant of *Podophyllum hexandrum* (Zuhra et al., 2021). Martinez et al. stated that 100% callus induction from root and hypocotyl explants of *Taraxacum officinale* on MS basal medium with NAA (0.5 mg L^{-1}) and BAP (0.5 mg L^{-1}) (Martinez et al., 2021). The maximum callus induction percentage (100%) was achieved on MS basal medium supplemented with PIC (2.0 mg L^{-1}), Kin (1.5 mg L^{-1}) and NAA (0.1 mg L^{-1}) from *Agapanthus praecox* (Tang et al., 2022). Tandon et al. observed the white compact calli in the combinations of 2,4-D (2.0 mg L^{-1}), IAA (0.2 mg L^{-1}) + BAP (2.0 mg L^{-1}) from *Mucuna pruriens* (Tandon et al., 2021).

Figure 11d. Effects of different concentrations of PGRs on callus induction from root explant of *C. tunicatum*

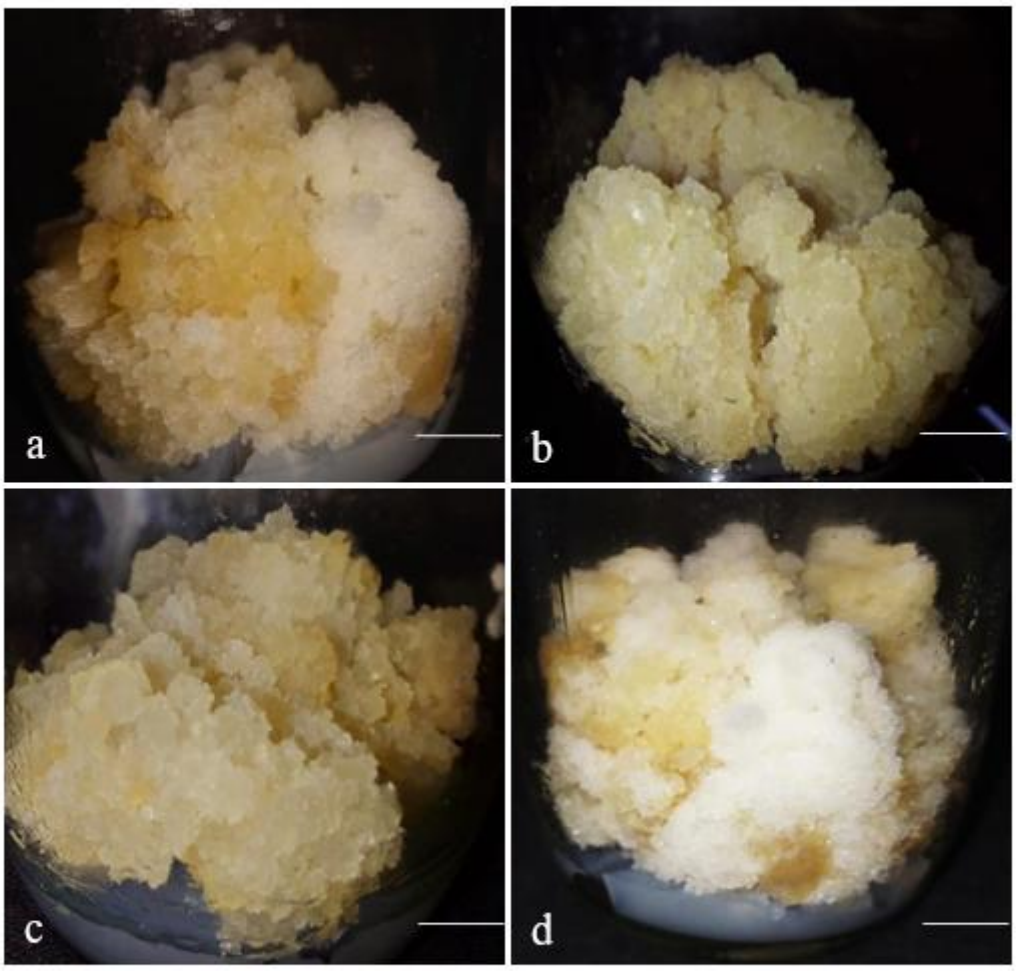

a) Yellowish white friable callus was observed on 2 mg L^{-1} 2,4 D + 2 mg L^{-1} IAA
b) Creamy friable callus was observed on 1 mg L^{-1} 2,4D + 2 mg L^{-1} IBA
c) Creamy friable callus was observed on 2 mg L^{-1} 2,4 D + 1 mg L^{-1} NAA
d) Brownish compact callus was observed on 2 mg L^{-1} 2,4 D + 1 mg L^{-1} IAA

Photographs were took at 45th day old calli. *Scale bar indicates 0.5 cm

4.4.14. Effect of cultural medium and PGRs on callus induction

Different cultural media like MS basal medium, Gamborg B5 medium, and Nitsch medium have been used, in which MS media is one of the most successful and widely used (Bhowmik et al., 2020; Indarwati et al., 2021; Widayat et al., 2020). The success of cell, tissue, or organ culture greatly depends on the choice of nutrients and PGRs. It played a great role in regulating the biological pathways and physiological pathways. It can greatly enhance the

efficiency of callogenesis and organogenesis in plant tissue culture (Basiri et al., 2022). Usually, auxin enhanced the development of callus (Krishnan et al., 2019; Rathore et al., 2020). Kilic & Onus proved that callus cannot be generated without the presence of growth hormone (Kilic & Onus, 2023). Callus formation results from cellular and tissue reprogramming, overcoming differentiation constraints like hormone gradients and chromatin regulation. It qualifies as dedifferentiated tissue within the plant-specific definition (Fehér, 2019).

Two different kinds of calli were observed when treated with different PGRs. Friable calli was formed when the medium was amended with the various combinations and combinations of IAA, NAA and 2,4 D in all explants of *C. tunicatum*. It was soft, friable in nature, and creamy white in color. The rigid and compact calli were observed when fortified with different concentration of BAP with NAA and IAA. These two different kinds of calli were morphologically different. Following our findings, Hesami et al. reported the two types of calli, namely Friable calli (FC) and Compact calli (CC) in *Ficus religiosa* of different explants such as leaf, internode, petiole, and root. Both the calli from the same explants are also achievable and these variations may be influenced by genetic, epigenetic, and culturing alterations (Hesami et al., 2018).

Our study corroborates the findings of Carsono and Yoshida; Benderradji et al. reported that the intensity of callogenesis differs from the different explants (Benderradji et al., 2012; Carsono & Yoshida, 2006). As PGRs were one of the most important factors in regulating mechanisms, leading to the formation of FC and CC. FC was beneficial for mass multiplication rather than CC. On the other hand, CC has more potential for regeneration (Martinez et al., 2021; Small & Degenhardt, 2018). CC was observed when a medium was supplemented with cytokinin, especially BAP for all the explants. Similar to our findings, fundamental PGRs like auxin play a major role in cell multiplication and cell elongation in callus culture. And also, the combination of auxin and cytokinin could enhance the proliferation of callus significantly (Al-Hussaini et al., 2015). In addition to that Tripathi et al. gave conformity to our results that 6-BA either combined with 2,4 D or alone acquired 100% somatic embryo initiation (Tripathi et al., 2021).

4.4.15. Direct organogenesis

The efficient protocol was established for direct *in vitro* organogenesis has been established from the nodal explant of *C. tunicatum.* Nodal explants were inoculated on MS media supplemented with 1 mg L^{-1} BAP and 1.5 mg L^{-1} 2,4 D (Figure 12). The explants were

proliferated into adventitious shoots when treated with IBA (2 mg L^{-1}) for root initiation of *C. tunicatum.*

Figure 12. Direct organogenesis from nodal explant of *C. tunicatum*

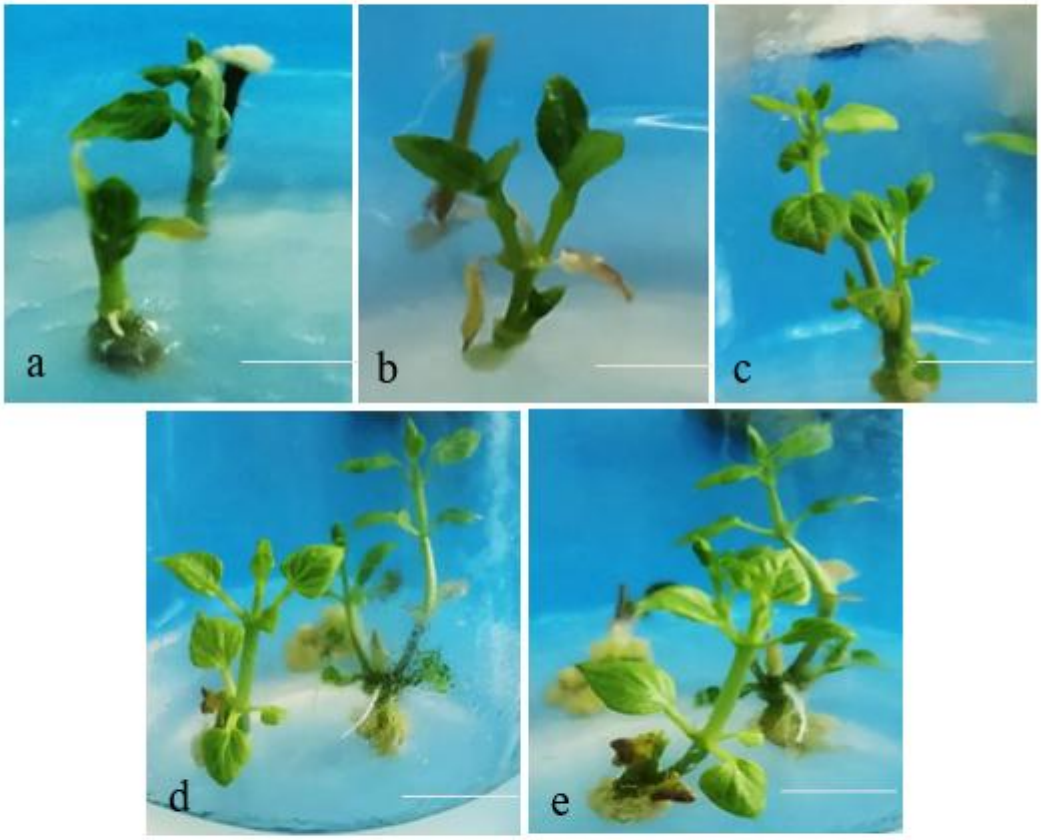

a) 7th day of inoculation b) 14th day of inoculation
b) 21st day of inoculation d) 25th day of inoculation
c) 30th day of inoculation
*Scale bar indicates 1 cm

The maximum shoots were obtained at BAP (2.0 mg L^{-1}) and TDZ (1.0 mg L^{-1}) using nodal explants from *Coscinium fenestratum* for direct organogenesis (Karthika, 2019). In *Coccinia cordifolia,* direct organogenesis from the internodal explant possessed the highest regeneration at BAP (1.5 mg L^{-1}) + NAA (0.1 mg L^{-1}) (Sarkar & Alam, 2022). Khan et al. studied the highest shoot bud formation from nodal explant of grapes at half MS basal media supplemented with BAP (2.0 mg L^{-1}) + GA_3 (0.5 mg L^{-1}) (Khan et al., 2015). Furthermore, cytokinin (BAP) induces cell division, helps to overcome apical dominance (Erfani et al., 2017;

Fallahpour et al., 2015; Miri & Roughani, 2018; Seran, 2013). The growth phases of the explant play a crucial role in the regeneration process (Xu, 2018).

Bansal et al. studied that nodal explants have a great potential for single and multiple shoot regeneration. MS basal medium fortified with cytokinin (Kin and 2-iP) proved to be highly effective for shoot regeneration (12.14 ± 1.58) and auxins IBA and IAA achieved 100% root induction. The nodal explants of *Lycium barbarum* showed the maximum shoots (23.33 ± 1.86) were observed when MS basal medium enriched with BAP (0.5 mg L^{-1}) (Karakas, 2020). Janarthanam and Sumathi optimized a method for the direct organogenesis from nodal explant of *Coleus forskohlii.* The MS medium fortified with 4.44 µM BAP induced the maximum shoots (24.3 ± 0.2). Shoots were then transferred into rooting media supplied with 2.46 µM IBA observed 7.8 ± 0.6 roots. *In vitro* grown developed plants were moved to hardening and it achieved 90% survival rate (Janarthanam & Sumathi, 2020).

4.4.16. Indirect Organogenesis

4.4.16.1. Somatic embryogenesis

The root-derived callus was cultured on MS medium augmented with BAP (1.0 mg L^{-1}) and 2,4-D (1.5 mg L^{-1}) (Figure 13a). Globular and heart-shaped calli were observed at 40th day. The totipotent tissue was generated and again sub-cultured on MS media containing 1.5 mg L^{-1} 2,4-D and 1.5 mg L^{-1} BAP as represented in (Figure 13b). The embryonic calli were transferred into MS medium supplemented with 1.5 mg L^{-1} 2,4-D and 1 mg L^{-1} TDZ after 70th day of inoculation. The cotyledonary embryos were developed gradually after the three months of embryogenic calli (Figure 13c, d). The callus was differentiated into axillary buds which become visible to the naked eye. Similar to our study, root-derived calli of *Vitis vinifera are* used for the process of somatic embryogenesis and organogenesis (Pathirana & Carimi, 2023).

The callus derived from internodal explants of *Scaevola sericea* showed the globular and heart-shaped embryos (Liang et al., 2020). In *Lycium barbarum,* MS medium without PGRs induced globular, heart, torpedo, cotyledon, and further development of plantlets (Khatri & Joshee, 2024). Subiramani et al. studied that the embryonic calli were obtained from MS basal medium fortified with 2,4-D (1.5 mg L^{-1}) and BAP (1 mg L^{-1}) in *Gloriosa superba* (Subiramani et al., 2019). Stress factors influenced the process of somatic embryogenesis significantly in *Picea Mongolica* (Wang et al., 2023).

Figure 13. Embryogenesis from root-derived calli of *C. tunicatum*

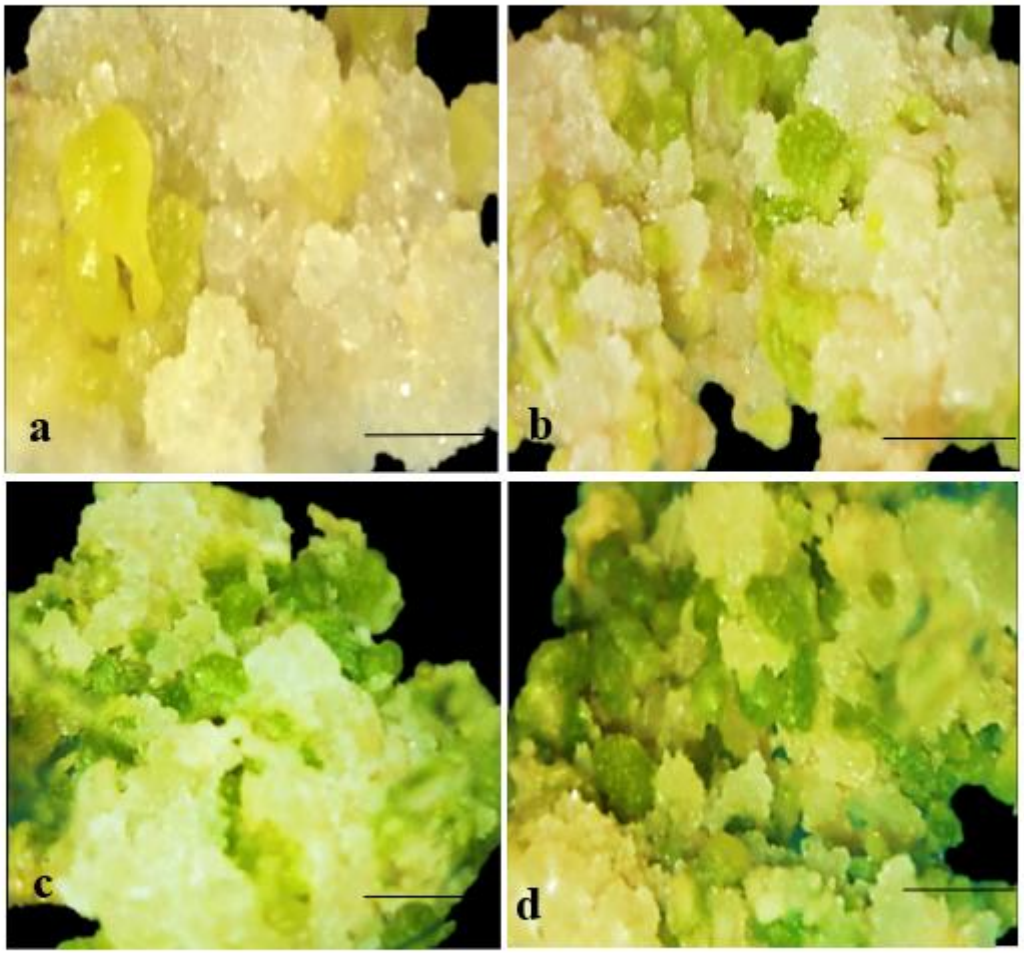

a, b) Globular calli was observed at 40th day of inoculation
c, d) Cotyledonary embryos were developed on 90th day

* Scale bar indicates 0.5 cm

4.4.16.2. Shoot Proliferation

Shoot proliferation was obtained on MS basal medium rejuvenated with different combinations of plant growth regulators such as BAP, TDZ, NAA and IBA. Shootlets were initiated from the calli represented in Figure 14a, b. The maximum shoots were proliferated (93.3%) at the concentration of 2 mg L^{-1} of BAP and 1 mg L^{-1} TDZ (Figure 14c and Table 4). The combination of 2 mg L^{-1} NAA + 1 mg L^{-1} BAP produced the least proliferation rate of 24.3% of *C. tunicatum*. According to Chen et al. effective adventitious shoots of *Chirita swinglei* reached 92.2% were formed on MS media fortified with NAA, BAP, and

Figure 14. Organogenesis from root-derived calli of *C. tunicatum*

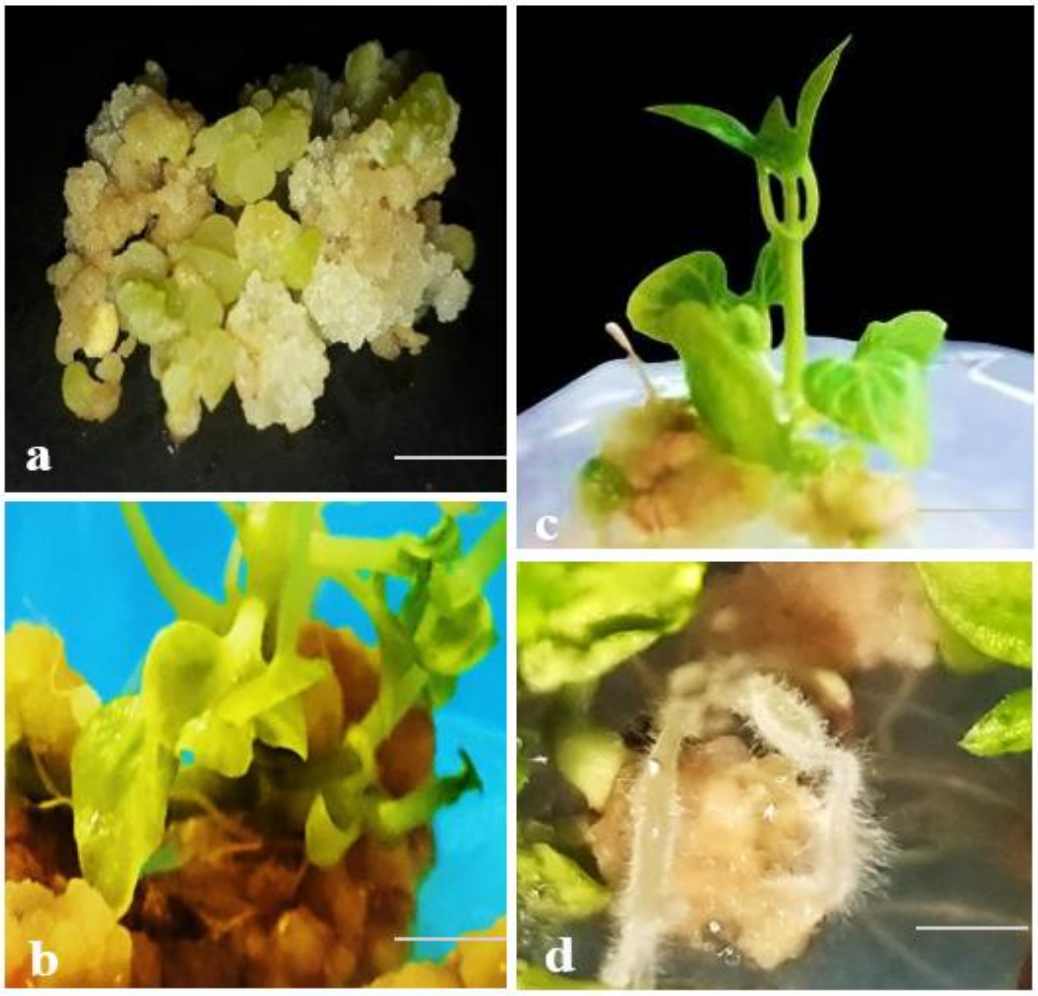

a, b) Callus modified into shoots
c) *In vitro* shoot regeneration on 2 mg L^{-1} BAP and 1 mg L^{-1} TDZ
d) *In vitro* root regeneration on 2.0 mg L^{-1}IBA
* 'a, b, d' Scale bar indicates 0.5 cm and 'c' indicates 1 cm

TDZ (Chen et al., 2016). Similarly, supplementation of 2.0 mg L^{-1} TDZ and 0.1 mg L^{-1} NAA to MS medium increased the regeneration frequency of 93.5% in *Nematanthus wettsteinii* (He et al., 2023). The highest number of micro tubers were obtained in *Gloriosa superba* when the fortification of TDZ (1.5 mg L^{-1}) (Subiramani et al., 2019). Lu et al. studied the adventitious buds were proliferated (40%) in *Rhodiola dumulosa* with MS medium enriched with BAP (1.0 mg L^{-1}) + NAA (0.5 mg L^{-1}) (Lu et al., 2023). Ranjan et al. studied that MS media supplemented with 1.0 mg L^{-1} BAP+ 0.5 mg L^{-1} NAA showed good results for shoot multiplication from the callus of leaf and nodal explant from *Bacopa monnieri* (Ranjan et al., 2018).

4.4.16.3. Root Proliferation

Multiple shoots were regenerated and mature shoots were transferred into rooting media with various concentrations of various growth hormones such as 2,4-D, IBA, BAP, TDZ, and their combinations. MS medium amended with IBA (2.0 mg L^{-1}) evoked a high efficiency of root formation (97.6 %) on MS medium after 85 days (Figure 14d and Table 4). In *Rhodiola dumulosa,* IBA (1.0 mg L^{-1}) induced maximum root induction of 10 to 15 roots per explant (Lu et al., 2023).

Table 4. Optimization of *in vitro* indirect regeneration of *C. tunicatum*

MS Medium with PGRs combinations (mg L^{-1})	*In vitro* regeneration (%)	
	Shoot	**Root**
C	-	-
1 NAA + 2 BAP	-	24.6 ± 1.5^{gh}
2 NAA + 1 BAP	24.3 ± 1.1^{f}	29.3 ± 0.5^{g}
1 NAA + 2 TDZ	52.6 ± 1.5^{d}	45.6 ± 1.1^{f}
2 NAA + 1 TDZ	63.6 ± 1.1^{c}	58.6 ± 1.1^{d}
1 BAP + 2 TDZ	89.6 ± 0.5^{b}	55 ± 2.6^{e}
2 BAP + 1 TDZ	**93.3 ± 0.5^{a}**	44.33 ± 1.5^{f}
1 IBA	24.6 ± 0.5^{f}	85.33 ± 1.1^{c}
1.5 IBA	26.6 ± 0.5^{f}	93.66 ± 1.1^{b}
2 IBA	30 ± 1^{e}	**97.66 ± 0.5^{a}**

Values represent mean ± standard deviation of tree replicates per treatment. Means in a column with same letter are significantly ($p \leq 0.05$) difference according to DMRT.

4.4.16.4. Acclimatization

The *in vitro* shoots and roots were detached from MS basal medium and gently washed with tap water to remove gelled agar. *In vitro* plantlets were transferred to hyco-pots containing vermiculite and organic manure in the ratio of 3:1 (v/v) and maintained in a greenhouse for 15 - 25 days. Then plants were transported into mud pots and 100% (after 6 weeks) survival rates of *C. tunicatum* were recorded (Figure 15). Nowakowska et al. described the rooted *in vitro* plantlets of *Helianthus verticillatus* were transferred into a soilless mixture and maintained in the greenhouse in which 96% survival rate was determined (Nowakowska et al., 2024). Okello et al. studied the survival rate of 95.7% of *in vitro* regenerated plantlets of *Aspilia africana* after

seven weeks of acclimatization (Okello et al., 2021). Galán-Ávila et al. evaluated the 100% acclimatization of *Cannabis sativa* plantlets from *in vitro* regeneration (Galán-Ávila et al., 2020).

Figure 15. Acclimatized a month-old plantlet of *C. tunicatum*

In *Aronia melanocarpa,* healthy plantlets were carefully removed and placed in the fertilizer-free peat and perlite mixture (1:10, v/v) of paper pots. The transparent lid of the culture vessel was fully covered fully for almost 10 days, and then the lid was partially opened to regulate humidity level for further hardening. All plantlets were then transferred to pots of relatively low humidity in a growth chamber with 15−25% (Bayhan & Yücesan, 2024). *In vitro* plantlets of *Pinus peuce* derived from IBA showed the highest acclimatization percentage than plants treated with NAA (Stojičić et al., 2024). The acclimatization of *in vitro* plants of Chickpea was transferred into a mixture of soil rite and agro peat and maintained in a culture room. All the hardened plants were then shifted into earthen pots with sterile soil and aloe to

grow in a greenhouse. The matured plantlets were observed after 30 -32 weeks and it was phenotypically normal and healthy (Jangid et al., 2024). In *Lycium barbarum,* well-developed plantlets were transferred to controlled climatic conditions. There are no morphological abnormalities were observed in regenerated plants, showing 100% success in acclimatization (Khatri & Joshee, 2024). *In vitro* plantlets successfully adapted to the natural climate during the process of acclimatization in *Rubia cordifolia* (Bansal et al., 2024).

For acclimatization of *Rhodiola imbricata,* well-rooted *in vitro* shoots were shifted into pots which comprising autoclaved soil: perlite: vermiculite (1:1:1, v/v/v). After hardening, 85% of plantlets survived and then moved to the greenhouse. Transferred plantlets showed a 100% survival rate (Dolker et al., 2024). In *Aspilia Africana,* plantlets were detached from *in vitro* culture bottles and washed thoroughly to remove the medium. It was maintained in hyco-pots containing sterile soil and perlite (2:1, v/v). It was enclosed with polythene bags with sufficient humidity and kept in the greenhouse. After acclimatizing the *in vitro* plants for 7 weeks the survival rate was observed as 95.7% (Okello et al., 2021).

4.4.17. Histological analysis

Thin section of non-embryogenic and embryogenic calli were taken for determining the characteristic features of the cells with the help of microtome and optical microscope. The anatomical study proved the dynamics of each stage of initiation and growth of organogenesis through somatic embryogenesis of *C. tunicatum*.

The non-embryogenic calli were observed as irregular and loosely packed parenchymatous cells. The intercellular space of the cells was visible under the optimal microscope. The meristematic multicellular cells were formed in the isodiametric-shaped and it was arranged compactly in an organized manner (Figure 16a, b). Somatic embryos are typically characterized by dense cytoplasm, abundant starch grains, and the presence of latex canals, as illustrated in Figure 16c, d. The development of somatic embryos encompassed different stages such as globular stages, heart-shaped and torpedo stage. The globular embryo with small cells rich in cytoplasm, protoderm, procambium and suspensor was detected (Figure 16e, f, g). The suspensor cells further divided into form heart shaped embryo (Figure 16h) significantly the heart shaped embryo gave rise to leaf primordia was shown in Figure 16i. Leaf primordia with intensive cell divisions, it forms epidermal layer with columnar shaped after a successful anticlinal division. It has prominent adaxial and abaxial epidermis, stomata, palisade cells, spongy cells, and formation of vascular tissues were observed in the leaf primordial stage

(Figure 16j, k). The formation of root portion was differentiated into medulla, chlorenchymatous cells, parenchymatous cells, developing vascular bundle and root hairs was shown in Figure 16l.

Figure 16. Histology of Callogenesis and Organogenesis of *C. tunicatum*

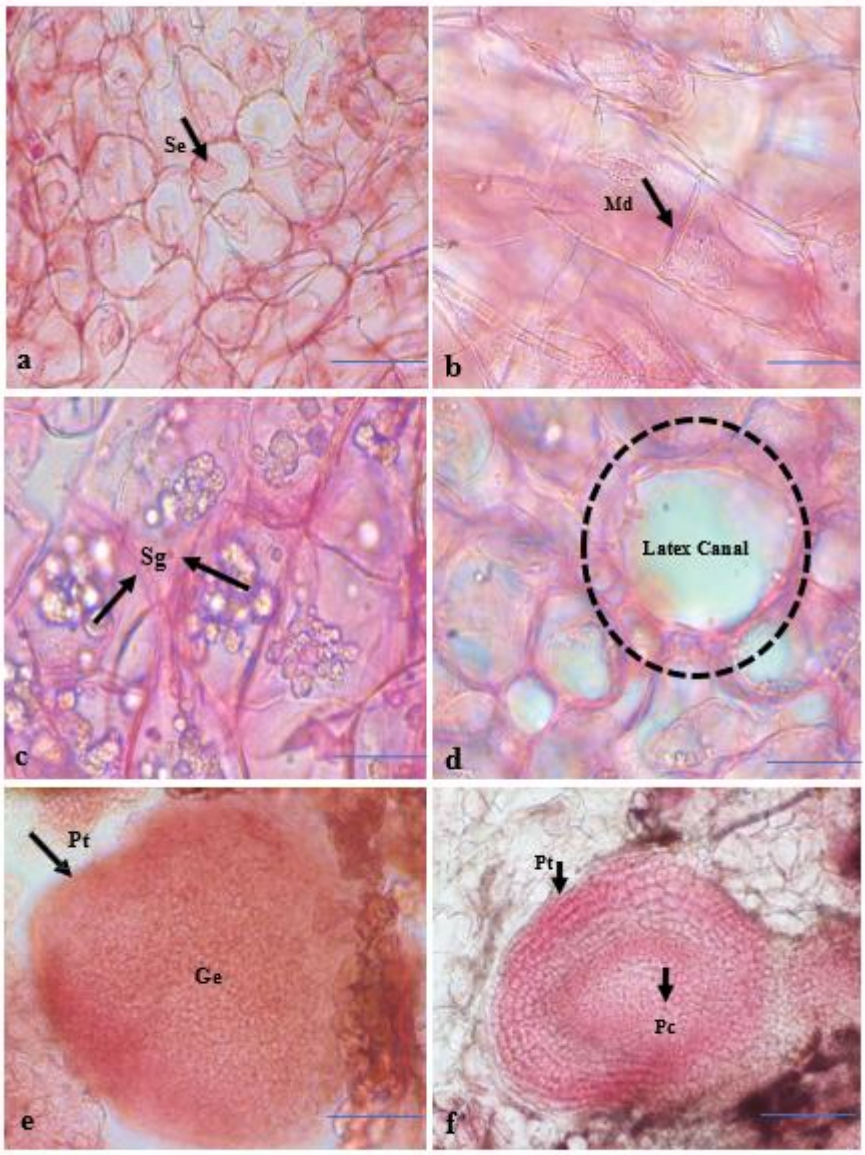

a) Somatic embryogenesis (Se) b) cell elongation and division, *arrow* indicates mitotic division (Md) c) embryonic cells with starch granules (Sg) d) Latex Canal e) formation of the protoderm (Pt) in globular embryo (Ge) at 45th day f) *Arrow* indicates the development of procambial cells (Pc)

In *Asparagus cochinchinensis,* newly formed cells were observed which consist of small, compact cells with dense cytoplasm. It contained highly vacuolated thin-walled spherical parenchyma cells with numerous starch granules. In initial stage, protruding shoots was observed under an optical microscope. Well-developed shoot buds showed the crystal idioblasts randomly

distributed in leaf primordia. The development of pre-vascular tissues was visible, xylem and phloem cells were formed in the vascular bundles. Similarly, the stomatal pores and protective spines were detected in the histological analysis (Kim et al., 2021).

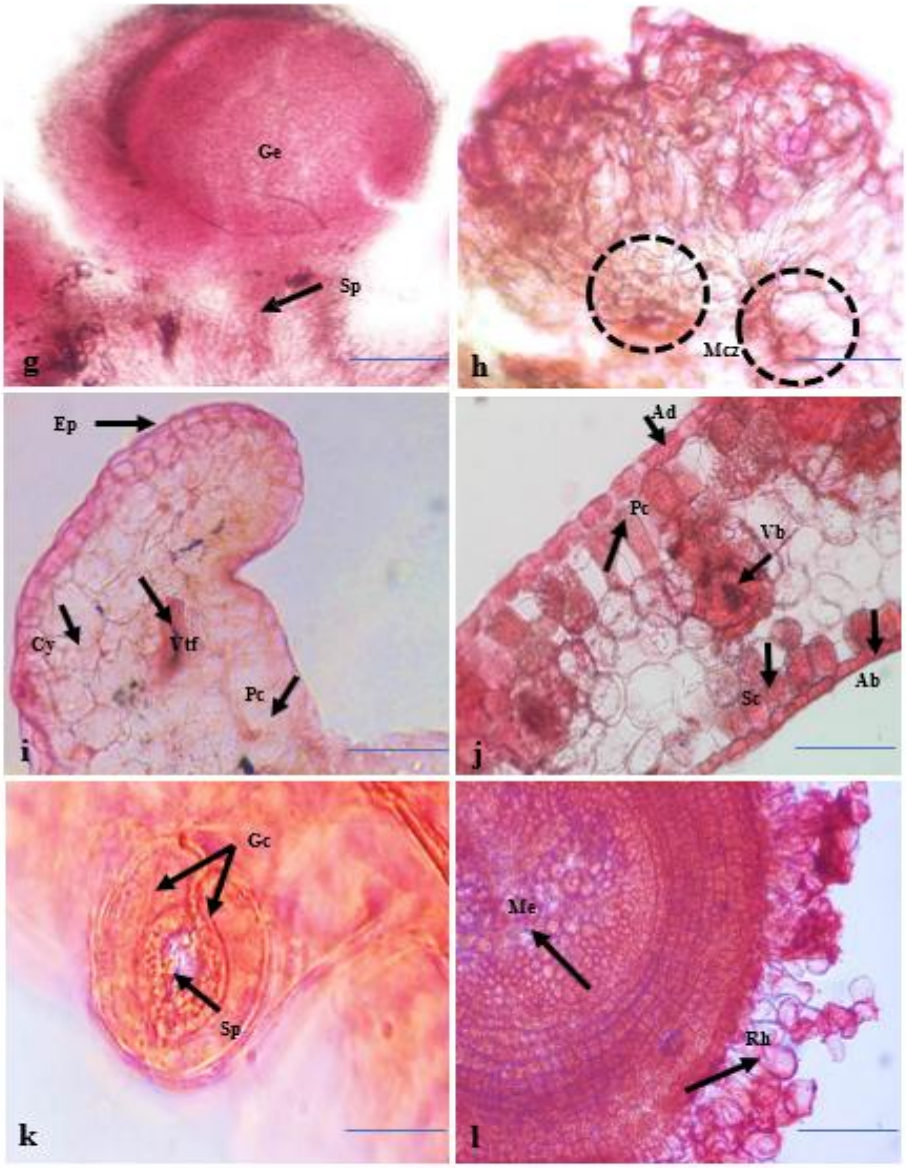

g) Arrow indicates the suspensor h) dotted circle indicates the Meristematic cell zone (Mcz) i) leaf primordia at 70th day, *arrow* indicates Epidermis (Ep), Cytoplasm (Cy), Palisade cells (Pc), Vascular tissue formation (Vtf) j) Formation of leaf, *arrow* indicates Adaxial Epidermis (Ad), Palisade cells (Pc), Developing Vascular Bundle (Vb), Spongy Cells (Sc), Abaxial Epidermis (Ab) k) Stomatal cells, arrow indicates Guard cell (Gc), Stomatal pore (Sp) l) Root formation, *arrow* indicates Medulla- Me (Pith), Root hairs (Rh).

*a, b, c, d, k - scale bar indicates 100 µm. *e, f, g, h, i, j, l - scale bar indicates 200 µm

Chen et al. observed globular embryo were developed on the leaf surface from primordial cells of *Chirita swinglei* (Chen et al., 2016). The detailed histological study revealed the internal structure of callus. The complex centre of meristematic cells was located in the small foci which

is closer to the surface, and it was covered by parenchymatous cells. The complex of parenchymatous cells was increased and the differentiation of vascular tissues observed in *Glycyrrhiza Glabra* (Akulow & Kostyukova, 2022). Interestingly, Klimek-Chodacka et al. also resembled our findings were observed in *Nigella damascene.* The callus sectioning revealed the internal structure of embryonic and non-embryonic zones. The non-embryonic cells were distinguished as loosely arranged with intercellular spaces while the embryonic cells were small, isodiametric-shaped cells along with prominent nuclei. The formation of each stage such as embryonic clumps, globular-shaped and heart-shaped were observed. The suspensor was located at the base of the pro-embryogenic stage was detected. Furthermore, hypocotyl, radical, and root meristem were fully developed from matured embryos (Klimek-Chodacka et al., 2020).

Dang et al. studied the microscopical observation of *Dioscorea nipponica* revealed the cell structure of callus formation. In the internal structure of the calli, there are a large number of parenchymatous cells and prominent nuclei were observed. The uneven thickening of cells, nest-like structure, was found in a few vascular tissue nodules. There are three types of calli were observed. One type of calli seems to be compactly arranged with more vascular tissue and a large quantity of tracheids. Type two cells showed the regularly distributed large parenchymatous cells and few vascular bundles were visible. Another type of cell was closely arranged with less interstitial substance and a well-developed tracheid. Comparatively, the type of three calli showed the strongest, cells were closely arranged and higher ability to regenerate in *Dioscorea nipponica* (Dang et al., 2022).

4.4. PHYTOCHEMISTRY

4.4.1 Extraction yield

The selection of solvent for the extraction process employed a significant impact of bioactive compounds in whole plant extracts. The higher extraction yield obtained in CME and PME showed 4.26 % and 4.86 % respectively. The other extracts such as PHE, PCE, PEAE, CHE, CCE, and CEAE exhibited 1.22 %, 1.43%, 2.97 %, 1.32 %, 1.62 %, 3.54 %, and 4.86% respectively (Table 5).

The phytochemical analysis was carried out qualitatively and quantitatively in both plant and callus using the preliminary analysis, FTIR, GC-MS and HPTLC. According to Hasan et al. the selection of solvents plays a significant role in the composition of bioactive compounds. The high-polar solvents tend to have more bioactive compounds (Hasan et al., 2024). The

comparative analysis of both wild plants and callus extracts of *C. tunicatum* were analysed. The bioactive compounds were rich in ethyl acetate and methanolic extract of *C. tunicatum*.

Table 5. Yield extraction of different solvents of *C. tunicatum*

Solvents	Quantity (%)	Solvents	Quantity (%)
PHE	1.223	**CHE**	1.32
PCE	1.43	**CCE**	1.624
PEAE	2.97	**CEAE**	3.543
PME	4.26	**CME**	4.865

4.4.2. Preliminary qualitative analysis

The preliminary phytochemical screening was carried out in eight crude extracts such as PHE, PCE, PEAE, PME, CHE, CCE, CEAE and CME of *C. tunicatum*. Comparatively, both ethyl acetate and methanolic extracts of wild and callus extracts observed rich secondary metabolites such as alkaloids, carbohydrates, glycosides, phenol, terpenoids, quinine, and phyto steroids were represented in Table 6. Also, hexane and chloroform observed fewer secondary metabolites compared to ethyl acetate and methanolic extract. Plant secondary metabolites have already been investigated by several research groups in various plant species. A similar result has been obtained in *Operculina codonantha* (Moncayo et al., 2021) and methanolic fruit extract of *Trichosanthes dioica* exhibited alkaloid, carbohydrates, terpenoids, flavonoids, tannins, saponins, steroids (Shrivastava et al., 2021). Rahman et al. analysed the *Ricinus communis* seed extract, in which various secondary metabolites were identified (Rahman et al., 2022).

In *Canthium parviflorum,* methanol and ethyl acetate extracts of leaf calli revealed the medicinally important bioactive compounds. The phytochemicals such as saponins, steroids, terpenoids, tannins, quinones and gums (Kala et al., 2012). Patel et al. investigated the preliminary qualitative analysis of ethanol and aqueous extract of both wild and callus of *Phyllanthus niruri* showed the presence of maximum phytochemicals like alkaloids, glycosides, flavonoids, steroids, phenolics, amino acids, carbohydrates, proteins, deterpines and saponins (Patel et al., 2018). The rich phytochemicals such as alkaloids, flavonoids, terpenoids, phenols,

steroids, saponins, tannins and glycosides were obtained in wild leaf and leaf-derived calli of *Allophylus serratus* (Jemal et al., 2022).

Table 6. Preliminary qualitative analysis of different extracts of *C. tunicatum*

S.No	Tests	PHE	PCE	PEAE	PME	CHE	CCE	CEAE	CME
1	**Alkaloids**								
a	Mayer's Test	-	-	++	+++	-	-	++	++
b	Wagner's Test	++	-	++	+	++	-	++	+
c	Drangendorff's Test	+	-	-	+	+	+	-	++
2	**Flavonoids**	+	-	++	+++	+	+	++	+++
3	**Carbohydrates and glycosides**								
a	Molisch's Test	++	++	+	+	+	+	+	+
b	Fehling Test	-	+	++	+	-	+	+	++
c	Barfoed Test	+	+	++	++	+	+	++	+
d	Bendict's Test	-	-	++	++	-	-	++	++
e	Borntrager's Test	+	+	+	++	+	+	+	++
4	**Saponin Test**	-	-	+	+	-	-	+	+
5	**Oils and fats test**								
a	Spot Test	-	-	-	+	-	-	-	-
6	**Phenolic test**	-		++	+++	-		++	++
a	Ferric chloride Test	-	+	-	-	-	+	-	-
b	Gelatin Test	-	-	-	++	-	-	-	++
c	Lead Acetate Test	++	-	-	++	+	-	+	+
d	Alkaline Reagent Test	-	+	++	++	-	+	++	++
e	Magnesium and Hydrochloric Acid Test	+	-	-	++	+	-	-	++
f	Phlobaterpenoids	-	-	-	-	-	-	-	-
7	**Quinone**	++	-	++	+	++	-	++	+
8	**Glycosides**	++	-	++	+++	+	-	++	+
9	**Cardiac glycosides**	+	-	-	-	+	-	-	-
10	**Terpenoid**	++	+	+	+++	+	+	+	++
11	**Coumarins**	-	-	-	+	-	-	-	+
12	**Steroids**	-	-	+	+	-	-	+	+
13	**Phytosterols**	-	++	++	++	-	++	+	++
14	**Protein**	+	-	++	+	+	-	++	++

"-" = absent, "+" = present

4.4.3. Quantitative analysis

4.4.3.1. Estimation of Total Alkaloid content

Alkaloids are effective in treating various diseases such as deterrence capability, anti-inflammatory activity, adaptogenic activities and general toxicity (Zhang & Hu, 2020). The

amount of alkaloid was measured in eight extracts of *C. tunicatum*. Interestingly, the maximum alkaloid content was found in PME (1.37±0.03 µg/mL), CME (1.074 µg/mL) followed by CEAE (0.92±0.11 µg/mL), and PEAE (0.78±0.05 µg/mL). Also, other extracts such as PHE, PCE, CHE, and CCE expressed the alkaloid content of 0.67±0.03 µg/mL, 0.53±0.04 µg/mL, 0.32±0.03 µg/mL and 0.71±0.04 µg/mL respectively of *C. tunicatum* were shown in Table 7 and Figure 17(e). Atropine was employed as a standard (Figure 17(a)) with level of significant ($p \leq 0.05$). Values were expressed in atropine equivalent per mg of extract. The differences in the values were statistically significant ($p \leq 0.05$). This information is the first report on this species and these results will help in the future to derive a novel drug. Nagalakshmi et al. also studied that the highest amount of alkaloid (5.62 mg) of methanol extract from *Tinospora cordifolia* were analysed (Nagalakshmi et al., 2023). In *Ephedra foliata,* the highest amount of alkaloid was showed in *in vitro* callus (200.40 ± 0.69 µg g^{-1}) and wild plants (100.00 ± 0.24 µg g^{-1}) showed minimal activity compared to *in vitro* callus extract (Lodha et al., 2014).

4.4.3.2. Estimation of Total Flavonoid content

The aluminium chloride method was analysed to determine the flavonoid content of different extracts of *C. tunicatum.*

The total flavonoid content was determined using the aluminium chloride method of various extracts. The highest flavonoid content was obtained in PME (3.58±0.02 µg/mL) followed by CME (3.36±0.05 µg/mL), CEAE (2.67±0.01 µg/mL), PEAE (2.37±0.01 µg/mL), CCE (1.71±0.01 µg/mL), CHE (1.64±0.01 µg/mL), PCE (1.28±0.02 µg/mL) and PHE (0.104±0.01 µg/mL) represented in Table 7 and Figure 17(e). Rutin was employed as a standard (Figure 17(b)) with level of significant ($p \leq 0.05$). Values were expressed in rutin equivalent per mg of extract. These results are statistically significant ($p \leq 0.05$). In *Ocimum sanctum,* the highest amount of flavonoid (4.75 mg /100 mg) was observed in methanol leaf extract (Garg & Garg, 2019). The leaf extract and leaf-derived calli extract in *Phyllanthus niruri* was experimented. The maximum quantity of flavonoids was obtained in ethanolic extract of leaf-derived calli (78.29 QE mg/gm) and leaf extract (49.51 QE mg/gm) (Patel et al., 2018). Similarly, this study proved the maximum quantity of flavonoid was obtained in callus (CEAE, CCE, and CHE) compared to plant extracts of *C. tunicatum.*

Figure 17. Quantitative analysis of secondary metabolites of *C. tunicatum*

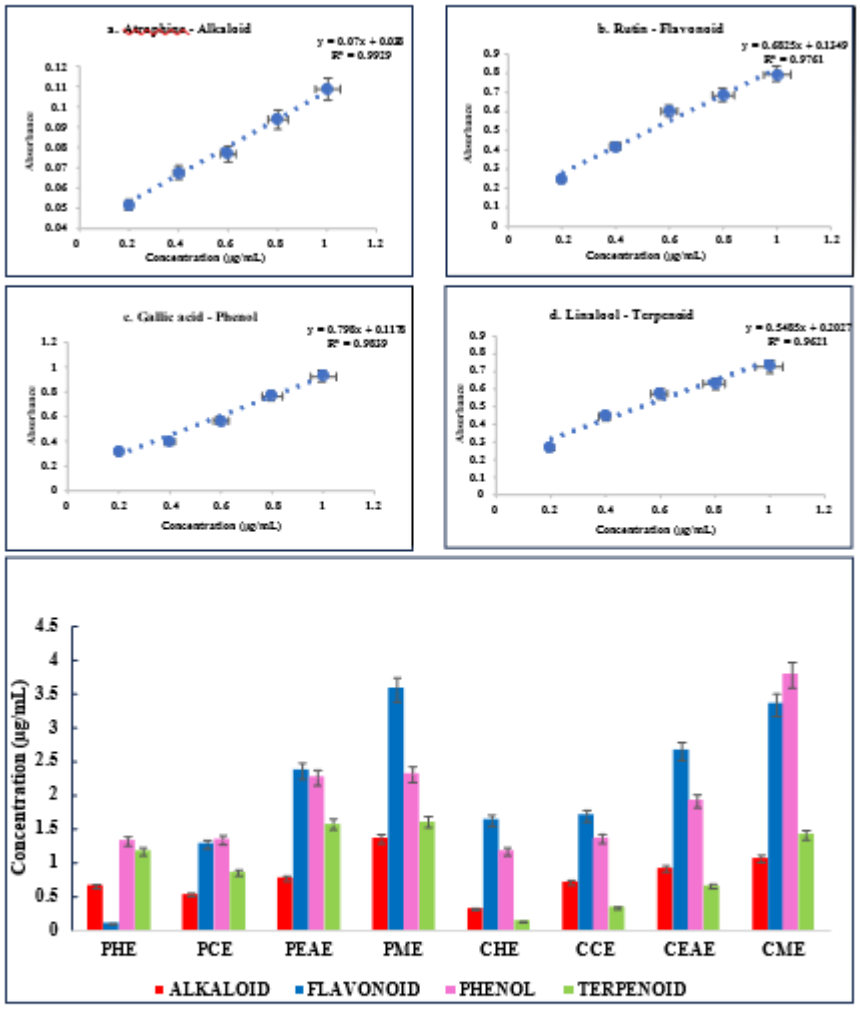

a) Calibration curve of standard atropine for the quantification of total alkaloid content b) Calibration curve of standard rutin for the quantification of total flavonoid content c) Calibration curve of standard gallic acid for the quantification of total phenol content d) Calibration curve of standard linalool for the quantification of total terpenoid content e) Graphical representation of quantitative secondary metabolite screening.

4.4.3.3. Estimation of Total Phenol Content

Phenolics have various therapeutic potentials for humans especially acting as a protective agent against free radicals (Kaur et al., 2019). The Phenolic content of PHE, PCE, PEAE, PME, CHE, CCE, CEAE and CME of *C. tunicatum* showed 1.33±0.01 µg/mL, 1.35±0.007 µg/mL, 2.27±0.063 µg/mL, 2.32±0.037 µg/mL, 1.18±0.05 µg/mL, 1.37±0.03 µg/mL, 1.93±0.04 µg/mL and 3.80±0.08 µg/mL respectively. The highest phenolic content was shown in the CME and PME as represented in Table 7 and Figure 17(e). Gallic acid was employed as a standard (Figure 17(c)) with level of significant ($p \leq 0.05$). The results were stated as equivalent of gallic acid

per mg of extracts. In *Cichorium intybus*, the highest phenolic content (302±0.251 mg/mL) was assessed in methanolic leaf extract (Arya et al., 2022).

Ahmed et al. studied the highest phenolic content (36.42±1.905 µg/mL) was observed in the methanolic extract of *Cannabis sativa* (Abdel-Azeem et al., 2020). Jemal et al. investigated the highest phenolic content of leaf extract showed 104.73±4.3 mg compared to callus extract 54.42±6.59 mg (Jemal et al., 2022).

4.4.3.4. Estimation of Total Terpenoid Content

Terpenoid content was analyzed using folin-ciocalteu method using various extracts of wild plant and callus extracts such as PHE, PCE, PEAE, PME, CHE, CCE, CEAE and CME of *C. tunicatum.* Linolool is used as a standard as shown in Figure 17 (d). The maximum terpenoid content of PME (1.60±0.02 µg/mL) subsequently, PEAE (1.57±0.14 µg/mL), CME (1.42±1.1 µg/mL), PCE (0.86±0.02 µg/mL), CEAE (0.66±0.5 µg/mL), PHE (0.4±0.04 µg/mL), CCE (0.34±0.3 µg/mL) and CHE (0.14±0.2 µg/mL) was obtained from *C. tunicatum* as shown in Table 7 and Figure 17(e). Results were expressed in linolool equivalent per mg of extract with the significant level of $p \leq 0.05$. In *Enicostemma litorrale,* the maximum amount of terpenoid was observed in methanol leaf extract (Indumathi et al., 2014). Terpenes and terpenoids contain various pharmaceutical properties such as antimicrobial, antihyperglycemic, antiparasitic, antioxidant, anti-inflammatory, analgesic etc., (Roaa, 2020).

Table 7. Quantitative analysis of secondary metabolites of *C. tunicatum*

Samples	Alkaloid	Flavonoid	Phenol	Terpenoid
PHE	0.67±0.03^{e}	0.10±0.01^{h}	1.33±0.01^{e}	0.4±0.04^{g}
PCE	0.53±0.04^{f}	1.28±0.02^{g}	1.35±0.007^{e}	0.86±0.02^{d}
PEAE	0.78±0.05^{d}	2.37±0.01^{d}	2.27±0.063^{c}	1.57±0.14^{b}
PME	**1.37±0.03^{a}**	**3.58±0.02^{a}**	2.32±0.037^{b}	**1.60±0.02^{a}**
CHE	0.32±0.03^{g}	1.64±0.01^{ef}	1.18±0.05^{f}	0.14±0.2^{g}
CCE	0.71±0.04^{d}	1.71±0.01^{e}	1.37±0.03^{e}	0.34±0.3^{f}
CEAE	0.92±0.11^{c}	2.67±0.01^{c}	1.93±0.04^{d}	0.66±0.5^{e}
CME	1.07±0.05^{b}	3.36±0.05^{b}	**3.80±0.08^{a}**	1.42±1.1^{c}

Values represent mean ± standard deviation of tree replicates per treatment. Means in a column with same letter are significantly ($p \leq 0.05$) difference according to DMRT.

Based on the quantitative identification of *C. tunicatum* extracts, demonstrated the presence of bioactive compounds. The secondary metabolites were quantified and results obtained in the following order such as phenols> flavonoids> terpenoids> alkaloids.

Cynanchum species encompasses 232 phytochemicals including alkaloids, flavonoids, phenols, terpenoids, acetophenones and C_{21} steroids (Wang et al., 2021). Comparatively, PEAE, PME, CEAE, and CME showed rich phytoconstituents compared to PHE, PCE, CHE, and CCE. These phytochemicals present in *C. tunicatum* are evidenced as therapeutic medicinal plant. For further analysis, extracts such as PEAE, PME, CEAE, and CME were chosen though these extracts showed maximum phytocompounds. Biological activities will be analysed based on the bioactive compounds to validate the pharmaceutical property *C. tunicatum.*

4.4.4. FTIR analysis

The functional groups of bioactive components in plant extracts such as PEAE, PME, CEAE and CME were identified by FTIR (Fourier transform infrared) spectra based on the peak value obtained in the region of infrared radiation. A maximum number of peaks have been found at the ethyl acetate and methanolic extract.

Steroids generally possess aliphatic groups (i.e., C-H) in the ring system and on the side chain and may also possess one or more carbonyl (C=O) and or ethylenic groups (C=C) (Osei et al., 2021). FTIR spectrum were analysed using PEAE, PME, CEAE and CME of *C. tunicatum*. The information in Figure 18 and Table 8 showed peak values along with their functional group of various extracts respectively. The main peak observed in FTIR spectra of CME extract at 2870.08 cm^{-1} (medium), 2924.09 cm^{-1} (strong), 2954.95 cm^{-1} (narrow sharp strong), 1728.22 cm^{-1} (weak), 1465.90 cm^{-1} (strong), 1381.03 cm^{-1} (medium), 1242.16 cm^{-1} (weak), 1172.72 cm^{-1} (weak), 1041.56 cm^{-1} (weak), 887.26 cm^{-1} (medium), 725.23 cm^{-1} (strong), 817.82 cm^{-1} (weak), 563.21 cm^{-1} (weak). Infrared spectrum of chemical constituents of CEAE exhibited peaks at 3325.28 cm^{-1} (broad strong), 2947.23 cm^{-1} (medium), 2831.50 cm^{-1} (sharp medium), 1666.50 cm^{-1} (very weak), 1404.18 cm^{-1} (weak), 1026.13 cm^{-1} (strong) and 686.66 cm^{-1} (medium). The peak of PME represented at 3633.89 cm^{-1} (weak), 2985.81 cm^{-1} (sharp medium), 2900.94 cm^{-1} (very weak), 1735.93 cm^{-1} (sharp narrow strong), 1442.75 cm^{-1} (medium), 1373.32 cm^{-1} (sharp medium), 1234.44 cm^{-1} (sharp strong), 1095.57 cm^{-1} (medium), 1041.56 cm^{-1} (sharp narrow strong), 786.96 cm^{-1} (broad medium), 848.68 cm^{-1} (sharp medium), 632.65 cm^{-1} (medium), 609.51 cm^{-1} (medium). The FTIR spectra of PEAE showed peaks at 3317.56 cm^{-1} (broad medium), 2831.50 cm^{-1} (sharp medium), 2939.52 cm^{-1}

(medium), 2522.89 cm^{-1} (weak), 2229.71 cm^{-1} (very weak), 2044.54 cm^{-1} (weak), 1666.50 cm^{-1} (weak), 1450.47 cm^{-1} (medium), 1111.00 cm^{-1} (medium), 1018.41 cm^{-1} (narrow strong), 671.23 cm^{-1} (broad medium), 601.79 cm^{-1} (medium), 524.64 cm^{-1} (medium).

TABLE 8. FTIR analysis of different extracts of *C. tunicatum*

Functional group	Frequency (cm^{-1})			
	PEAE	PME	CEAE	CME
Alcohol (O-H stretching)	3317.56 2831.50	3633.89 -	3325.28	- -
Alkane (C-H stretching)	2939.52	2985.81 2900.94	2947.23 2831.50	2870.08 2924.09 2954.95
Carboxylic acid (O-H stretching)	2522.89	-	-	-
Nitriles (C≡N stretching)	2229.71	-	-	-
Isothiocyanate (N=C=S Stretching)	2044.54	-	-	-
Aromatic compounds (C-H bending)	1666.50	1735.93	1666.50	1728.22
Alkane (C-H Bending)	1450.47	-	-	1465.90
Carboxylic acid (O-H bending)	-	1442.75	1404.18	-
Alcohol (O-H bending)	-	1373.32	-	1381.03
Amine (C-N stretching)	-	1234.44	-	1242.16 1172.72
Aliphatic ether (C-O stretching)	1111.00	1095.57	-	-
Sulfoxide (S=O stretching)	1018.41	1041.56	1026.13	1041.56
Alkene (C=C bending)	-	-	-	887.26
Halo Compound (C-Cl stretching)	671.23 601.79	786.96 848.68 632.65 609.51	686.66	725.23 817.82 563.21
Halo Compound (C-I stretching)	524.64	-	-	-

The spectra of *C. tunicatum* with the frequency range from 2831.50 to 2985.81 represented the presence of an alkane group (C-H stretch). The peak at 3325.28 and 3633.89 corresponds to the presence of alcohol (O-H stretch) (Vahur et al., 2016). The peak at 2522.89 was observed as carboxylic acid (O-H stretch). The peak at 2229.71 showed the presence of nitriles (C≡N stretch). The peak at 2044.54 signified the presence of isothiocyanate (N=C=S stretch). The peak at 1666.50 and 1728.22 to 1735.93 unveiled the presence of aromatic compounds (C-H bending). The peak at 1450.47 and 1465.90 displayed alkane (O-H bending) (Reignier et al., 2021). The peak at 1404.18 and 1442.75 showed carboxylic acid (O-H bending). The peak at 1381.03 and 1373.32 exhibited alcohol (O-H bending). The peak ranges from 1172.72 to 1242.16 represented by amine (C-H stretch). The peak ranges from 1018.41 to 1041.56 showed a sulfoxide group (S=O stretch) (Müller et al., 2014). The medium peak at 887.26 exhibited alkene (C=C bending). The peak ranges from 563.21 to 848.68 showing a halo compound (C-Cl stretch). The medium peak at 524.64 contained a halo compound (C-I stretch) (Papakosta et al., 2020). The FTIR spectrum confirmed to the presence of alkaloids, flavonoids, phenols, terpenoids, carboxylic acid, alkane, and aromatic alkenes in both wild plants and the callus of *C. tunicatum*.

Figure 18. FTIR analysis of different extracts of *C. tunicatum*

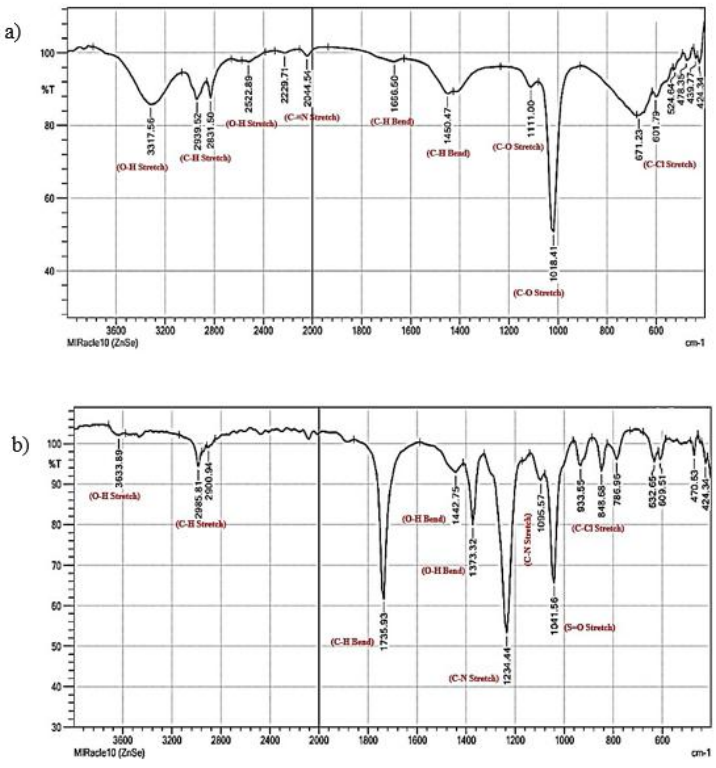

a) PEAE b) PME

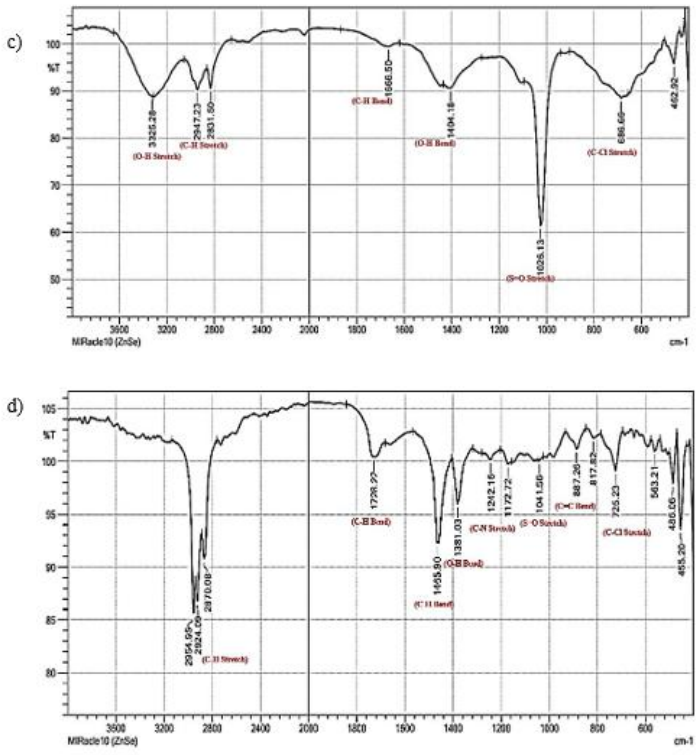

c) CEAE d) CME

4.4.5. GCMS analysis

The GCMS analysis was determined with two extracts such as PME and CME of exhibited the highest phytoconstituents *C. tunicatum*.

The GC-MS analysis of C. *tunicatum* were identified 45 bioactive compounds using spectral data. The main bioactive compounds were present in both PME and CME such as 1,3-Dioxolane, 3,7,11,15-Tetramethyl-2-hexadecen-1-ol, 9,12-Octadecadienoic acid, 9-Hexadecenoic acid, Octadecanoic acid, Colchicine, Phytol, Tetradecanoic acid and l-(+)-Ascorbic acid 2,6-dihexadecanoate. The area (%) of both extracts exhibited in different ranges represented in Table 9a.

The compounds present only in PME are of Beta-Amyrin (10.614 %), 1-Hexacosene (0.145%), 14-Dimethyl-5. alpha. -ergosta-8 (0.430%), 5-Cholestene-3-ol (5.243%), 9,19-Cyclolanost-24-en-3-ol (10.728%), Cholesta-22,24-dien-5-ol (3.224%), Lup-20(29)-en-3-one (0.306%), Megastigmatrienone (0.116%), Rutin (4.54%), Pregn-5-en-20-one (0.136%) and syn-Tricyclo [5.1.0.0(2,4)] oct-5-ene (0.048%) were represented in Table 9b. Conversely, in

TABLE 9a. Similar compounds present in both PME and CME of GC-MS analysis from *C. tunicatum*

Peak	Molecular weight	PME		CME		Formula	PME/CME
		Area (%)	Retention time	Area (%)	Retention time		
1.	74.08	0.382	3.104	0.33	25.48	$C_3H_6O_2$	1,3-Dioxolane
2.	296.5	0.363	13.602	4.35	18.18	$C_{20}H_{40}O$	3,7,11,15-Tetramethyl-2-hexadecen-1-ol
3.	280.4	0.355	29.977	0.67	21.52	$C_{18}H_{32}O_2$	9,12-Octadecadienoic acid
4.	254.41	0.119	14.929	0.25	15.19	$C_{16}H_{30}O_2$	9-Hexadecenoic acid
5.	284.5	0.751	18.714	0.17	12.35	$C_{18}H_{36}O_2$	Octadecanoic acid
6.	399.4	8.129	25.998	7.90	22.35	$C_{22}H_{25}NO_6$	Colchicine
7.	296.5	1.455	17.572	0.20	13.202	$C_{20}H_{40}O$	Phytol
8.	228.37	0.141	12.490	0.19	6.317	$C_{14}H_{28}O_2$	Tetradecanoic acid
9.	652.9	8.129	15.336	0.17	9.29	$C_{38}H_{68}O_8$	l-(+)-Ascorbic acid 2,6-dihexadecanoate

CME have exhibited bioactive compounds such as Furfural (1.73%), 3-Methylenedihydro-2,5-furandione (1.24%), 2,3-dihydro-3,5-dihydroxy-6-methyl- (3.69%), 5-(Hydroxymethyl)-2-Furaldehyde (28.48%), n-Hexadecanoic acid (13.76%), Phthalic acid (4.69%), 9-Octadecenoic acid (2.76%), Bis(2-ethylhexyl) phthalate (3.42%), Cyclopentanecarboxylic acid (1.08%), 3-Nonenoic-3,4-D2 acid (2.70%), Chromone (2.82%), Acetic acid (3.14%), Benzoic acid (4.91%), 3-Butoxypropylamine (6.29%), 1,5-Pentandiol (7.89%), Acetoxyacetic acid (1.88%), Furazane (1.14%), Piperazine (4.35%) and 2,5-Furandione (2.92%) as shown in Table 9c. The structures were shown in Figure 19. Soliman et al. studied bioactive chemicals of *C. acutum* using GC-MS observed lupeol, hexadecanoic acid, neophytadiene, octadecanoic acid, and phytol were found with percentages of 15.36%, 10.72%, 9.15%, 8.78%, and 6.51%, respectively (Soliman et al., 2022).

TABLE 9b. Bioactive compounds present only in PME of GC-MS analysis from *C. tunicatum*

Peak	Molecular weight	Area (%)	Retention time	Formula	PME
1.	426.72	10.614	44.767	$C_{30}H_{50}O$	Beta-Amyrin
2.	364.7	0.145	34.306	$C_{26}H_{52}$	1-Hexacosene
3.	426.7	0.430	42.870	$C_{30}H_{50}O$	14-Dimethyl-5. alpha. -ergosta-8
4.	540.9	5.243	41.252	$C_{37}H_{64}O_2$	5-Cholestene-3-ol
5.	468.8	10.728	46.126	$C_{32}H_{52}O_2$	9,19-Cyclolanost-24-en-3-ol
6.	384.6	3.224	41.877	$C_{29}H_{48}O$	Cholesta-22,24-dien-5-ol
7.	424.7	0.306	45.271	$C_{30}H_{48}O$	Lup-20(29)-en-3-one
8.	190.28	0.116	11.065	$C_{13}H_{18}O$	Megastigmatrienone
9.	610.5	4.54	18.382	$C_{27}H_{30}O_{16}$	Rutin
10.	300.5	0.136	38.302	$C_{21}H_{32}O$	Pregn-5-en-20-one
11.	190.32	0.048	10.489	$C_{14}H_{22}$	syn-Tricyclo [5.1.0.0(2,4)] oct-5-ene

Fattahi et al. analysed GC-MS of *Deracocephalum moldavica* essential oil, and seventy compounds were identified (Fattahi et al., 2021). Mariyammal et al. evaluated 42 compounds across various solvents (petroleum ether, chloroform, ethyl acetate, methanol, and hydro-alcoholic), with consistent compounds like neophytadiene, palmitic acid, phytol, trans-δ9-octadecenoic acid, oleic acid, dichloroacetic acid, tridec-2-ynyl ester, z, z-8,10-hexadecadien-1-ol, phytyl palmitate, phthalic acid, phytyl tetradecanoate, ergost-5-en-3-ol, (3beta,24r)-, stigmasterol, and tetrapentacontane from *Aristolochia tagala* leaf extracts (Mariyammal et al., 2023).

Similarly, many bioactive compounds (23 nos.) were identified by GC-MS analysis such as 9,12,15-octadecatrien-1-ol, n-Hexadecanoic acid, octadecatrienol acid, methyl palmitate and phytol in *Hibiscus asper* leaf extracts (Olivia et al., 2021). The GC-MS analysis of *Amomum*

TABLE 9c. Bioactive compounds present only in CME GC-MS analysis from *C. tunicatum*

Peak	Molecular weight	Area %	Retention time	Formula	CME
1.	96.08	1.73	20.814	$C_5H_4O_2$	Furfural
2.	112.08	1.24	18.00	$C_5H_4O_3$	3-Methylenedihydro-2,5-furandione
3.	144.12	3.69	21.24	$C_6H_8O_4$	2,3-dihydro-3,5-dihydroxy-6-methyl-
4.	132.066	28.48	20.38	$C_6H_6O_3$	5-(Hydroxymethyl)-2-Furaldehyde
5.	256.42	13.76	11.328	$C_{16}H_{32}O_2$	n-Hexadecanoic acid
6.	166.13	4.69	22.165	$C_8H_6O_4$	Phthalic acid
7.	282.5	2.76	19.1	$C_{18}H_{34}O_2$	9-Octadecenoic acid
8.	390.6	3.42	9.928	$C_{24}H_{38}O_4$	Bis(2-ethylhexyl) phthalate
9.	372	1.08	12.325	$C_{18}H_{28}O_2$	Cyclopentanecarboxylic acid
11.	172	2.70	15.364	$C_{10}H_{16}D_2O_2$	3-Nonenoic acid
12.	146.14	2.82	16.297	$C_9H_6O_2$	Chromone
13.	232	3.14	16.483	$C_{10}H_{16}O_6$	Acetic acid
14.	273	4.91	18.181	$C_{15}H_{12}FNO_3$	Benzoic acid
15.	131	6.29	20.386	$C_7H_{17}NO$	3-Butoxypropylamine
16.	188	7.89	21.243	$C_9H_{16}O_4$	1,5-Pentandiol
17.	242	1.88	21.525	$C_{15}H_{30}O_2$	Acetoxyacetic acid
18.	211	1.14	21.750	$C_2H_2IN_3O$	Furazane
19.	100	4.35	22.165	$C_5H_{12}N_2$	Piperazine
20.	98	2.92	22.359	$C_4H_2O_3$	2,5-Furandione

nilgiricum leaf extracts showed the presence of 25 peaks corresponding to bioactive compounds. Among these, the methanol leaf extracts contained 9 identified compounds, the ethyl acetate leaf extracts had 6, and the methanol rhizome extract showed 10 peaks (Konappa et al., 2020). Jayakar et al. explored the bioactive compounds in hexane and methanol leaf extracts of *Garcinia cambogia* using GC-MS analysis, in addition, eleven and seventeen phytoconstituents were identified respectively and fourteen compounds in each of the hexane and methanol leaf extracts of *Garcinia indica* were emphasized the medicinal properties

(Jayakar et al., 2020). El-Beltagi et al. investigated phytochemicals of *Ficus sycomorus* from methanol extracts using GC-MS analysis, in which 12 from fruit and 29 from leaf bioactive compounds were identified, respectively (El-Beltagi et al., 2019). Idris et al. investigated chemical constituents in essential oils of the *Rumex crispus* in both the leaf and root. The bioactive compounds present in the essential oil of the leaves such as 5-Eicosene, (E)-, docos-1-ene, trans-5-Octadecene, tetradecane while those found in the root are 1-Heptacosanol, 4-Methyloctane, ethylcyclohexane, eucalyptol, m-Xylene, octadecane, phytol, and tetradecane (Idris et al., 2019).

Figure 19. GCMS chromatogram of *C. tunicatum*

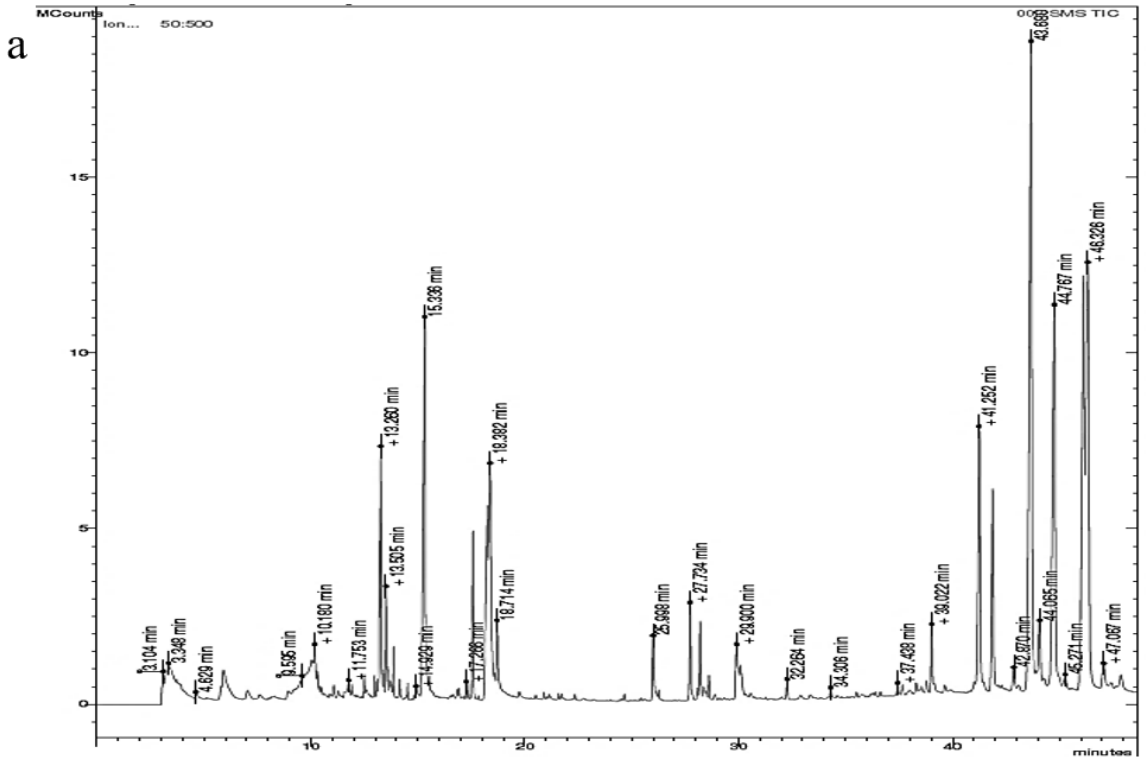

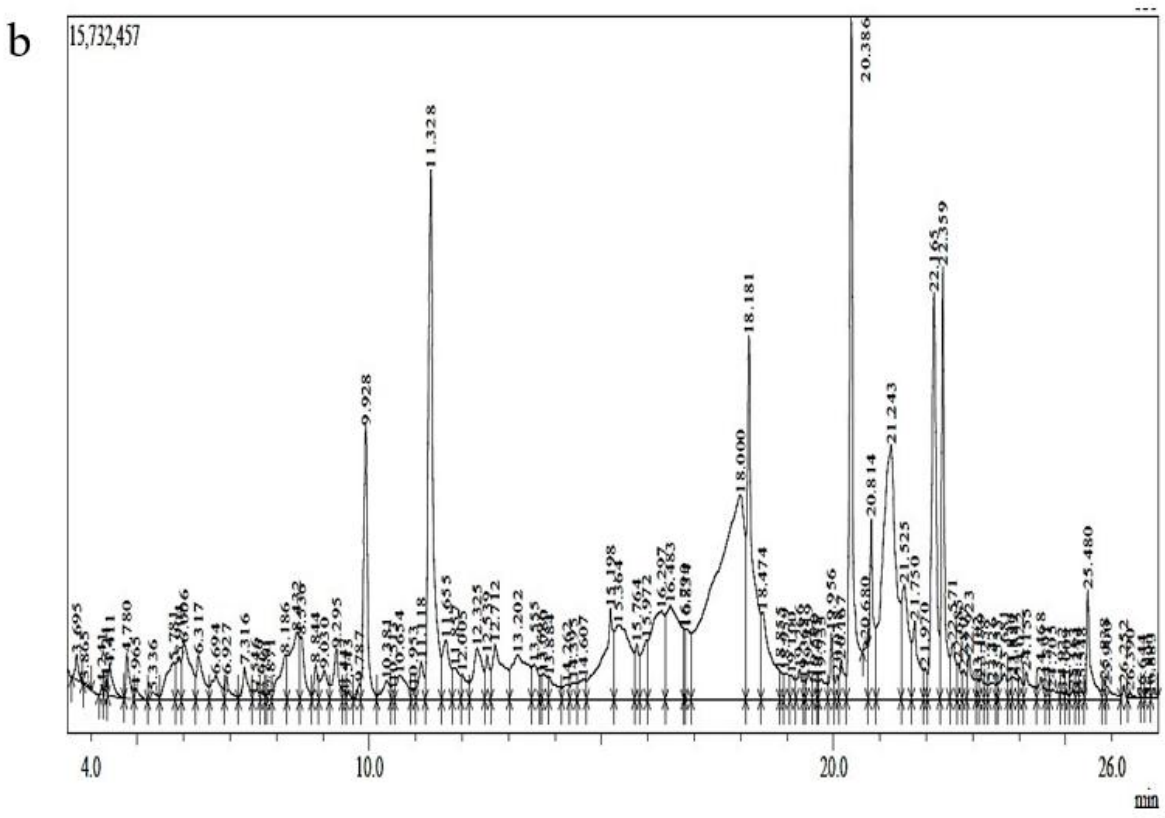

a) PME and b) CME

Anand et al. studied the GC-MS analysis in both callus and plant extract and showed the major compounds identified in both extracts were Furfural, Campesterol, Malonic acid, Beta-sitosterol, Myristic acid, Stigmasterol, Diethyl phthalate, Propanoic acid, Furyl hydroxymethyl alcohol, Linoleic acid, Butanedioic acid, Dodecanoic acid, Octadecanoic acid, Caproic acid, etc (Anand et al., 2018).

The composition of fatty acids in plants is diverse and essential for various biological processes. Palmitic acid, stearic acid, myristic acid, and linoleic acid are among the key fatty acids found in plants and contribute to plant structural integrity, membrane function, energy storage and responses to environmental factors (Rustan & Drevon, 2001). Lupeol demonstrated a promising compound for drug development due to its wide-ranging beneficial effects which include its anti-diabetic, anti-asthma, anti-arthritic, cardioprotective, hepatoprotective, nephroprotective, neuroprotective, and anticancer properties (Tsai et al., 2016). Terpene compounds were derived from mevalonate which are isoprene polymers with diverse biological activities such as antibacterial, anti-tumor, anti-inflammatory, and anti-viral effects (Fan et al., 2023). Phytosterols possess various properties like antifungal, anti-inflammatory, antibacterial, anti-tumor, antioxidant, and anti-ulcerative effects which play their multifunctional biological

roles (Abdul et al., 2016; Ito et al., 2017). Spectral data provided valuable evidence of phytochemical compounds present in the plant species. The bioactive compounds obtained from medicinal plants contain various drug and pharmaceutical applications, offered potential opportunity for advanced research (Babouongolo et al., 2021; Dash et al., 2023; Nimbeshaho et al., 2020).

4.4.6. HPTLC profiling

According to FTIR results, many secondary metabolites were obtained in the methanol extract of both wild plant and callus extract from *C. tunicatum*. So, the HPTLC fingerprinting analyses were performed with only two extracts such as PME and CME of *C. tunicatum* to exhibit the quantity of phytoconstituents.

Figure 20. HPTLC analysis of colchicine

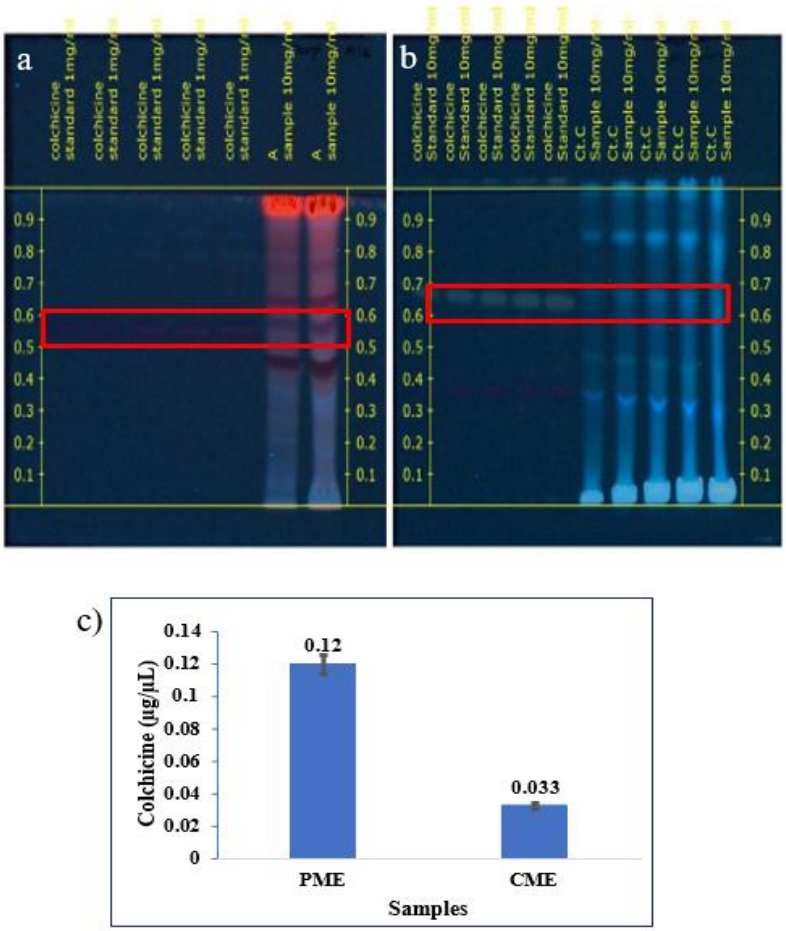

a), b) Short and long UV of HPTLC plates
c) Graphical representation of colchicine

In PME and CME, the bioactive compounds were isolated on HPTLC plates by different mobile phases such as Ethyl acetate: Methanol: Water (20:3:2), and Ethyl acetate: methanol:

formic acid: water (20:3:1:2) for colchicine and rutin respectively. Various solvent systems have been documented for the concurrent determination and quantification of bioactive substances in fruits, vegetables, and medicinal plants (Chewchinda & Kongkiatpaiboon, 2020; Hashim et al., 2016; Patel et al., 2015).

HPTLC fingerprinting of alkaloids of methanolic extract from *C. tunicatum* demonstrated eight spots with an increasing order of Retention factor such as 0.032, 0.224, 0.302, 0.474, 0.597, 0.669, 0.776, 0.976 at 2.5 µL. The colchicine was observed as 0.12 µg and 0.033 µg in 1 µL of PME and CME respectively of *C. tunicatum* (Figure 20). Spot 1 (strychnine), 2 (colchicine) 3 (alkaloid 1), and 5 (alkaloid 2) were identified (Senguttuvan & Subramaniam, 2016; Kalaiselvi et al., 2012). The seven spots with the R_f value of 0.071, 0.258, 0.460, 0.585, 0.669, 0.781, 0.979 at 5 µL of extract, in which 0.46 was identified as alkaloid 4 (Deepika & Maurya, 2022).

Figure 21. HPTLC analysis of rutin

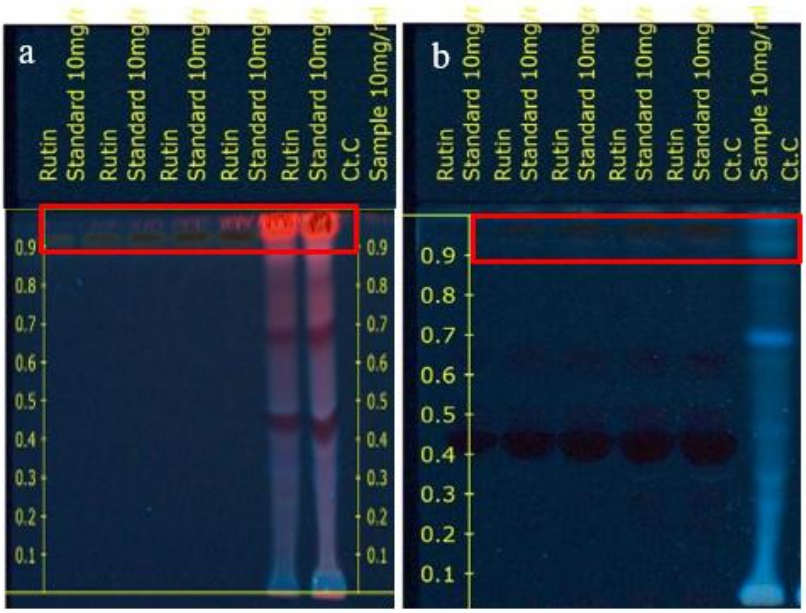

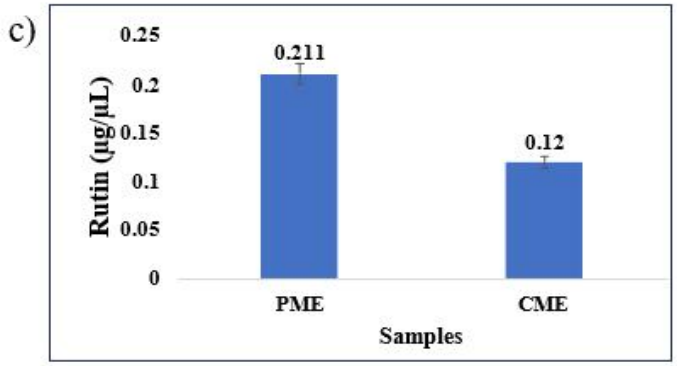

a), b) Short and long UV of PME
c) Graphical representation of rutin

Flavonoid showed eight bands with R_f value such as 0.048, 0.082, 0.310, 0.456, 0.684, 0.813, 0.890 and 0.966 at 2.5 µL of methanolic extract. Six bands with R_f value such as 0.076, 0.460, 0.703, 0.834, 0.900, and 0.971 were identified at 5 µL. The rutin was observed as 0.211 µg and 0.12 µg in PME and CME respectively of *C. tunicatum* (Figure 21). Similarly, Senguttuvan et al. reported that R_f values indicated that 0.27, 0.56, and 0.62 were identified as Terpenoid 1, Coumarin, and Terpenoid 5 in methanolic leaf extract of *Hypochaeris radicata* (Senguttuvan & Subramaniam, 2016). These bioactive components were reported strong antimicrobial, anti-hemostatic, antioxidant, anticancer, anti-inflammatory, anti-cardiovascular disease, cardioprotective, and chemopreventive activities (Bae & Kim, 2016; Deepika & Maurya, 2022; Kalaiselvi et al., 2012; Tessema et al., 2023). The obtained fingerprint of the HPTLC chromatogram of *C. tunicatum* represented unique biologically active components. Flavonoids such as quercetin and myricetin leads to protect the cells from oxidative damage and aging process (Bae & Kim, 2016; Paul et al., 2020). The validation parameters for HPTLC analysis were found to be within the acceptable range for the intended purpose (Paul et al., 2020; Tessema et al., 2023). The bioactive compounds present in *C. tunicatum* exhibit various therapeutic potential.

4.4.7. Column Chromatography

In Column chromatography, silica gel was used as a stationary phase, mobile phase such as hexane, chloroform, ethyl acetate and methanol based on the polarity level. Since fractionization using column chromatography was largely influenced by the polarity of the mobile phase and the compounds for each solvent (Figure 22).

As a result, 80 fractions were collected based on various solvent system. The chloroform and ethyl acetate fraction showed a single band in TLC with R_f value of 0.7 (Figure 23a). The eluted fraction was further subjected to characterization using UV, FTIR and GC-MS analysis. The UV analysis showed a peak at 290 nm (Figure 23b). FTIR analysis helps to explore different functional groups such as 1735, 1242, 1041 cm^{-1} represented the functional groups as Carboxyl, Amine and Sulfoxide (Figure 23c). And, further GC-MS spectra identified the compound as 1,3 Benzenedicarboxylic acid as represented in Figure 23d. Similarly, Nasiru et al. isolate and purify the phenolic compounds of *Cynanchum auriculatum* through thin- layer, silica gel column chromatography and reverse-phase silica gel column chromatography. The characterization of the isolated compounds such as cynandione A, 2,5-dihydroxyacetophenone and radix piperacanthone (Nasiru et al., 2024).

Figure 22. Column Chromatography of PME of *C. tunicatum*

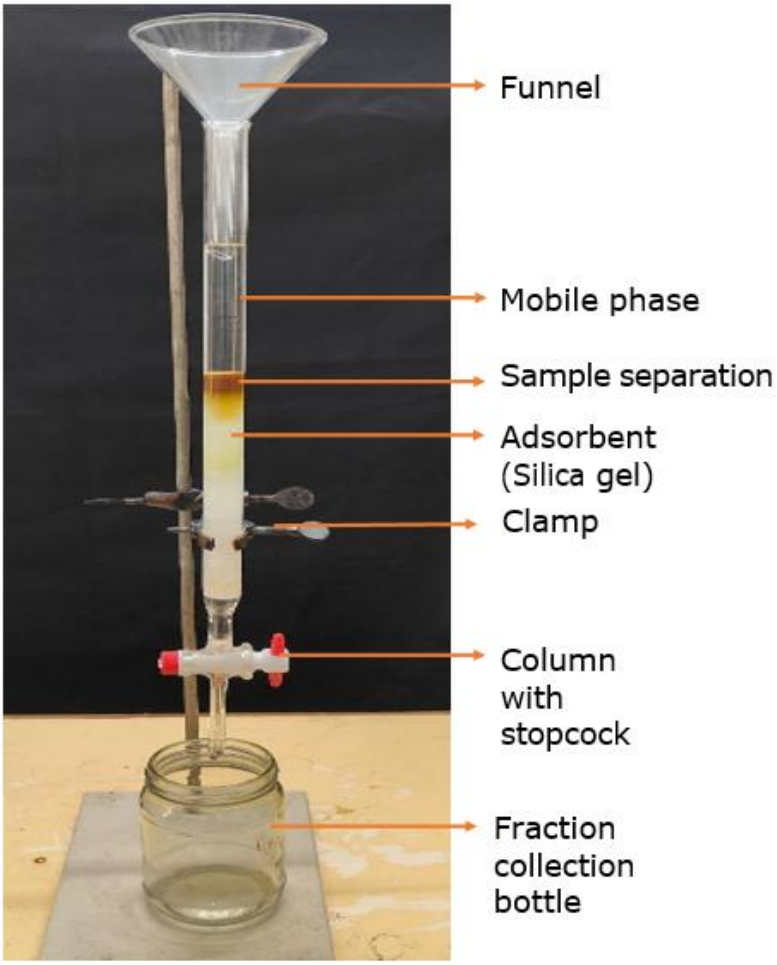

Figure 23b. UV analysis of isolated compound (fraction 1) from PME of *C. tunicatum*

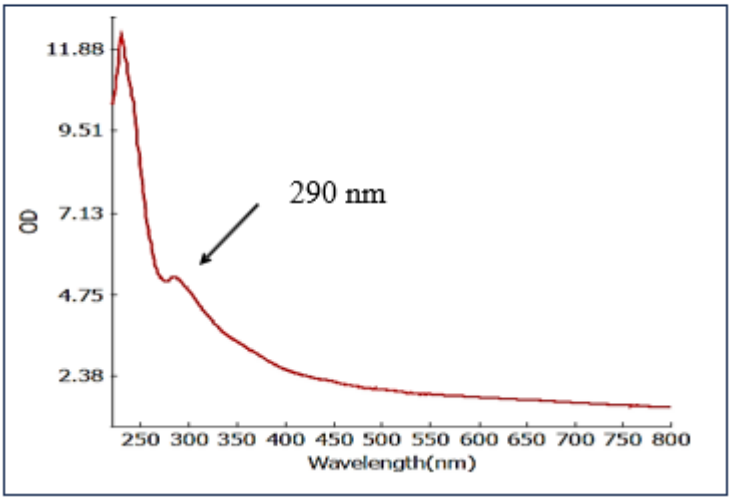

Figure 23c. FTIR analysis of isolated compound (fraction 1) from PME of *C. tunicatum*

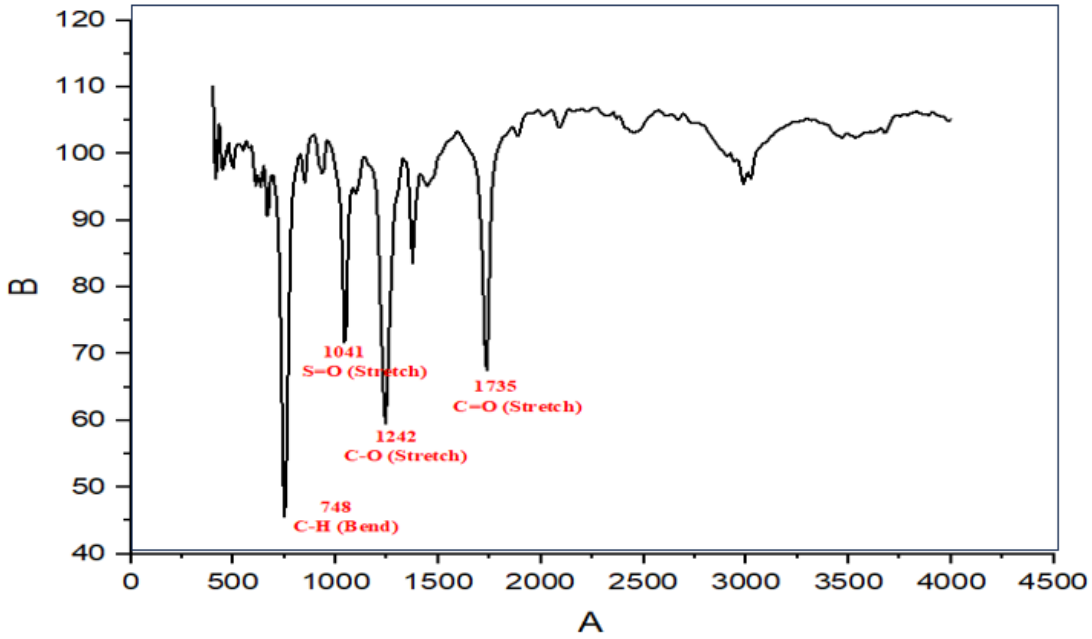

Figure 23d. GCMS analysis of isolated compound (fraction 1) from PME of *C. tunicatum*

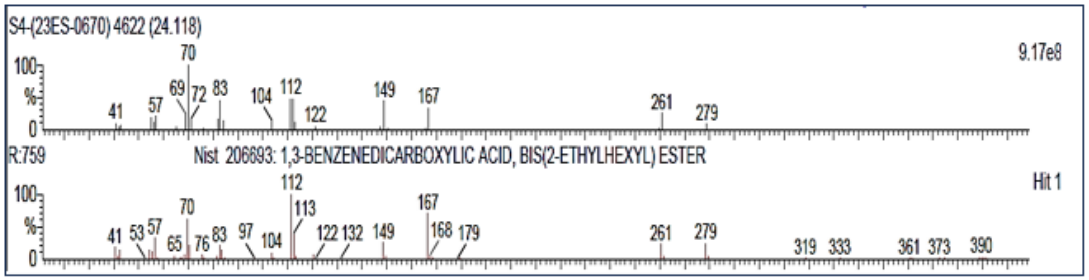

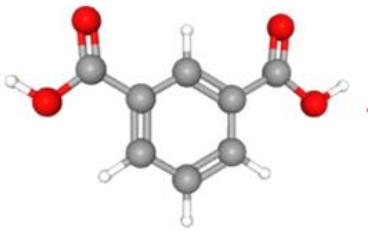

Structure of the compound

4.5. BIOLOGICAL ACTIVITIES

4.5.1. Evaluation of anti-microbial activity

The anti-microbial activity was carried out in PEAE, PME, CEAE and CME of *C. tunicatum.*

4.5.1.1. Anti-bacterial activity

Three bacteria which include *Salmonella enterica* (MTCC-3858), *Enterococcus faecalis* (MTCC-439) and *Escherichia coli* (MTCC-1687) were used to analyse antibacterial activity using well-diffusion method. Amphicilin and DMSO are the positive and negative controls.

The CME exhibited a strong antibacterial activity and it achieved a maximum inhibition zone of 32.5±1.8 mm at 100 µL, 29.7±0.7 mm at 75 µL, 27.5±0.9 mm at 50 µL and 23.8±1.8 mm at 25 µL was observed against *Salmonella enterica* whereas the positive control Amphicilin inhibited 14±2 mm. Followed by another pathogenic bacteria *Enterococcus faecalis* showed the highest inhibition zone (15.2±1.4 mm) at the concentrations of 100 µL, 12.4±0.6 mm (75 µL), 11.7±1.6 mm (50 µL), 11.39±0.9 mm (25 µL) and Amphicilin inhibited 15.1±1.2 mm. The *Escherichia coli* inhibited the maximum zone of 13.8±1.2 mm at concentration of 100 µL, 13.1±0.8 mm (75 µL), 10.8±1.2 mm (50 µL), and 12.8±1 mm (25 µL) whereas positive control showed 15.1±1 mm.

The PME was active against *Salmonella enterica,* and it achieved the highest inhibition zone of 26.2±0.6 mm at the concentrations of 100 µL, 24.5±1.4 mm (75 µL), 23.2±0.6 mm (50 µL) and 17.3±1.5 mm (25 µL). In *Enterococcus faecalis***,** 13.4±1 mm at the concentration of 100 µL, 13±0.6 mm (75 µL), 8.3±0.6 mm (50 µL), and 0.6±1.1 mm (25 µL). *Escherichia coli* achieved 13.1±0.7 mm at the concentration of 100 µL, 12.3±0.6 mm (75 µL), 10.6±1.5 mm (50 µL), 9.3±0.6 mm (25 µL).

The CEAE was effective against the *Enterococcus faecalis*, the maximum inhibition zone of 12.8±1.2 mm was obtained at the concentration of 100 µL. In *Salmonella enterica,* the maximum inhibition zone of 12.8±0.8 mm was achieved. The *Escherichia coli* showed the highest inhibition zone of 12.4±0.9 mm. The PEAE showed the highest inhibition zone (12.3±1.1 mm) in *Enterococcus faecalis.* In *Salmonella enterica*, the maximum inhibition zone of 11.3±0.3 mm was observed. *Escherichia coli* showed the highest zone of inhibition was 12.3±0.5 mm. Thus, the anti-bacterial activity of callus extracts evoked a great inhibition zone compared to the plant extract of *C. tunicatum* as represented in Table 10 and Figure 24.

Table 10. Antimicrobial and Antifungal activity of *C. tunicatum*

Sample	Antibacterial activity Positive control (Ampicillin)			Antifungal activity Positive control (Amphotericin)	
	***Escherichia coli* (mm)**	***Salmonella enterica* (mm)**	***Enterococcus faecalis* (mm)**	***Aspergillus niger* (mm)**	***Candida albicans* (mm)**
Positive control	15.1±1	14±2	15.1±1.2	13±2	10.9±1.5
Negative control	0	0	0	0	0
PEAE					
25µL	11 ± 1^{b}	9 ± 1^{c}	7.6 ± 0.5^{c}	3 ± 1^{c}	3.3 ± 0.5^{c}
50µL	10.3 ± 0.5^{c}	11 ± 1^{a}	12 ± 1^{a}	4.6 ± 1.1^{b}	4.6 ± 1.5^{b}
75µL	11.6 ± 0.5^{b}	10 ± 0.5^{b}	11 ± 1^{b}	4 ± 1^{b}	4.6 ± 0.5^{b}
100µL	**12.3 ± 0.5^{a}**	**11.3 ± 0.3^{a}**	**12.3 ± 1.1^{a}**	**10 ± 1.1^{a}**	**7.1 ± 0.3^{a}**
PME					
25µL	9.3 ± 0.6^{d}	17.3 ± 1.5^{d}	0.6 ± 1.1^{d}	12.4 ± 0.5^{d}	8 ± 1^{c}
50µL	10.6 ± 1.5^{c}	23.2 ± 0.6^{c}	8.3 ± 0.6^{c}	11.8 ± 1^{c}	10.1 ± 1^{b}
75µL	12.3 ± 0.6^{b}	24.5 ± 1.4^{b}	13 ± 0.6^{b}	12.8 ± 1^{b}	10.1 ± 0.8^{b}
100µL	**13.1 ± 0.7^{a}**	**26.2 ± 0.6^{a}**	**13.4 ± 1^{a}**	**15.3 ± 0.9^{a}**	**10.9 ± 1.1^{a}**
CEAE					
25µL	7.7 ± 0.4^{c}	8.1 ± 0.6^{d}	11.2 ± 1^{bc}	2.5 ± 0.5^{d}	0
50µL	11.1 ± 1^{b}	10.3 ± 1.5^{c}	11.8 ± 1.2^{b}	4.9 ± 1^{c}	0
75µL	11 ± 1.9^{b}	11.6 ± 1.1^{b}	11.8 ± 1.2^{b}	6.1 ± 1.2^{b}	0
100µL	**12.4 ± 0.9^{a}**	**12.8 ± 0.8^{a}**	**12.8 ± 1.2^{a}**	**10.2 ± 1^{a}**	0
CME					
25µL	12.8 ± 1^{c}	23.8 ± 1.8^{d}	11.39 ± 0.9^{c}	8.1 ± 1.2^{c}	0
50µL	10.8 ± 1.2^{b}	27.5 ± 0.9^{c}	11.7 ± 1.6^{c}	8 ± 1^{c}	0
75µL	13.1 ± 0.8^{a}	29.7 ± 0.7^{b}	12.4 ± 0.6^{b}	9.1 ± 1.2^{b}	11 ± 1^{b}
100µL	**13.8 ± 1.2^{a}**	**32.5 ± 1.8^{a}**	**15.2 ± 1.4^{a}**	**11.2 ± 1^{a}**	**13.7 ± 1.4^{a}**

Group 'a' has the best treatment and group 'd' has the poorest performance treatments. Values represent mean ± standard deviation of tree replicates per treatment. Means in a column with same letter are significantly ($p \leq 0.05$) difference according to DMRT.

Plant derived phytochemicals possessed remarkable antimicrobial potential without side effects compared to synthetic drugs. Because they're natural, they might even offer additional benefits in terms of safety and efficacy (Prasad et al., 2016). Similar to our study, in *Solanum trilobatum*, the maximum inhibition zone (22 mm) was achieved in leaf callus extract against *S. aureus* compared to natural leaf extract (16 mm). Also, *E. coli* achieved a highest inhibition

zone was 18 mm in leaf callus extract compared to 15 mm in natural leaf extract (Nagarajan et al., 2009).

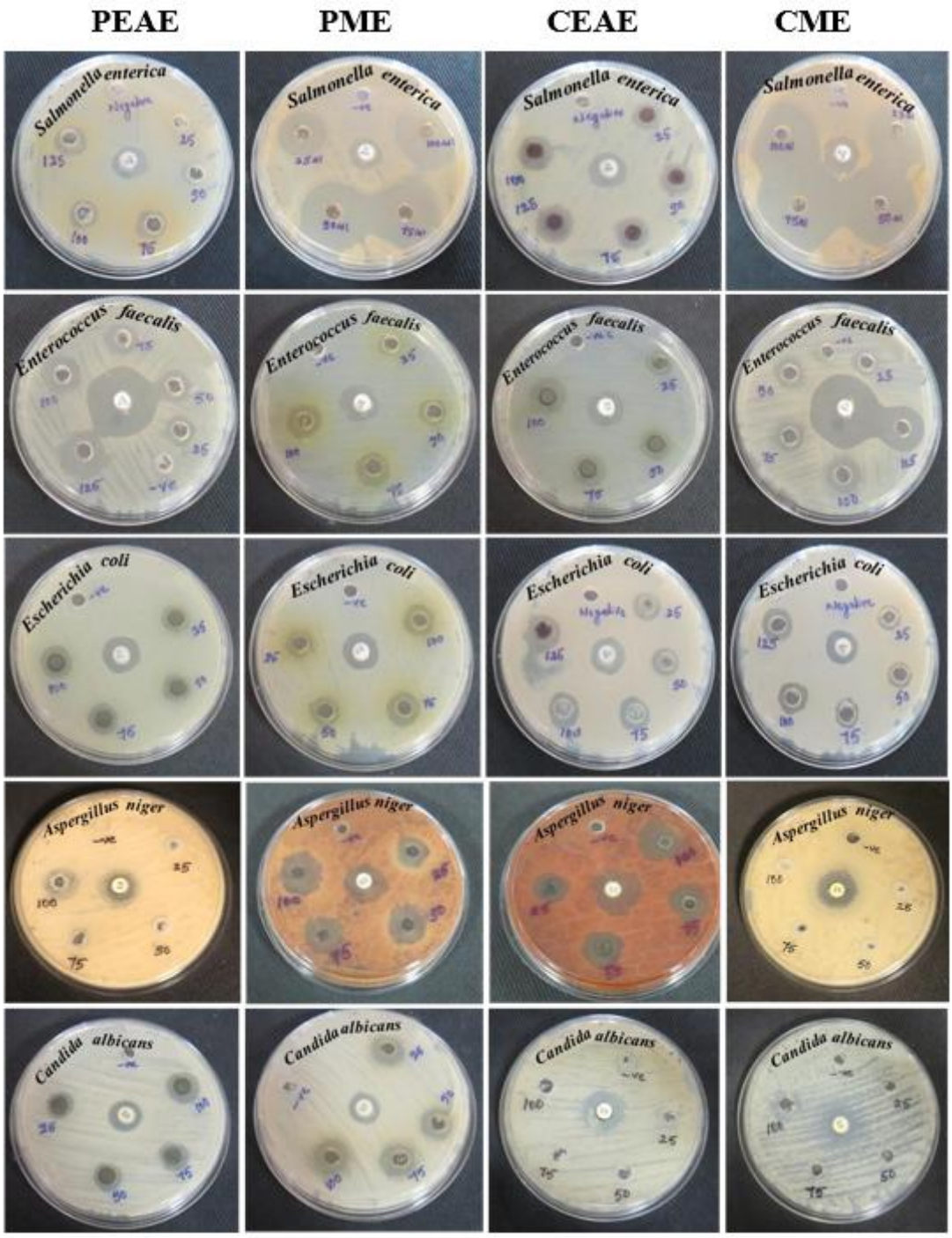

Figure 24. Antimicrobial activity of different extracts of *C. tunicatum* against five microbes

In *Thianthema decandra* the comparative analysis of both root and root callus was observed. The strong inhibition activity was exhibited in root callus against gram-negative

bacteria such as *Alcaligens faecalis, Escherichia coli, Klebsiella pneumonia, Proteus vulgaris, Salmonella enterica, Salmonella paratyphi A, Salmonella typhi* and *Salmonella tyhimurium* (Radfar et al., 2012). The methanolic extract of hypocotyl callus was effective against *Escherichia coli* and maximum inhibition zone of 19 mm was recorded in *Trigonella foenum-graecum* (Osman et al., 2020). The methanolic extract of leaf callus in *Saracaasoca* exhibited a strong inhibition zone (17 mm) against the *Enterococcus faecium* and 14 mm was achieved against *Salmonella typhi* (Vignesh et al., 2022).

4.5.1.2. Evaluation of anti-fungal activity

Two fungi which include *Aspergillus niger* (MTCC - 281), *and Candida albicans* (MTCC-183) were used to analyse antifungal activity using well diffusion method. Amphotericin and DMSO are the positive and negative controls.

PME exhibited potent anti-fungal activity against *Aspergillus niger,* the highest inhibition zone of 15.3±0.9 mm was observed at the concentration of 100 µL, 12.8±1 mm in 75 µL, 11.8±1 mm in 50 µL and 12.4±0.5 mm in 25 µL. After that, the maximum inhibition zone was observed (10.9±1.1 mm) at the concentration of 100 µL and 10.1±0.8 mm (75 µL) against the *Candida albicans.* CME showed a maximum zone of inhibition (13.7±1.4 mm) at the concentrations of 100 µL, 11±1 mm (75 µL) was observed against *Candida albicans*. CME extract showed the maximum inhibition zone 11.2±1 mm at 100 µL against *Aspergillus niger*.

PEAE showed the highest inhibition zone of 10±1.1 mm at the concentration of 100 µL against *Aspergillus niger*. The inhibition zone 7.1±0.3 mm (100 µL), 4.6±0.5 mm (75 µL), 4.6±1.5 mm (50 µL) and 3.3±0.5 mm (25 µL) was obtained against *Candida albicans*. The zone of inhibition (10.2±1 mm) recorded for CEAE against the *Aspergillus niger* (Table 10 and Figure 24). This activity displayed a dose-dependent pattern, where increasing the concentration of the extract correlated positively with increasing the antibacterial efficacy.

The strongest anti-fungal activity of PME against *Candida albicans* and *Aspergillus niger* were observed. Hasan et al. highlighted the antimicrobial activity, when the concentration increases which is directly proportional to the zone of inhibition (Hasan et al., 2024). The essential oil of leaf and seeds of *Ocimum basilicum* exhibited a strong antibacterial activity of 20.06 mm at a concentration of 50% against *Pseudomonas aeruginosa* (Sahu et al., 2024). Owusu et al. observed the highest inhibition zone of 16.1 mm and 17.6 mm in the aqueous and ethanol extract of *A. cordifolia* against *S. aureus* (Owusu et al., 2021). In *Prosopis juliflora,* the aqueous extract exhibited highest inhibition zone (23 mm) against *Escherichia coli,* 18 mm

against *Salmonella enterica* and 12 mm against *Candida albicans* (Alkaabi et al., 2020). Abaka et al. studied methanolic extract of seed callus and exhibited maximum zone of inhibition (17 mm) in *Balanites aegyptiaca* against *C. albicans* (Abaka et al., 2020).

4.5.1.3. Minimum Inhibitory Concentration (MIC)

The values for MIC of four different extracts against five microbes including three bacteria and two fungi. The concentration of 50 µg/mL, 25 µg/mL, and 12.5 µg/mL of CME suspension showed no turbidity in *Salmonella enterica.* So, the MIC value of CME against *Salmonella enterica* was 6.25 µg/mL, and PEAE against *Aspergillus niger* was 6.25 µg/mL. PME showed the clear suspension at 50 µg/mL, 25 µg/mL, and 12.5 µg/mL against two bacteria including *Escherichia coli, Enterococcus faecalis,* and two fungi including *Aspergillus niger* and *Candida albicans.* The CEAE of *Candida albicans* showed no activity (Table 11). The concentration of MIC and MBC was found to be 312.5 µg/disc and 625 µg/disc, respectively. Whereas MFC was found to be 1250 µg/disc against *Candida albicans* (Misbah et al., 2020). The MIC of *Moringa oleifera* and *Gongronema latifolium* was observed between 12.5mg/mL to 25.0mg/mL against *Salmonella typhi* and *Staphylococcus aureus* (Olise et al., 2021).

4.5.1.4. Minimum Bactericidal Concentration (MBC) and Minimum Fungicidal Concentration (MFC)

The MBC of different concentrations ranging from 50 µg/mL, 25 µg/mL, 12.5 µg/mL, 6.25 µg/mL, 3.12 µg/mL and 1.56 µg/mL were tested. The killed every single cell in the suspension of all extracts against *Escherichia coli, Enterococcus faecalis,* and *Salmonella enterica* at 25 µg/mL. On the other hand, the PEAE showed MBC at the concentration of 50 µg/mL against *Enterococcus faecalis.* The PEAE of MFC values showed 12.5 µg/mL and the CEAE showed no activity against *Candida albicans.* All other concentrations and extracts (CME, PME) were found to be efficient at 25 µg/mL against two bacteria including *Escherichia coli, Enterococcus faecalis,* and two fungi including *Aspergillus niger* and *Candida albicans* shown in Table 11. Olise et al. determined the MBC was observed between the range of 6.25 mg/mL-12.5 mg/mL and 6.25 mg/mL to 12.5 mg/mL against the bacteria *Salmonella typhi* and *Staphylococcus aureus* (Olise et al., 2021). The MIC and MBC assessment of silver nanoparticles against *S. aureus* observed growth inhibition of 0.625, 1.25, 2.5, and 5 mg/mL. It confirmed the value of MIC and MBC was observed as 0.625 mg/mL against *S. aureus* (Parvekar et al., 2020).

Table 11. MIC, MBC and MFC of different microbes of *C. tunicatum*

Name of the bacteria	PEAE		PME		CEAE		CME	
	MIC (µg/mL)	MBC (µg/mL)	MIC (µg/mL)	MBC (µg/mL)	MIC (µg/mL)	MBC (µg/mL)	MIC (µg/mL)	MBC (µg/mL)
Escherichia coli	25	25	12.5	25	12.5	25	12.5	25
Salmonella enterica	12.5	25	12.5	25	12.5	25	6.25	25
Bacillus substilis	25	50	12.5	25	12.5	25	12.5	25
Name of the fungi	**MIC (µg/mL)**	**MFC (µg/mL)**	**MIC (µg/mL)**	**MFC (µg/mL)**	**MIC (µg/mL)**	**MFC (µg/mL)**	**MIC (µg/mL)**	**MFC (µg/mL)**
Aspergillus niger	6.25	12.5	12.5	25	12.5	25	12.5	25
Candida albicans	12.5	25	12.5	25	0	0	12.5	25

4.5.2. Antioxidant assays

Interest in antioxidants is growing due to their role in preventing free radical damage in human metabolism and preserving fatty foods. Natural antioxidants are favoured over synthetic ones. Free radicals, which are produced inevitably in biological systems, are linked to many degenerative diseases, including cancer, inflammation, hypertension, diabetes, preeclampsia, renal failure, atherosclerosis, Alzheimer's, Parkinson's, aging, and cardiovascular disorders (Mary & Merina, 2021). Consumption of herbal products rich in phenolics, known for their antioxidant effects, reduces disease risk and prevents degenerative disorders. However, the antioxidant capacity and quality of these natural extracts depend on both the source and the extraction processes used (Askın et al., 2018).

The comparative analysis of ethyl acetate and methanolic extract of wild plant and *in vitro* callus was determined. The extracts such as PEAE, PME, CEAE and CME were tested with four antioxidant assays. The evaluation of DPPH (2,2-diphenyl-1-picrylhydrazyl), FRAP (Ferric ion Reducing Antioxidant Power) assay, ABTS (2,2-azino-bis-3-ethylbenzothiazoline-6-sulphonic acid) and TAA (Total antioxidant activity) showed the maximum inhibition percentage in PME and CME.

4.5.2.1. Evaluation of DPPH assay

DPPH assay is a commonly used, simple, and cost-effective method for evaluating antioxidant activity (Baliyan et al., 2022). Free radicles lead to cell damage, antioxidants such as phenol and flavonoid have an ability to protect cells from damage (Karale et al., 2022). The radical scavenging activity was analysed from *C. tunicatum* using ethyl acetate and methanolic extract of wild and callus extracts. PME showed maximum inhibition rate (86.82%), whereas standard ascorbic acid displayed 85.9% (IC_{50} = 38.9 µg/mL). Followed by, CME (84.08%), CEAE (70.82%) and PEAE (69.11%). The Half-maximal inhibitory concentration was examined as PEAE (IC_{50} = 76.15 µg/mL), PME (IC_{50} = 53.1 µg/mL), CEAE (IC_{50} = 63.4 µg/mL) and CME (IC_{50} = 52.2 µg/mL) at the concentration of 100 µg/mL, and as shown in Table 12 and Figure 25. It established the PME and CME of *C. tunicatum* have capability to prevent oxidative damage with significant level ($p \leq 0.05$) by DMRT test. So far, there is no antioxidant activity have been reported from *C. tunicatum.* According to Lamichhane et al. ethanolic leaf extract of *Rubus ellipticus* showed IC_{50} value almost like the standard ascorbic acid and it was more potent as standard ascorbic acid (Lamichhane et al., 2023). In *Euphorbia eriophora*, the highest inhibition rate (68.721±1.694) was obtained in EtOH extract (Akgül et al., 2022). The ethyl acetate extract (IC_{50} = 640 ± 1.9 µg/mL) and hexane extract (IC_{50} = 80 ± 1.2 µg/mL) of callus culture of *Vigna unguiculata* showed maximum inhibition rate (Vats, 2012).

Figure 25. DPPH assay of different extracts of *C. tunicatum*

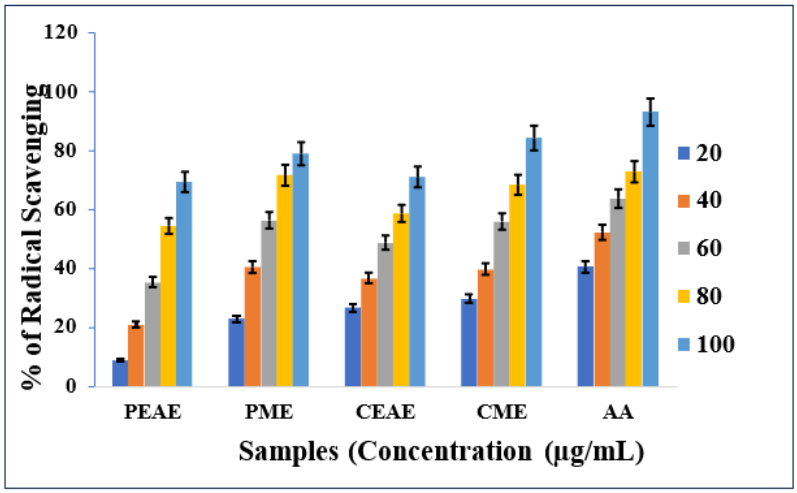

Table 12. DPPH Radical Scavenging activity of *C. tunicatum*

Concentration (µg/mL)	PEAE (%)	PME (%)	CEAE (%)	CME (%)	AA (%)
20	8.67±0.003^{e}	22.76±0.004^{e}	26.49±0.01^{e}	29.38±0.004^{e}	40.34±0.007^{e}
40	20.75±0.003^{d}	40.4±0.004^{d}	36.41±0.006^{d}	39.48±0.009^{d}	52.09±0.004^{d}
60	35.01±0.002^{c}	56.05±0.007^{c}	48.44±0.005^{c}	55.63±0.002^{c}	63.43±0.006^{c}
80	54.12±0.008^{b}	71.39±0.006^{b}	58.39±0.005^{b}	68.13±0.005^{b}	72.58±0.004^{b}
100	69.11±0.004^{a}	86.82±0.002^{a}	70.82±0.01^{a}	84.08±0.01^{a}	85.9±0.005^{a}
IC_{50} (µg/mL)	**76.15**	**53.1**	**63.4**	**52.2**	**38.9**

Group 'a' has the best treatment and group 'e' has the poorest performance treatments. Values represent mean ± standard deviation of tree replicates per treatment. Means in a column with same letter are significantly ($p \leq 0.05$) difference according to DMRT.

4.5.2.2. Evaluation of FRAP assay

The assessment of FRAP assay involved the reduction of Ferric ion (Fe_3+) to Ferrous ion (Fe_2+) (Ene-Obong et al., 2018) using ethyl acetate and methanol extracts of *C. tunicatum* of both wild and *in vitro* callus extract. The FRAP value of CME (1.6 µg/mL), CEAE (1.09 µg/mL), PME (1.27 µg/mL) and PEAE (0.98 µg/mL) at 100 µg/mL were represented in Table 13 and Figure 26. It depicted the more antioxidant potential in callus extract compared to plant extract. FRAP assay of methanol extract showed maximum radicle scavenging activity with significance of $p \leq 0.05$ using DMRT's test. In *Coronopus didymus*, the maximum FRAP value (0.304 µg/mL) was obtained at 50 µg/mL in aerial parts of ethanolic extract (Noreen et al., 2017).

Figure 26. FRAP assay of different extracts of *C. tunicatum*

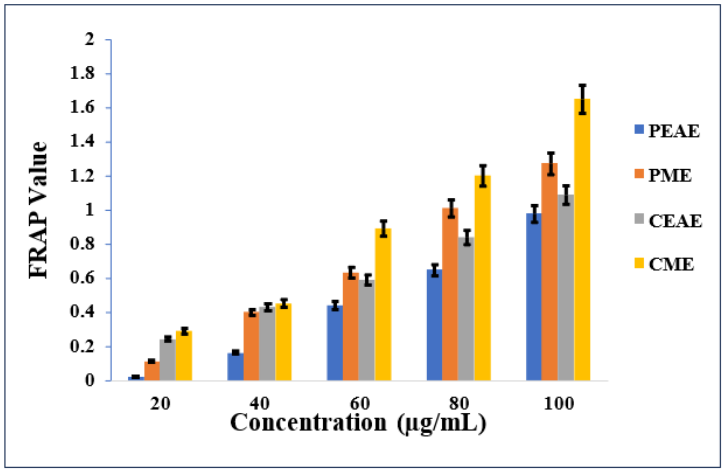

Table 13. FRAP analysis of different extracts of *C. tunicatum*

Concentration (µg/mL)	PEAE (µM Fe+2/g)	PME (µM Fe+2/g)	CEAE (µM Fe+2/g)	CME (µM Fe+2/g)
20	0.02^{e}	0.11^{e}	0.24^{e}	0.29^{e}
40	0.16^{d}	0.4^{d}	0.43^{d}	0.45^{d}
60	0.44^{c}	0.63^{c}	0.59^{c}	0.89^{c}
80	0.65^{b}	1.008^{b}	0.84^{b}	1.2^{b}
100	0.98^{a}	**1.27^{a}**	1.09^{a}	1.65^{a}

Group 'a' has the best treatment and group 'e' has the poorest performance treatments. Values represent mean ± standard deviation of tree replicates per treatment. Means in a column with same letter are significantly ($p \leq 0.05$) difference according to DMRT.

4.5.2.3. Evaluation of ABTS assay

The ABTS assay was performed to determine with four extracts PEAE, PME, CEAE and CME of *C. tunicatum.* The percentage scavenging activity of all four extracts showed CME (89.69%), followed by CEAE (65.5%), PME (57.07%) and PEAE (56.42%) were observed at 100 µg/mL (Table 14 and Figure 27). The standard ascorbic acid showed 82.24%. The IC_{50} values of PEAE, PME, CEAE, CME and ascorbic acid showed 99.58, 72.99, 75.73, 60.24 and 51.39 µg/mL respectively. The radical scavenging activity of polysaccharides of *Cynanchum auriculatum* CAP2-1 was determined by Chai et al. The ABTS showed a maximum inhibition percentage of 71.22 % at 0.8 mg/mL (Chai et al., 2018).

Table 14. ABTS Radicle Scavenging of different extracts

Concentration (µg/mL)	PEAE (%)	PME (%)	CEAE (%)	CME (%)	AA (%)
20	4.3 ± 0.1^{e}	36.87 ± 0.1^{e}	17.1 ± 0.1^{e}	14.5 ± 0.05^{e}	35.51 ± 0.11^{e}
40	13.49 ± 0.1^{d}	44.51 ± 0.09^{d}	35.27 ± 0.11^{d}	35.55 ± 0.07^{d}	45.55 ± 0.06^{d}
60	17.06 ± 0.07^{c}	47.56 ± 0.13^{c}	39.94 ± 0.07^{c}	44.96 ± 0.06^{c}	46.64 ± 0.11^{c}
80	34.79 ± 0.1^{b}	49.29 ± 0.11^{b}	48.92 ± 0.14^{b}	64.23 ± 0.12^{b}	64.44 ± 0.08^{b}
100	56.42 ± 0.1^{a}	57.07 ± 0.09^{a}	65.5 ± 0.1^{a}	89.69 ± 0.1^{a}	82.24 ± 0.1^{a}
IC_{50} (µg/mL)	**99.58**	**72.99**	**75.73**	**60.24**	**51.39**

Group 'a' has the best treatment and group 'e' has the poorest performance treatments. Values represent mean ± standard deviation of tree replicates per treatment. Means in a column with same letter are significantly ($p \leq 0.05$) difference according to DMRT.

Figure 27. ABTS of different extracts of *C. tunicatum*

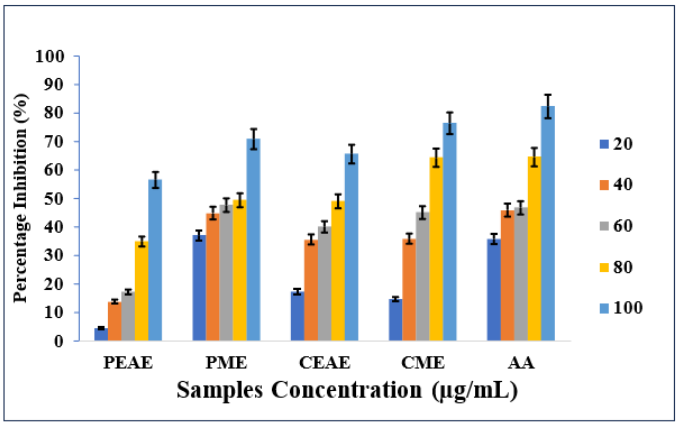

4.5.2.4. Evaluation of Total Antioxidant Activity

The antioxidants from *C. tunicatum* phytochemicals have ability to convert Molybdenum VI to Molybdenum V by Phosphomolybdenum method. The reduced molybdate forms a blue complex that can be measured using spectrophotometry (Phatak & Hendre, 2014). TAA was evaluated from *C. tunicatum* using four extracts such as PEAE, PME, CEAE and CME at different concentrations. The maximum scavenging activity was obtained at 100 µg/mL in CME (83.68%) followed by PME (81.83%), CEAE (62.19%) and PEAE (58.63%) as shown in Table 15 and Figure 28. The IC_{50} values of PEAE, PME, CEAE, CME and AA showed 82.11, 47.11, 86, 53.38 and 32.91 µg/mL respectively.

Table 15. Total antioxidant activity of different extracts of *C. tunicatum*

Concentration (µg/mL)	PEAE (%)	PME (%)	CEAE (%)	CME (%)	AA (%)
20	13.66±0.03^{e}	29.97±0.01^{e}	15.4±0.07^{e}	27.32±0.02^{e}	44.25±0.005^{e}
40	21.1±0.02^{d}	48.05±0.008^{d}	17.57±0.04^{d}	40.89±0.02^{d}	54.1±0.008^{d}
60	30.09±0.009^{c}	60.35±0.007^{c}	31.23±0.02^{c}	53.13±0.01^{c}	62.46±0.007^{c}
80	57.03±0.1^{b}	70.38±0.009^{b}	45.17±0.05^{b}	68.16±0.02^{b}	75.12±0.002^{b}
100	58.63±0.02^{a}	81.83±0.006^{a}	62.19±0.01^{a}	83.68±0.002^{a}	86.37±0.003^{a}
IC_{50} (µg/mL)	**82.11**	**47.11**	**86**	**53.38**	**32.91**

Group 'a' has the best treatment and group 'e' has the poorest performance treatments. Values represent mean ± standard deviation of tree replicates per treatment. Means in a column with same letter are significantly ($p \leq 0.05$) difference according to DMRT.

Hence, it proved that the callus extracts of *C. tunicatum* has essential ability for antioxidant properties compared to plant extracts with significant level of $p \leq 0.05$. Similarly, *Limonia acidissima* exhibited maximum radical scavenging activity (5.055 µL) in ethanolic leaf extract (Parvez & Sarker, 2021). In *Rhodiola rosea*, maximum scavenging activity (3.66 ± 0.24 mg/mL) in aqueous extract (Bayliak et al., 2016).

Figure 28. TAA of different extracts of *C. tunicatum*

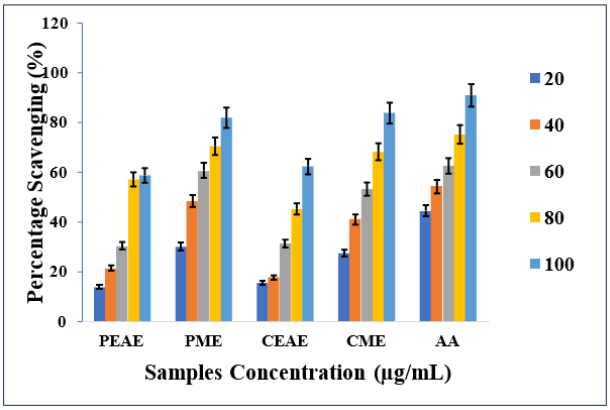

4.5.3. Determination of Anti-inflammatory activity

Protein may undergo denaturation due to adverse microorganism or oxidative stress. The vascular tissue response is known as inflammation (Ferrero-Miliani et al., 2007) and inhibited by inflammatory response due to mechanism of action (Yesmin et al., 2020). The maximum inhibition percentage of CME (310.74%), PME (85.71%), CEAE (374.53%) and PEAE (130.81%). Result displayed in Table 16 and Figure 29, the IC_{50} value of PEAE (70.1 µg/mL), PME (57.03 µg/mL), CEAE (60.14 µg/mL), CME (59.23 µg/mL) and Diclofenac sodium (42.31 µg/mL). PEAE<CEAE<Diclofenac sodium<PME<CME are percentage of inhibition results of *C. tunicatum*.

Table 16. Anti-inflammatory activity of different extracts of *C. tunicatum*

Conc. (µg/mL)	PEAE (%)	PME (%)	CEAE (%)	CME (%)	Diclofenac
20	2.51±0.002^{e}	13.22±0.0005^{e}	39.32±0.003^{e}	24.8±0.002^{e}	49.27±0.002^{e}
40	29.55±0.004^{d}	28.12±0.003^{d}	122.09±0.011^{d}	118±0.002^{d}	71.01±0.002^{d}
60	62.89±0.002^{c}	50.79±0.002^{c}	221.72±0.007^{c}	194.62±0.001^{c}	102.89±0.001^{c}
80	97.48±0.004^{b}	71.42±0.001^{b}	301.12±0.004^{b}	268.08±0.003^{b}	147.82±0.004^{b}
100	130.81±0.001^{a}	85.71±0.002^{a}	374.53±0.009^{a}	310.74±0.002^{a}	171.01±0.001^{a}
IC_{50} (µg/mL)	**70.1**	**57.03**	**60.14**	**59.23**	**42.31**

Group 'a' has the best treatment and group 'e' has the poorest performance treatments. Values represent mean ± standard deviation of tree replicates per treatment. Means in a column with same letter are significantly ($p \leq 0.05$) difference according to DMRT.

Yesmin et al. studied the highest anti-inflammatory activity (60%) at 1000 µg/mL by egg albumin denaturation assay from *Piper chaba* (Yesmin et al., 2020). Previously, Truong et al. investigated albumin denaturation assay in *Severinia buxifolia* observed the highest inhibition percentage with IC_{50} value of methanol > ethyl acetate > acetone > dichloromethane > chloroform > water (Truong et al., 2019). Agarwal & Shanmugam demonstrated albumin denaturation assay in *Kalanchoe pinnata* showed maximum inhibitory activity in a methanolic extract with an IC_{50} value of 490 µg/mL (Agarwal & Shanmugam, 2019). It can be postulated from the observed results that the anti-inflammatory activity of wild and *in vitro* callus extracts of *C. tunicatum* could be due to its inhibition of protein denaturation and minimum inhibitory concentration.

Figure 29. Anti-inflammatory activity of different extracts of *C. tunicatum*

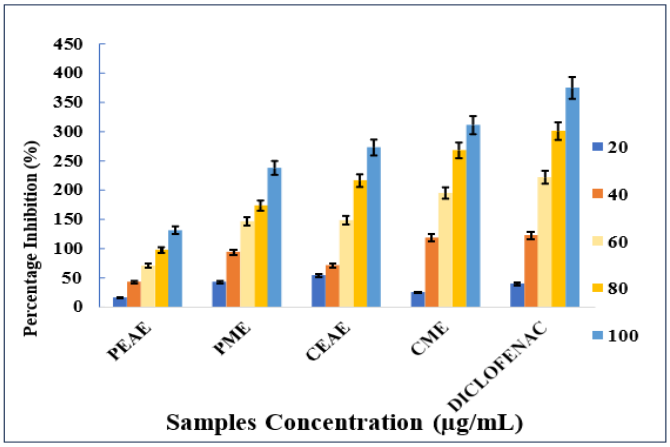

4.5.4. Determination of anti- cancer activity

The anticancer activity was evaluated using different crude extracts such as PEAE, PME, CEAE, and CME of *C. tunicatum.* The *in vitro* cytotoxicity was performed using the HCT-116 cell line initiated from an adult male. SDS was used as a positive control.

4.5.4.1. MTT (Methylthiazolyldiphenyl-tetrazolium bromide) assay

The percentage of cytotoxicity against the HCT-116 at different concentrations ranged from 1.56 to 50 µg/mL of various crude extracts of *C. tunicatum* (Figure 30, 31, 32, 33). The maximum percentage of cytotoxicity of CEAE was observed as 88 % at the concentrations of 50 µg/mL (Figure 34). Followed by, CME exhibited 84.64 % of cytotoxicity. Next to that, PEAE and PME showed cytotoxicity percentage was 85.49% and 75.41%. Whereas the CME showed the highest inhibition percentage of cytotoxicity using MTT assay. The IC_{50} Values of

CME, CEAE, PME and PEAE were obtained as 16.71 µg/mL, 17.81 µg/mL, 24.15 µg/mL and 26.47 µg/mL respectively shown in Table 17. The present study showed that *C. tunicatum* had potential activity against colorectal cancer cells HCT-116.

Figure 30. Anticancer activity of HCT-116 cell line of PEAE of *C. tunicatum*

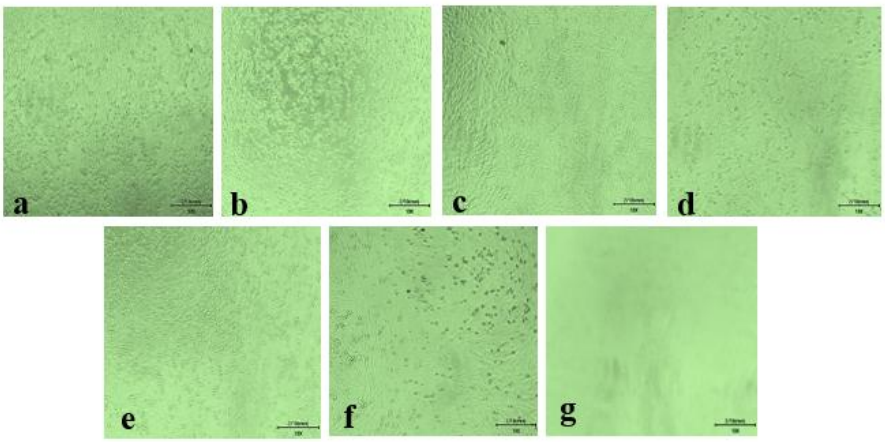

a) 1.562 µg/mL of extract b) 3.125 µg/mL of extract c) 6.25 µg/mL of extract d) 12.5 µg/mL of extract e) 25 µg/mL of extract f) 50 µg/mL of extract g) positive control

Figure 31. Anticancer activity of HCT-116 cell line of PME of *C. tunicatum*

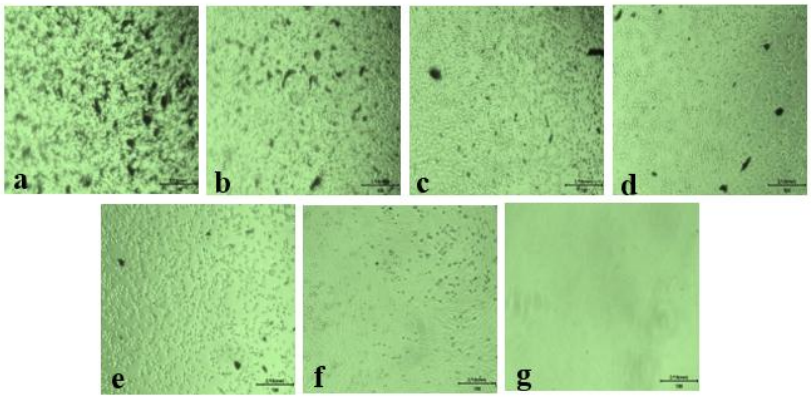

a) 1.562 µg/mL of extract b) 3.125 µg/mL of extract c) 6.25 µg/mL of extract d) 12.5 µg/mL of extract e) 25 µg/mL of extract f) 50 µg/mL of extract g) positive control

Figure 32. Anticancer activity of HCT-116 cell line of CEAE of *C. tunicatum*

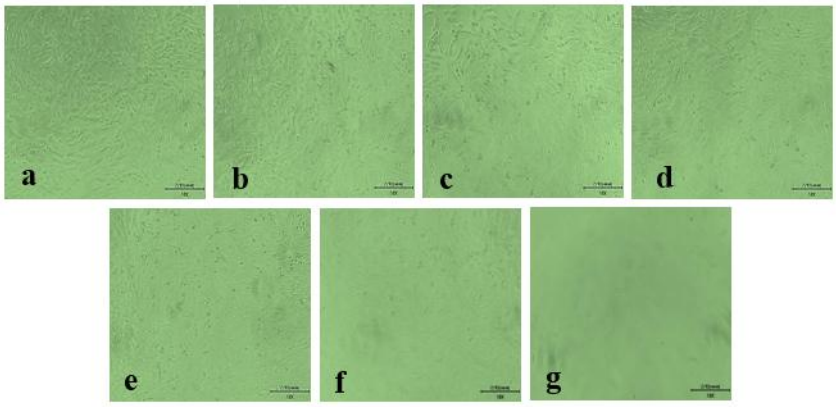

a) 1.562 µg/mL of extract b) 3.125 µg/mL of extract c) 6.25 µg/mL of extract d) 12.5 µg/mL of extract e) 25 µg/mL of extract f) 50 µg/mL of extract g) positive control

Figure 33. Anticancer activity of HCT-116 cell line of CME of *C. tunicatum*

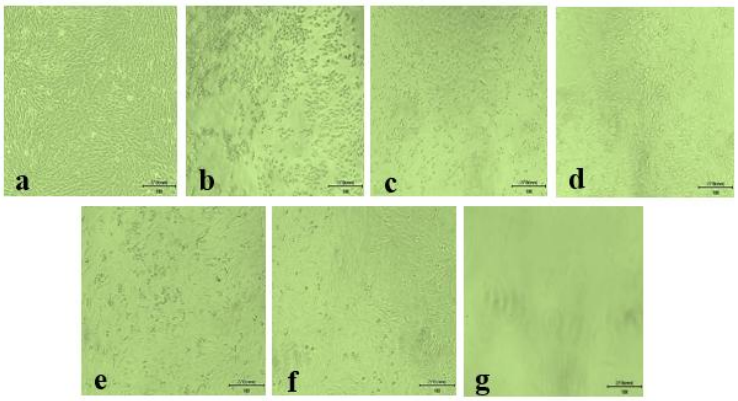

a) 1.562 µg/mL of extract b) 3.125 µg/mL of extract c) 6.25 µg/mL of extract d) 12.5 µg/mL of extract e) 25 µg/mL of extract f) 50 µg/mL of extract g) positive control

Nelson et al. studied the cytotoxicity effect of HCT-116 cell line in *Eclipta alba*. It showed a level of significant ($p \leq 0.05$) and cytotoxicity effect was increased as concentration increases. The IC_{50} value of colorectal cancer cell line was obtained as 179 ± 0.81 µg/mL in methanolic extract of *Eclipta alba* (Nelson et al., 2020). In *Catharanthus roseus* and *Emblica officinalis,* the inhibitory concentration (IC_{50}) of 46.21 µg/mL and 35.21 µg/mL respectively in colorectal cancer using HCT-116 cell line was observed (Bandopadhyaya et al., 2015). Cytotoxic activity was examined in methanolic extract from *Origanum vulgare* using MTT assay. The IC_{50} value was obtained as 140.77 ± 2.13 µg/mL in colorectal cancer using HCT-116 cell line (Grbović et al., 2013). In *Turbinaria decurrens*, the IC_{50} values of n-hexane, and ethyl acetate fraction were observed as 1.51 µg/ml, 3.058 µg/mL respectively (Zakaria et al.,

2018). The hexane extract from *Clerodendrum infortunatum* obtained best cytotoxic activity of 68.17 ± 1.36 % at 100 µg/mL (Haris et al., 2016). The ethanol stamen crude extract of *Nelumbo nucifera* was observed maximum percentage (86.3%) using colorectal cancer at 400 µg/mL (Zhao et al., 2017).

Table 17. Anticancer activity of HCT-116 cell line of different extracts of *C. tunicatum*

Drug Concentration (µg/mL)	% of Cytotoxicity			
	PEAE	PME	CEAE	CME
1.56	-	-	7.22	8.13
3.125	4.4	14.27	24.14	28.15
6.25	16.03	35.71	38.16	41.62
12.5	30.46	49.36	53.16	64.68
25	57.25	62.44	76.15	70.44
50	85.49	75.41	88.42	84.64
Negative	-	-	-	-
Positive	100	100	100	100
Blank	100	100	100	100
IC_{50} (µg/mL)	26.47	24.15	17.81	16.71

Excessive ROS can push tumour cells into free radicle damage, potentially leads to death. Unlike normal cells, cancer cells have a compromised antioxidant defence system, which limits their ability to neutralize excess ROS and prevent cellular damage. The anticancer activity observed in stem extract that disrupt the redox balance critical for the survival of HCT-116 cells. This disruption could either involve increasing or inhibiting ROS levels within the cancer cells (Nelson et al., 2020).

Figure 34. Percentage of Cytotoxicity of different extracts of *C. tunicatum* against HCT-116 cell line

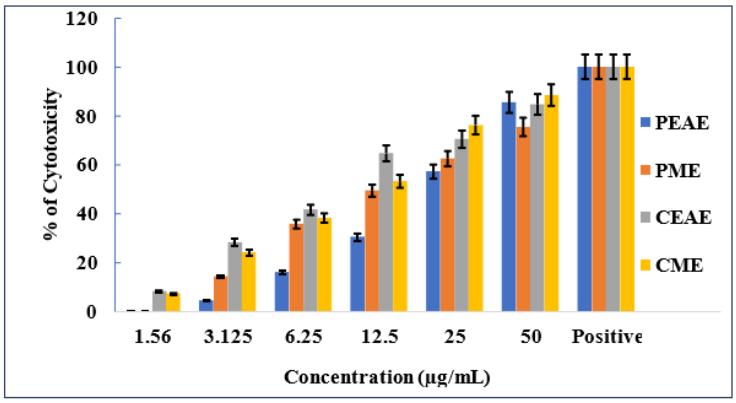

4.5.5. Brine Shrimp Lethality Assay

The brine shrimp (*Artemia salina*) lethality assay was assessed to identify the toxicity level of plant extracts such as PEAE, PME, CEAE and CME of *C. tunicatum*. Kala & Mallikarjuna studied the toxicity of bioactive compounds being tested, which led to the discover the new cytotoxic compounds (Kala & Mallikarjuna, 2014). The Potassium Dichromate (Positive) and saline water (negative) were acted as a control.

The lowest toxicity was observed in the CME, percentage mortality was calculated after 24 hours observed as 53%. This extract showed the lowest toxicity and is considered for pharmaceutical activities. The increasing drug concentration is directly proportional to the mortality rate. The percentage showed as 17, 20, 27, 40 and 53% at the concentration of 100, 250, 500, 1000, 1500 µg/mL respectively. Subsequently, the CEAE showed the second lowest mortality rate was observed as 17, 20, 27, 40, 53% at 100, 250, 500, 1000, 1500 µg/mL correspondingly. The PME was observed as 17, 17, 23, 43 and 67% followed by PEAE was recorded as 7, 10, 17, 33, and 87% at same concentrations. The only concentration of 1500 µg/mL showed a sudden increase of lethality rate of *Artemia salina*. All extracts showed fewer toxic effects when compared to potassium dichromate (positive control). All nauplii survived in the saline water (negative control). The callus methanolic extract showed less toxicity was observed compared to plant extracts (Table 18).

Similarly, Mannan et al. studied that a 100% mortality rate was observed in methanolic leaf extract of *Artemisia dubia* at the concentration of 1000 ppm after 24 hours (Mannan et al., 2012). In *Aedes aegypti*, the cytotoxicity test confirmed the toxic percentage of leaf and callus hexane extracts. Comparatively, callus extract showed a very lower toxicity percentage of 16.67%, whereas a 100% mortality rate was obtained in leaf extract (Kulathilaka & Senarath, 2014).

Similar to our results, Agha et al. the mortality rate of *Artemia salina* increased as the drug concentration increased. In *Trigonella foenum-graecum*, the highest mortality percentage was observed as 23.33% at 250 µg/mL in whole plant extracts. The lowest toxic range was obtained in the callus extract at 16.66% at 250 µg/mL and it exhibited less toxicity (Agha et al., 2022).

Table 18. Brine shrimp lethality assay of different extracts of *C. tunicatum*

S.No	Sample Code	Concentration (µg/mL)	Mortality of Brine shrimp (No. of shrimps dead) (h)					
			1	2	4	6	24	%Mortality (24h)
1.	PEAE	100	0	0	0	1	2	7
		250	0	0	0	1	3	10
		500	0	0	0	1	5	17
		1000	0	0	0	10	10	33
		1500	0	0	3	20	26	87
		LC_{50}						1024.638
2.	PME	100	0	0	0	0	5	17
		250	0	0	0	0	5	17
		500	0	0	0	0	7	23
		1000	0	0	1	1	13	43
		1500	0	0	0	14	20	67
		LC_{50}						1120.642
3.	CEAE	100	0	0	1	7	3	10
		250	0	0	1	8	5	17
		500	0	0	2	4	12	40
		1000	0	0	2	3	14	46
		1500	0	0	1	7	18	60
		LC_{50}						1122.434
4.	CME	100	1	1	1	1	8	17
		250	0	0	0	0	6	20
		500	1	1	1	1	5	27
		1000	1	2	2	2	12	40
		1500	0	0	0	2	16	53
		LC_{50}						1385.038
3.	Positive control ($K_2Cr_2O_7$)	1 mg/ml	30	-	-	-	-	100
4.	Negative control	Saline water	0	0	0	0	0	0

4.6. *IN SILICO* STUDIES

4.6.1. Molecular docking

The inference from the *in vitro* anticancer assay provided valuable evidence which support *in silico* studies of *C. tunicatum*. Docking studies are crucial in drug discovery for predicting ligand-receptor interactions and ranking compounds based on binding energies or

fitness scores. The bioactive compounds were obtained from GCMS analysis of *C. tunicatum* associated with the primary drug pathway for human colorectal cancer. The responsible ligand and protein (6 GUE) were docked between ligand and protein molecules. The highest affinity score was achieved as shown in Table 19. The protein structure (6 GUE) was obtained from PDB database which is human cyclin-dependent kinase 2 (CDK_2 enzyme). Enzyme-ligand interactions were performed using Schrödinger which conformed the strong interaction. Subsequent computational analysis identified 9 compounds significantly enhanced cytotoxicity assay against 6 GUE.

Table 19. Docking studies for natural plant-based compounds with HCT-116 cell line of *C. tunicatum*

Protein	Compound	Pub chem ID	Molecular weight (g/mol)	Molecular formula	Binding energy	Ligand efficiency	Glide emodel	Canonical Smiles
6GUE	Chromone	10286	146.14	$C_9H_6O_2$	**-7.625**	-0.693	-31.136	C1=CC=C2C(=C1)C(=O)C=CO2
	5-(Hydroxymethyl)-2-Furaldehyde	237332	126.11	$C_6H_6O_3$	-6.231	-0.692	-28.671	C1=C(OC(=C1)C=O)CO
	4H-Pyran-4-one	119838	144.12	$C_6H_8O_4$	-6.09	-0.609	-26.082	CC1=C(C(=O)C(CO1)O)O
	Megastigmatrienone	5375190	190.28	$C_{13}H_{18}O$	-5.905	-0.422	-23.482	CC1=CC(=O)CC(C1/C=C/C=C)(C)C
	Furfural	7362	96.08	$C_5H_4O_2$	-5.859	-0.837	-21.432	C1=COC(=C1)C=O
	Phenol	996	94.11	C_6H_6O	-5.686	-0.812	-21.955	C1=CC=C(C=C1)O

Chromone had the maximum binding affinity score of −7.62 Kcal/mol. The compound chromone was the most active compound in the dataset and presents a conventional hydrogen bond with the carbonyl group attached with a residue LUE83. The designed compounds formed

the amino acids fractions such as phenylalanine (PHE82, PHE80), glutamic acid (GLU81), alanine (ALA31, ALA144) (VAL64, VAL18), lysine (LYS33), aspartic acid (ASP145), leucine (LEU134) and isoleucine (ILE10) of the CDK_2 enzyme. The 2D and 3D interactions of the compound chromone and the enzyme were presented in Figure 35. The highest binding score of other compounds such as 5-(Hydroxymethyl)-2-Furaldehyde (-6.231 Kcal/mol), 4H-Pyran-4-one (-6.09 Kcal/mol), Megastigmatrienone (-5.905 Kcal/mol), Furfural (-5.859 Kcal/mol) and Phenol (-5.686 Kcal/mol). Salem et al. studied the derivatives of chromone showed the high potential cytotoxic effects (HCT-116) against protein (PDB ID:7SJ3) owing to induce DNA fragmentation in cancer cell lines up-regulate the expression of the pro-apoptotic genes P53 and Bax and down-regulate the expression level of CDK_4 as well as the anti-apoptotic gene Bcl-2 (Abo-Salem et al., 2024). Wang et al. observed the wide range of pharmaceutical properties of chromone derivates including antimicrobial, anti-inflammatory, anti-HIV, antioxidant, anticancer and antibacterial activities. Even in clinical medicines, numerous chromone containing drugs have been utilized such as nedocromil (anti-inflammatory), cromolyn (anti-inflammatory), diosmin (phlebotropic) and flavoxate (anticholinergic) for so many years (Wang et al., 2017).

Figure 35. 2D and 3D interaction of ligands with HCT-116 proteins (6gue)

a)

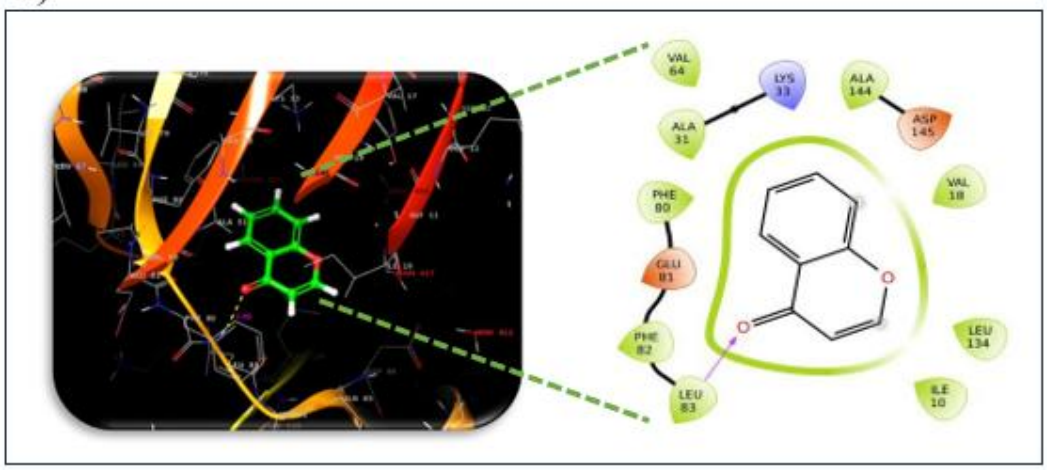

b)

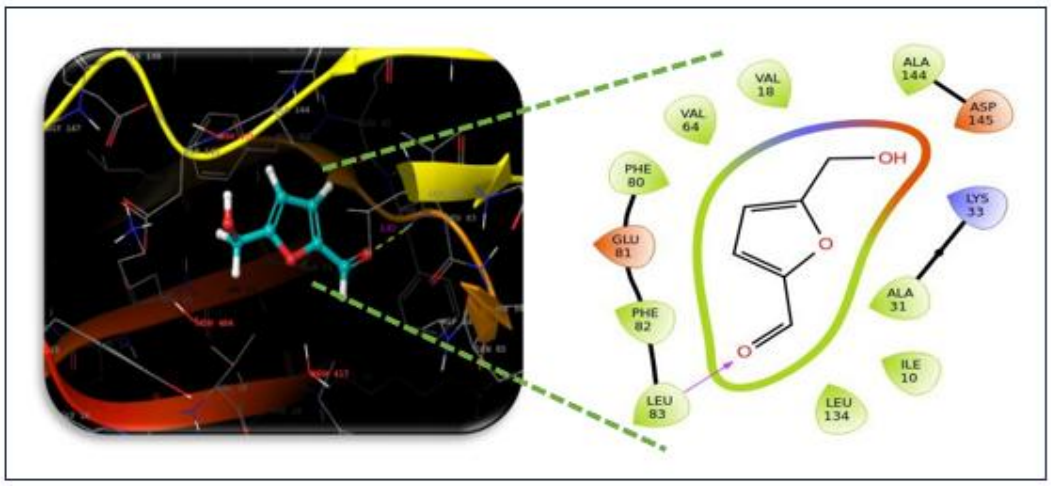

a) Chromone
b) 5-(Hydroxymethyl)-2-Furaldehyde

c)

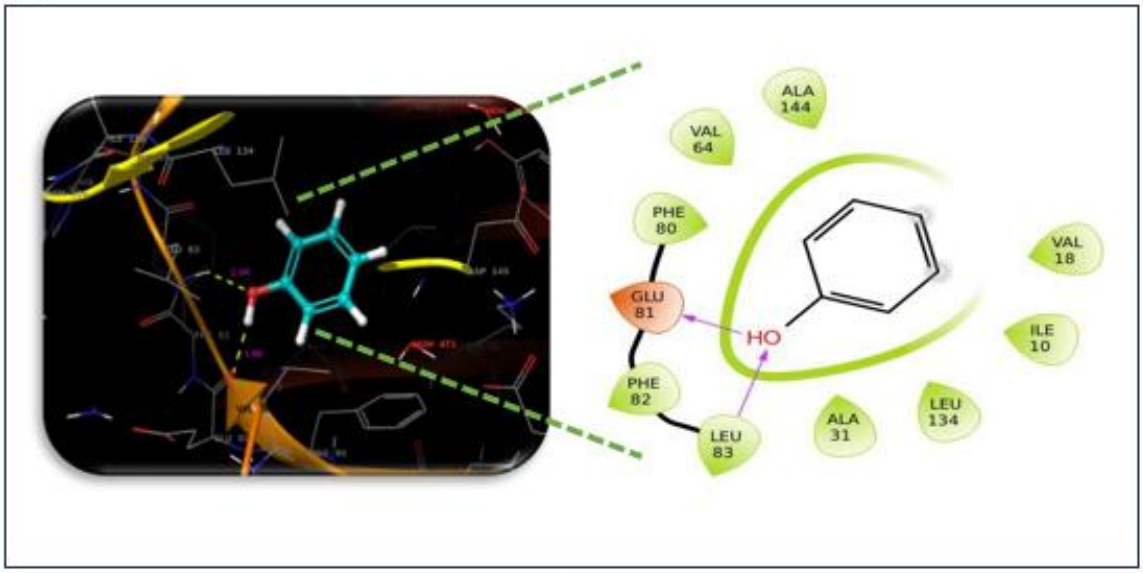

d)

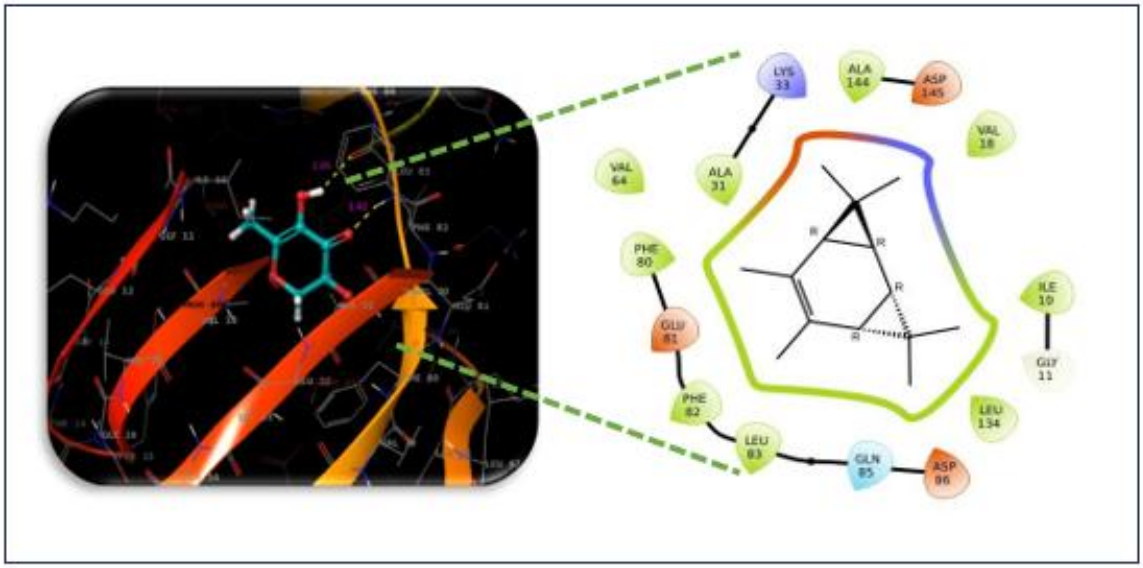

c) Phenol
d) 4H-Pyran-4-one

e)

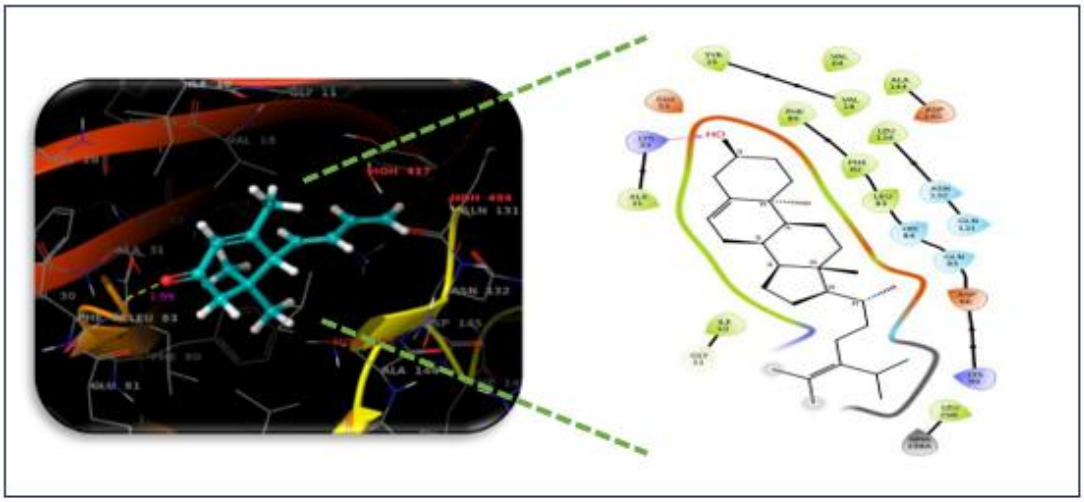

f)

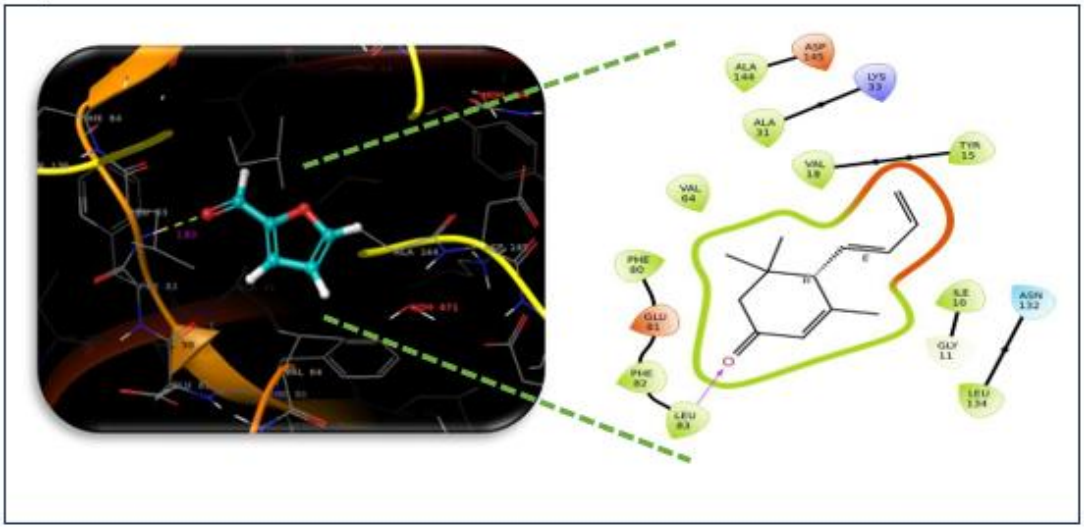

e) Megastigmatrienone
f) Furfural